FACTORS THAT LIMIT CONTROL EFFECTIVENESS IN SELF-EXCITED NOISE DRIVEN COMBUSTORS

A Dissertation
Presented to
The Academic Faculty

by

Jackie H. Crawford III

In Partial Fulfillment
of the Requirements for the Degree
Doctor of Philosophy in the
School of Aerospace Engineering

Georgia Institute of Technology
May 2012

FACTORS THE LIMIT CONTROL EFFECTIVENESS IN SELF-EXCITED NOISE DRIVEN COMBUSTORS

Approved by:

Dr. Tim Lieuwen, Advisor
School of Aerospace Engineering
Georgia Institute of Technology

Dr. Erik Verriest, Co-Advisor
School of Electrical and Computer Engineering
Georgia Institute of Technology

Dr. Wassim Haddad
School of Aerospace Engineering
Georgia Institute of Technology

Dr. Jerry Seitzman
School of Aerospace Engineering
Georgia Institute of Technology

Dr. Massimo Ruzzene
School of Aerospace Engineering
Georgia Institute of Technology

Date Approved: March 26, 2012

ACKNOWLEDGEMENTS

While doing the research for this thesis I have been repeated struck by how much serendipity plays a role in guiding events. Research involves more than searching for the right piece of information or analysis tool. Having the correct people around me have helped tremendously in seeing this thesis to completion. I would like to thank my advisor Tim Lieuwen for putting up with my unique brand of stubbornness and independent mindedness. Despite this, he has placed a large amount of trust in the vision I had for this research and in giving me the leeway to accomplish things in the order and matter I thought was most important and efficient. I always had his ear available when I need it. Most importantly, I appreciate the freedom to perform research without compromising my sense of self. My co-advisor Erik Verriest served as my tour guide to the exciting and exotic world of time delay and stochastic system. His willingness to show me where to look saved me from countless dead ends and his ability to express mathematical details in very simple language is astounding. I cannot begin to express how this positively influenced my style of thinking. Finally, I would also like to thank Wassim Haddad for taking the time to make extraordinary detailed and insightful comments during my thesis proposal. The influence of those comments can definitely be felt in certain sections of this thesis.

My peers also helped me greatly. This thesis is very multi-disciplinary which prevented me from delving as deeply in the details on certain physical process as I would like because I was focused on how to make mutually antagonistic modeling frameworks interact with each other in a physically and mathematically consistent matter. Jacqueline

O'Conner was always available to talk about fluid mechanics and turbulence. Shreekrishna could always be counted on to discuss concept ranging from analysis to heat release perturbation modeling. Finally, Prabhakar Venkateswaran was someone who I could always discuss general concepts in combustion with to make sure I understood their physical ramifications. Many other people have befriended me in Atlanta that made my stay a pleasurable one. This gift of friendship is not forgotten. I will miss you guys.

The vast majority of this thesis was enabled by the financial support of NASA Glenn through their Fundamental Aeronautics program. John DeLaat served as technical monitor and Jerry Seitzman as primary investigator. They were both very patient in giving me the time needed to teach myself new mathematical techniques which allowed me to focus on more long sighted and impactful contributions to the combustion instability community. Additional financial support was provided by the Sloan Foundation during the final semester.

Long distance support came from my family. Being able to visit home has always been a motivator to push through hard times when research was not going anywhere and in some cases backwards. Finally, I would like to thank God for always being there for me for the things I cannot mention. I am under no illusion that there are more deserving people for his help and yet I'm still here doing what I want to do with my life as if it was meant to be. This has been a deeply humbling experience and one I hope not to lose sight of in whatever future adventures life has in store for me.

TABLE OF CONTENTS

LIST OF TABLES

Page

LIST OF FIGURES

Page

LIST OF SYMBOLS AND ABBREVIATIONS

Abbreviations:

ARE	Algebraic Riccati Equation
dB	Decibel
FTF	Flame Transfer Function
LDI	Lean Direct Injection
LHCP	Left Hand Complex Plane
LPM	Lean Premixed
LPP	Lean Premixed Prevaporized
LQG	Linear Quadratic Gaussian
LQR	Linear Quadratic Regulator
MIMO	Multiple Input Multiple Output
MSP	Modified Smith Predictor
PDF	Probability Density Function
PID	Proportional Integral Derivative
RHCP	Right Hand Complex Plane
RQL	Rich Quench Lean Burn
SISO	Single Input Single Output
SPL	Sound Pressure Level
STR	Self-Tunning Regulator
UTRC	United Technologies Research Center

Symbols:

$\mathscr{A}$	Infinitesimal Generator
$\mathscr{B}$	Control Operator
c	Speed of Sound or Generic Coefficient
c_p	Specific Heat at Constant Pressure
c_v	Coefficient of Variation
$\mathbb{C}$	Space of Complex Numbers
$\mathscr{D}$	Differentiation Operator
e	Internal Energy
E	Acoustic Energy
F	Function
$\mathscr{F}$	Non-Unitary Fourier Transform
h_R	Heat of Reaction
I	Acoustic Intensity
J	Jacobian or Cost Function
k	Control Gain
k_n	Axial Wave Number
l	Langrage Basis Polynomial
L	Combustor Length
L_f	Flame Length
$\mathbb{L}$	Lebesgue Space
M	Mach Number
$\mathbb{M}$	M Space

$\vec{n}$	Normal Vector
n_C	Heat Release Gain
n_H	Heat of Reaction Sensitivity
n_S	Laminar Flame Speed Sensitivity
p	Pressure
$\mathscr{P}$	Solution to the ARE
q'''	Volumetric Heat Release Rate
$\mathscr{Q}$	Acoustic Energy Operator
R	Amplitude
$\mathbb{R}$	Space of Real Numbers
$\mathscr{R}$	Control Weight
s	Entropy or Complex Argument
S_L	Laminar Flame Speed
St	Strouhal Number
$\mathscr{S}$	Shift Operator
t	Time
T	Temperature
u	Control Input
v	Velocity
V	Volume
$\mathscr{V}$	Eigenvector
x	Spatial Coordinate
x_f	Position of Mean Heat Release
y	Output
Z	Acoustic Impedance

Greek Letters:

β	Flame Geometry Factor
χ	Velocity Temporal Mode Shape
δ	Dirac Delta Function
Δ	Characteristic Equation
ε	Small Parameter
η	Pressure Temporal Mode Shape
γ	Ratio of Specific Heats
κ	Dummy Variable
λ	Eigenvalue
O	Order of …
ω	Frequency
φ	Equivalence Ratio
Φ	Spectral Density
ψ	Spatial Mode Shape
ρ	Density
σ	Standard Deviation
τ	Time Delay
θ	Total Phase
ϑ	Density Temporal Mode Shape
υ	Fourier Frequency
$\mathcal{W}$	Noise Operator
ξ	Stochastic Process
ζ	Damping Coefficient

Subscripts:

$(\bullet)_0$	0^{th} Order Perturbation
$(\bullet)_1$	1^{st} Order Perturbation
$(\bullet)_A$	Advection
$(\bullet)_c$	Cutoff
$(\bullet)_{comb}$	Combustor
$(\bullet)_D$	Denominator
$(\bullet)_f$	Flame
$(\bullet)_L$	Lower Bound
$(\bullet)_{max}$	Maximum
$(\bullet)_N$	Numerator
$(\bullet)_{net}$	Net
$(\bullet)_{noz}$	Nozzle
$(\bullet)_{stoc}$	Stochastic
$(\bullet)_U$	Upper Bound
$(\bullet)_V$	Velocity

SUMMARY

This thesis considers what limits control effectiveness in self-excited, noise driven, combustors using a full Strouhal number thermo-acoustic model with the ultimate aim of learning how to design combustors to be responsive to feedback control of combustion instabilities. The inclusion of time delays in the volumetric heat release perturbation models create unique behavioral characteristics which are not properly reproduced within current low Strouhal number thermo-acoustic models used for feedback control. New analysis tools using probability density functions are introduced in this thesis which enable exact expressions for the statistics of a time delayed system. Additionally, preexisting tools from applied mathematics and control theory for spectral analysis of time delay systems are introduced to the combustion community. These new analysis tools can be used to extend sensitivity function analysis used in control theory to explain limits to control effectiveness in self-excited combustors. The control effectiveness of self-excited combustors with actuator constraints are found to be most sensitive to the location of non-minimum phase zeros. Modeling the non-minimum phase zeros correctly require accurate volumetric heat release perturbation models. Designs that removes non-minimum phase zeros are more likely to have poles in the right hand complex plane. As a result, unstable combustors are inherently more responsive to feedback control.

CHAPTER 1

INTRODUCTION

Design of gas turbine combustors for propulsion and power generation is facing challenges posed by increasingly stringent environmental regulations of pollutants. Emission standards for mono-nitrogen oxides such as NO and NO_2 are currently the most difficult for the combustion engineer to meet and is often an impetus for new combustor designs. NO_x emission requirements are met by burning lean, with excess air, to keep the temperature low since their formation rates are strongly temperature sensitive. Unfortunately, this combustion regime is prone to self-excited, combustion driven, pressure and velocity oscillations called combustion instabilities, which are very damaging to combustor components.

Mitigation of combustion instabilities requires the disruption of multiple mechanisms responsible for the accumulation of acoustic energy inside a combustor. This design goal must be carefully balanced with the ability to maintain a wide operation envelope. Combustors need to stabilize acoustic energy growth rates so that existing combustion instabilities will have tolerable pressure amplitudes by having sufficient acoustic damping. One way to get around the lack of acoustic damping in low NO_x combustors is to artificially create it by using feedback control to modify the combustor flame response. Successful demonstrations of this technique date back to the 1980's; however, the results of feedback control are highly variable. A large number of demonstrations show control systems that do not always fully attenuate combustion instability amplitudes and introduce unwanted secondary combustor dynamics. Widespread industrial adoption of combustion instability control systems will not occur until the reasons for control failures are understood and are predictable.

This thesis concerns itself with understanding the causes of failure in current combustion instability control systems to enable improved combustor and control system design in the future. The existence of these control system failures implies that important combustion physics may be unmodeled in current thermo-acoustic models. Once these thermo-acoustic models are corrected, attention can be turned to how the mathematical structure inherent in thermo-acoustic models leads to fundamental limits to control system effectiveness. These limits can be quantified with the development of performance predictions tools. Accomplishing all of these goals hinges upon identifying the missing combustion physics. This introductory chapter is meant to explain why combustion instabilities are so detrimental to combustor performance and the history of attempts to mitigate their impact. The historical review will also elucidate the combustion instability community's inability to explain and predict the behavior of combustion control systems which will provide clues for how to improve current thermo-acoustic models.

1.1 Combustion Instabilities

Large amplitude pressure and velocity oscillations in combustors present a number of potential risks to safe gas turbine operation which can lead to mechanical failure. Vibratory stresses in the combustor liner and other components can cause fatigue failure due to fretting and crack propagation. Examples of combustion liner fracture in gas turbine power plants are shown by Sewell and Sobieski[1] as well as Goy et al.[2] Fracture and fatigue failure can also be accelerated indirectly through the enhancement of heat transfer by acoustic streaming.[3] Sound waves at the wall boundaries[4] excite vorticity waves to satisfy the no-slip condition which increases the local Nusselt number. The higher heat flux to the combustor components increases their temperature, and hence, reduces the number of cycles to achieve fatigue failure. Larger heat fluxes are possible through boundary layer separation if the amplitude of oscillation is large enough.

Beyond structural concerns, combustion instabilities also pose problems for combustor aerodynamics. Velocity perturbations can create flame stabilization issues through blowout[5] and flashback.[6] In blowout the flame propagates downstream and out of the combustor which requires the combustor to be relit. This is much more problematic in aircraft engines because relight altitude is lower than cruise altitude.[7] Flashback causes the flame to move upstream into cold-section components not designed for high temperatures. Premature auto ignition can then occur in a combustor premixing section which is a critical safety concern.

Understanding of the mechanism leading to combustion instabilities and its behavior has been heavily driven by military and government aerospace applications, ranging from afterburners and ramjets to solid and liquid fueled rockets. When combustion instabilities were found in a given type of combustor they were followed by intense periods of study until the instability was eliminated or the project canceled. The state of knowledge and understanding about combustion instability behavior developed a patchwork quality to it. Appreciating what knowledge was inherited by the gas turbine community requires a brief history lesson which has ramifications for the limitations in thermo-acoustic modeling which is covered in Chapter 2 of this thesis. A detailed history of combustion instabilities is provided by Culick.[8]

Early experimental work on combustion instabilities was driven by conjectures on combustion physics often leading to a progression of tests for different flow field and geometry changes in the combustor and recording the results. At NACA Lewis,[9] now called NASA Glenn, this process applied to afterburners lead to the discovery that perforated liners can fully attenuate high frequency transverse mode instabilities. Similarly, combustion instabilities for the F-1 engine[10] in the first stage of the Saturn V were finally addressed by testing a large series of baffles and improving fuel injector designs. The legacy of these projects is the identification of the relevant physical processes that needed to be understood in much more detail such as sources of acoustic

damping and heat release perturbations. This work set the stage for future analytical work.

During the same era, transfer function based modeling was used to describe chugging in fuel feed systems[11] due to strong coupling between acoustic oscillations and structural vibrations called a pogo instability. Natural acoustic responses of a combustor was also studied heavily in the late 1960's and early 1970's, particularly by Zinn[12] and Culick[13] relying on Galerkin expansion methods. Linearly unstable combustors were found to have a limit cycle response due to nonlinear gas dynamics. Early work on limit cycle amplitudes was undertaken by Awad and Culick.[14] Future work would add multidimensionality and modal coupling effects to these thermo-acoustic models.[15] Combustion instabilities can also be sustained indirectly in a combustion chamber.

Entropy waves can serve as a source of acoustic noise particularly when interacting with boundaries. Marble and Candel[16] showed that when non-isentropic temperature fluctuations are advected through a compact nozzle, or diffuser, they can be a significant source of sound. Experimental studies on RQL combustors[17] and the BR710 engine[18] has shown that combustion instabilities triggered by entropy waves are generally caused by sound waves affecting the fuel injection system which results in modulations in the equivalence ratio. These equivalence ratio modulations then cause entropy fluctuations in the products of combustion. The study of entropy waves is still an active field of research in which fundamental studies on dispersion[19] and multidimensional effects[20] are ongoing.

How vorticity waves lead to combustion instabilities are not as well understood as entropy waves. Knowledge about them tends to be of an experimental nature. Flow visualization experiments in dump combustors for ramjets[21] support the idea that vortex shedding leads to acoustic energy production by perturbing the strength and location of heat release in a combustor. Similar results exist for investigations of combustion instabilities for the P230 solid rocket boosters used by the Ariane 5[22] and the retired Titan

family[23] of launch vehicles. Vorticity can also perturb the flame indirectly by interacting with boundary to create sound.[24]

Combustion instabilities in industrial applications prior to the 1990's was mostly confined to diffusion flames in boilers and furnaces,[25] yet they were not common enough to lead to sustained research efforts by industry. This changed drastically when NO_x regulations were strengthened in the United States by the Clean Air Act Amendments of 1990. Tightening of international emission regulations followed from recommendations by the International Civil Aviation Organization in 1996 for aircraft engines. Anticipated NO_x regulations are now a major combustor design consideration. Low NO_x combustors strive for low flame temperatures because the NO_x production rate is strongly sensitive to temperature. This is achieved in ground power applications by using lean premixed flames while aircraft engines rely on rapid fuel air mixing to achieve lean burning and to avoid autoignition caused by high operational pressures. Both of these designs suffer from low acoustic damping. Traditionally, dilution air is used to cool combustor liners, which is a major source of acoustic damping. Modern combustors divert most of the dilution air into the main flow to burn at lean equivalence ratios. As a result, combustion instabilities became a pressing concern for industry and lead to a fruitful era of research and collaboration between academia, government, and industry to tackle the combustion instability problem.

A key contribution from this collaboration on combustion instabilities in gas turbine combustors was the understanding that the dominant nonlinearity in the combustor response is due to heat release nonlinearities and not acoustic nonlinearities.[26] This led to the development of physically based volumetric heat release perturbations models. These models are reviewed by Lieuwen[27] for acoustic interactions with premixed flames while Annaswamy[28] reviews a more general class of heat release perturbations. The importance of having proper volumetric heat release perturbation models cannot be understated. They are mathematical descriptions of different

self-excitation mechanisms and hence describe a feedback response in the flame behavior. Combustion instability work done prior to the development of volumetric heat release perturbation models focused on the combustion chamber and its acoustics. From a control theory point of view this represents the response of the system plant. Proper feedback control requires knowledge of both the plant and the feedback mechanism with an appreciation of how they interact.

1.2 The Promise of Control

Feedback control of combustion instabilities work by modifying the balance of acoustic energy, Eq. (1.1), inside a combustor.

$$\frac{\partial E_2}{\partial t} + \nabla \cdot I_2 = \frac{\gamma - 1}{\gamma p_0} p_1 \frac{\partial q_1'''}{\partial t} \tag{1.1}$$

Equation (1.1) shows that the rate of change of acoustic energy, E_2, is equal to the difference of the acoustic energy flux, I_2, with an acoustic energy generation/dissipation term that depends upon perturbations in the pressure field, p_1, and volumetric heat release rate, q_1'''. When these perturbations are cyclical (in phase within 90º) they act as an acoustic energy source, but when they are anti-cyclical they act as a sink of acoustic energy. This criteria was first observed by Lord Rayleigh,[29] but it would not be formally derived until much later by Chu.[30] Most reported attempts at controlling combustion instabilities work by modifying the Rayleigh source term; although a few schemes exist that modify the acoustic energy flux out of the combustor.

The first proposal of using feedback control to handle combustion instabilities was by Tsien[31] in 1952. Tsien's idea was that appropriate modulation of a servo-valve in the fuel feed system could suppress a pogo instability in a monopropellant rocket engine. Several more papers[32] shortly appeared on how to apply feedback control for bipropellant rockets; however, experimental demonstration proved unattainable due to the

technological limitations of that era. Three more decades would pass before the idea of performing feedback control was revisited at Cambridge University.

The first proof of concept experiment was performed on flames in a Rijke tube by using a speaker to change the acoustic boundary conditions. Dines[33] used an empirically tuned phase shifting controller based on CH^* chemiluminescence to achieve a 35 dB reduction in the sound pressure level (SPL) which was repeated by Heckl[34] using a microphone. Concrete steps towards more practical systems came from Langhorne et al.,[35] whom performed feedback control based on a pressure transducer driving a secondary fuel injector to disrupt the Rayleigh source term to achieve a 12 dB reduction in the SPL. Future work, particularly in the 1990's, saw rapid diversification in experimental demonstrations of combustor and control design. A concise review of feedback control of combustion instabilities is given by Huang and Yang[36] as part of a larger article on combustion dynamics.

Suppression of combustion instabilities by feedback control has shown great potential over the last two decades. Multiple control schemes[37] have been used successfully with a wide selection of sensors, actuators, and combustor geometries.[38] Experiments often show significant suppression of combustion instabilities accompanied by an overall lowering of low frequency broadband combustion noise[39] as shown in Figure 1-1. A feedback control system has been successfully commercialized and fielded by Siemens for control of azimuthal instabilities in their V94.3A heavy duty gas turbines.[40] Other successful industrial demonstrations include the afterburner on the Turbo Union RB199 engine[41] and the Siemens-Westinghouse W501F Dry Low NO_x combustor.[42] History has shown that feedback control of combustion instabilities can work at particular operating conditions. If they can perform reliably over a large operability envelope then the stage will be set widespread industrial operation.

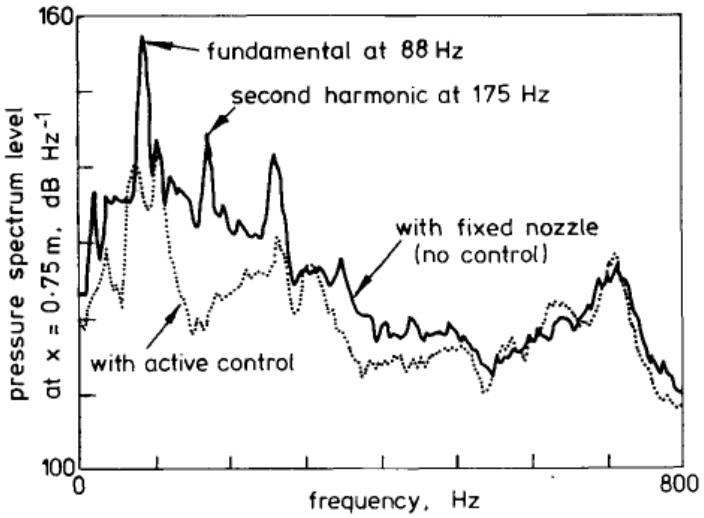

Figure 1-1: SPL of uncontrolled (solid) vs. controlled (dash) combustor pressure demonstrating approximately a 20 dB decrease at low frequencies. Reproduced from Bloxsidge et al.[39]

1.3 Challenges of Control

While significant progress has been made in demonstrating that feedback control of combustion instabilities is feasible, much work remains in understanding the factors influencing how effective control will be for a given combustor. The results of control implementation are highly variable. For example, even with their success, Siemens reported operating conditions where feedback control would excite combustion instabilities at other frequencies. Siemens' experience with feedback control limitations is not atypical; new combustion dynamics induced by feedback control is well documented in compilations in the combustion instability literature.[43] In many applications feedback control fails to fully suppress the original instability. Full-scale adoption of control systems for combustion instabilities requires consistently reproducible results.

Early control systems for combustion instabilities relied upon empirical transfer functions and phenomenological proportional phase shifting controllers based upon Rayleigh's criterion; however, the physical interpretation of Rayleigh's criterion is often

oversimplified leading to suboptimal results. This is best seen if the Rayleigh source term in the acoustic energy equation (1.1) is integrated spatially over a volume V and temporally over a period T to give the Rayleigh index: Eq. (1.2).

$$R.I. = \frac{\gamma - 1}{\gamma p_0} \iiint_V \left[\int_T p_1 \frac{\partial q_1'''}{\partial t} dt \right] dV \tag{1.2}$$

Combustion engineers designing control systems want to minimize the Rayleigh index. As mentioned in the previous section, this is done by keeping volumetric heat release perturbations anti-cyclical to pressure perturbations. In practice, this is implemented on an instantaneous basis without regard to the future. This is problematic because pressure and volumetric heat release perturbations are not independent variables. A controller can be designed to satisfy Rayleigh's criterion in the present while limiting its future ability to satisfy the same criterion because it is changing the pressure perturbation field in an unanticipated way. Furthermore, feedback control is often assumed to be driving the dominant volumetric heat release perturbation mechanism, but the volumetric heat release perturbation term in the Rayleigh index is a summation of all volumetric heat release perturbation mechanisms. If the combustor is self-excited then these other mechanisms can be of comparable magnitude and indirectly influence the control system by the changes they induce in the combustor's acoustics.

Additional problems arise with common system identification practices in the combustion community due to system transfer functions being identified at a preselected operating condition that may not be representative of other required operating conditions. As a result, they have limited validity, particularly due to the presence of unaccounted time delays and system nonlinearities. This creates difficulties in trying to compare the performance levels of different control systems on different combustors because only the best control results are reported at the operating condition the system identification was performed under. Typical results that are likely to be seen in practice are hard to find, and hence, little is known about the robustness of combustion instability control systems.

For gas turbine power plants and aircraft engines, understanding how to properly handle time delays is a fundamental unresolved issue in combustion dynamics.

The presence of time delays in combustion response models dates back to the 1950's when Summerfield[44] first proposed a proportional delay model which was popularized by Crocco and Cheng[45] as the n-τ model. Mathematical tools used to handle time delays in the combustion instability community have not evolved much since then despite major progress[46] in the fields of applied mathematics and control theory. Combustion control systems create an additional time delay in the thermo-acoustic model due to the advection time needed for fuel oscillations to travel between the fuel actuators to the flame front. Many experiments incorrectly treat the time delay as equivalent to a phase shift. Typical justification for this is that a time delay compensator and a phase lag/lead compensator can be designed to give the same response at a single fixed frequency such that this approach should be valid when the power spectrum of the combustor response is predominately narrowband; however, once control is applied and begins suppressing a combustion instability the response spectra can lose its narrowband characteristics leading to limited control effectiveness. Comparing a delay compensator to a phase lag/lead compensator in the frequency domain makes it obvious that they are not the same because the delay compensator has a complex exponential in its transfer function which makes it anharmonic and infinite dimensional.

Increasingly sophisticated tools for handling time delays came from the control community but tended to follow the same strategy of indirectly dealing with the time delay or finding clever tricks to hide it which often involves invoking assumptions that limits their applicability. Model based controllers such as the Linear Quadratic Gaussian[47] (LQG), H-Infinity[48] ($\mathcal{H}_\infty$), and the Self-Tuning Regulator[49] (STR) used Padé approximates to rationalize terms in the transfer function due to time delays; however, this is only valid for small delays and cases exists where the Padé approximates incorrectly predict stability.[50] Another common approach is to hide the entire time delay

term in a bounded uncertainty matrix for the plant transfer function.[51] Black box adaptive controllers based on least mean squares algorithms have also been tried[52] but these controllers cannot guarantee stability nor an ability to positively affect system performance. On the other hand, model based adaptive controllers are able to handle the time delay explicitly, such as a Posi-Cast controller[53] (also known as a Smith Predictor[54]) which can be paired with a STR, but this design requires exact knowledge of the value of the time delay and has difficulty coping with non-minimum plane zeros.[55]

This short history of combustion instability control systems illustrates the difficulty of properly incorporate arbitrary large time delays into system modeling and control system design. Clearly, a need for new analytic tools exists to understand how time delays limit control effectiveness. Furthermore, all of the examples cited so far have a single time delay in the control system. If a combustor is self-excited then it will also have an independent time delay in the plant transfer function. This fact is well recognized but it is often not included in models intended for control system design. A notable exception include STR's based on a thermo-acoustic model by Dowling[26] which includes the effects of reflected acoustic waves from the combustor's inlet and outlet; however, the STR's that use this model use Padé approximates for the acoustic propagation time which is problematic for the reasons previously mentioned. Multiple independent time delays in the system's state and control input have not been explicitly studied in combustion instability control systems.

Time delays are not the sole barriers to increased control system performance. A variety of factors can lead to compromised capabilities to suppress combustion instabilities. These include background noise floor levels, actuator control authority, actuator bandwidth, sensor location, and controlled combustor dynamics. Under the influence of feedback control, the steady state pressure response can exhibit a variety of behaviors associated with limited control effectiveness such as peak splitting[56] and amplitude breathing.[57]

Peak splitting, known as the water bed effect in the control community,[58] is a growth in oscillation amplitude at closely spaced frequencies above and below the nominal instability frequency. An example of peak splitting due to feedback control is illustrated in Figure 1-2, which contrasts the SPL of an adaptive controller from Kopasakis and Delaat[56] with the uncontrolled case. Generally, increased control authority attenuates the oscillation amplitude at the nominal instability frequency but sideband frequencies intensify and move away from each other in the frequency domain. This peak splitting behavior has been observed across a wide selection of control designs such as a phase shifter from Cohen et al.,[59] a LQG from Murugappan et al.,[47] fuzzy logic control from Coker et al.,[60] and an adaptive sliding phase controller from Kopasakis et al.[61] The overall effect of peak splitting is to limit the maximum degree to which the oscillation amplitude can be suppressed.

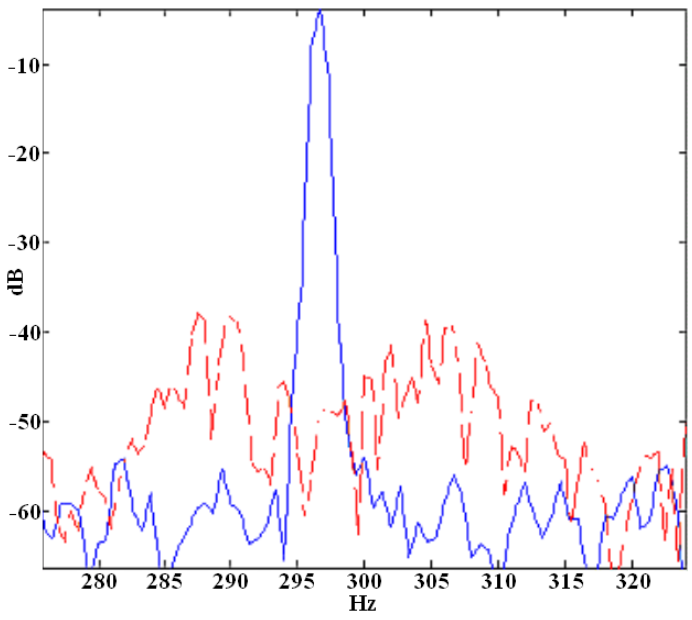

Figure 1-2: Demonstration of peak splitting in the SPL of uncontrolled (solid) vs. controlled (dash) combustor pressure. Reproduced from Kopasakis & Delaat.[56]

Investigations into the causes of peak splitting have focused on the discrepancy between modeled control systems and their realizations. Fleifil et al.[62] looked at the

phase of the closed loop transfer function between the combustor, controller, and filter dynamics using acoustic feedback. This analysis built upon earlier work on linear acoustic modal coupling.[63] They noted that ignoring phase effects across a frequency range around the instability frequency by only concentrating on oscillations at the nominally unstable frequency can lead to peak splitting. An example is feeding the band-pass filtered output of the flame transfer function into the controller, leading to excitation of a lower frequency instability compared to the nominally unstable frequency. In the frequency region between the stop-band and the pass-band of the band-pass filter is a region of rapid phase variation that can constructively add if paired incorrectly with the phase roll-off region of the flame transfer function.[64] Simultaneously, higher frequency combustion instability can be excited from the effect of anti-resonance interacting with a phase shifting controller. The system transfer function has zeros in it due to linear modal coupling, which creates a dip in the pressure response. In frequencies adjacent to the system zero is a region of rapid phase roll-off exist which can be excited if paired incorrectly with a phase shifting controller. The combination of the suppression of the nominally unstable frequency and the excitation of two adjacent frequencies results in observing peak splitting.

Further studies of peak splitting came from Banaszuk et al.,[65] using sensitivity function analysis[58] to investigate combustors forced by background noise with time delayed control and self-excitation. Both time delays from the controller and the self-excitation mechanism were assumed to be the same time. The sensitivity function used to analyze the effect of control is defined as the transfer function between output disturbances and the system output. Amplification or attenuation of a given frequency is dictated by the magnitude of the sensitivity function. Finite bandwidth control actuators (such as on-off valves) are limited over the range of frequencies that they can manipulate in the sensitivity function. As the magnitude of the sensitivity function is attenuated at the instability frequency, it must be accompanied by a magnification of adjacent

frequencies, because the Bode integral[66] requires the area of the logarithm of the sensitivity function to be constant. This amplification of adjacent frequencies manifests itself as peak splitting. The presence of time delays is not needed for peak splitting, but their presence aggravates the problem. Simulations correctly reproduced peak splitting frequencies and amplitude trends seen in experimental results.

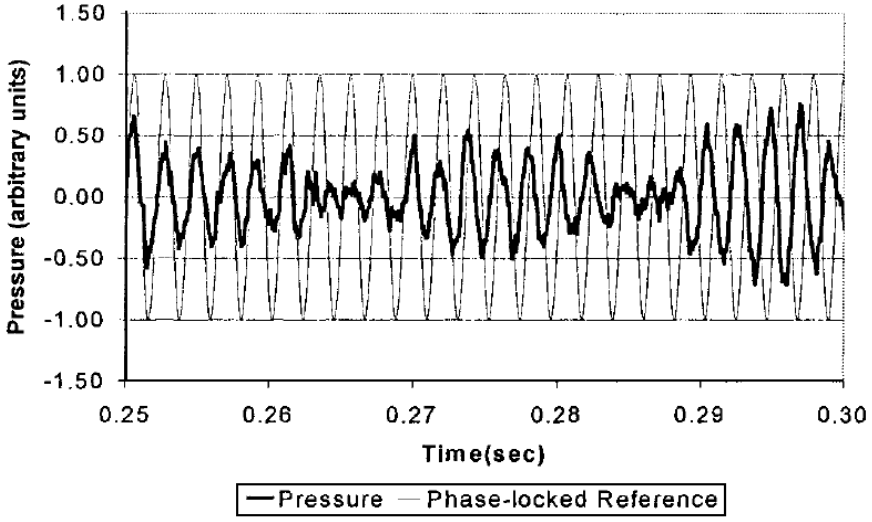

Figure 1-3: Comparison of the time variation of pressure in a controlled combustor and a phased locked reference showing amplitude breathing. Reproduced from Johnson et al.[57]

Significant breathing in instability amplitude is another typical observation in controlled combustors.[67] In this case, the average instability amplitude of the controlled combustor might be reduced significantly, but is associated with significant variations in instability amplitude on a cycle to cycle basis. This is a serious issue given that one of these significant amplitude bursts could result in blowoff of the flame, among other problems. Typical data illustrating this breathing phenomenon was reported by Johnson et al.[57] and is reproduced in Figure 1-3. Also shown on this plot is a sinusoidal signal with fixed phase. Comparison of the phases of the pressure with a fixed phase signal reveal the existence of time intervals of rapid phase drift in the combustor at low instability amplitude values. This can be seen at t = 0.265 and 0.285 seconds, where the

phase of the pressure signal abruptly changes by almost 180 degrees relative to the phase locked reference signal. The instability then grows in amplitude until the observer can converge to the correct phase. Phase drift coupled with observer dynamics at low signal to noise ratios of the coherent signal could be leading to this phenomenon. In a related study, Lieuwen[68] found similar stochastic behavior in the phase of the uncontrolled combustor dynamics, where the phase drift per cycle is found to resemble a random walk. Typically, stochastic behavior is attributed to combustion noise which is known to affect combustor performance and stability[69] but it has not been well studied.

1.4 Feedback Control Outside of Combustion

Mathematically, most of the emphasis in this thesis is placed on how to handle time delays. Combustion instabilities do not have a monopoly on having time delays in their models. A lot can be learned about time delays by looking outside the combustion community to more established fields of study. Some of the earliest encounters with time delays come from economics dealing with price fluctuations,[70] phenomena associated with solid state lasers,[71] modeling visco-elasticity[72] in solid mechanics, modeling nuclear reactor kinetics,[73] and machine tool vibration.[74] Collectively, these models date back to the first half of the 20th century. Attempts to develop control systems for these models would quickly follow.

Early control system designs focused on time delays in the system input/output because they were much more common than delays in the state variables. Linear systems with input delays allow for easy factoring of the contribution of delays from the plant transfer function which facilitates reusing pre-existing tools from finite dimensional systems. PID (proportional integral derivative) controllers were commonly designed for time delay systems using tuning rules for non-delayed systems such as the widely used Ziegler-Nichols method.[75] Other popular design techniques that actually acknowledge the existence of the time delay try to hide it by manipulating the delay in such a way so

that the resulting system looks like a delay free system. Examples of this include controllers using Padé approximates, the Smith predictor,[76] and finite spectrum assignment.[77] Padé approximates turn the time delay terms in the frequency domain into a rational function of frequency such that the governing equations looks like a high order ordinary differential equation. The Smith predictor forecasts what the future sensor output will be so that the control loop looks delay free when using the predicted output. Smith predictors cannot handle unstable systems but Watanabe and Ito[78] came up with a modified Smith predictor (MSP) to handle this case. Finite spectrum assignment designs the controller to cancel the delay term, an approach general enough to also incorporate state delays too. A comparison of all of these classical approaches is discussed in more detail in the monograph by Zhong.[79]

All of the just discussed design methods are not optimized in the modern control sense with respect to some type of norm and also have poor robustness characteristics because they rely heavily on knowing the delays exactly. Despite this, these controllers have found a home within the control community because they do work for a class of transfer functions and they are relatively simple to design and implement. Furthermore, most of these controllers are the same controllers that have been predominately used for the feedback control of combustion instabilities, if the control designs that neglect time delays are temporally disregarded. These controllers were state of the art in the late 1970's but decades worth of new knowledge exists in control theory along with a half century worth of applied analysis that have not been absorbed by the combustion instability community. The only real exception to this comes from adaptive control theory, which lead to the use of STR's,[49] fuzzy logic,[60] and other adaptive schemes based on Rayleigh's criterion. This means potential exists for improving the performance of control systems and understanding their behavior on the feedback control of combustion instabilities through more advanced control system design.

While control theory was developing the first generation of controllers for time delay systems the theoretical and applied mathematics community was laying the foundation that would lead to a large diversification of available analysis tools to enable the next generation of controllers for time delay systems. Several influential monographs appeared by the late 1970's on time delays from Bellman and Cooke[80] covering the spectral theory, Hale[81] covering the time domain behavior, and Curtain and Pritchard[82] covering the operator-theoretic approach. Future controllers would lean on all three of these monographs. Historically, the infinite dimensional LQR problem was the first to see development followed by the $\mathcal{H}_\infty$ problem. Eventually the idea of pole placement without hiding the time delay would also be revisited.

The development of the LQR problem followed several prolonged but distinct stages: how to formulate the problem, what equation needs to be solved, how to solve that equation, and how to implement the resulting controller. By the mid 1990's the first two of these stages were largely complete. These are well covered by the monographs from Bensoussan et al.[83] and Curtain and Zwart.[84] Recent work on how to solve the resulting equations in the most computationally efficient way have hinged upon how to discretize the time delay. A particular version of this technique based on a pseudospectral method[85] that will end up being very useful in this thesis is covered in Appendix A. The final step on how to implement the resulting infinite dimensional controller is still an open problem and active area of research.

Many of the developments in robust control for infinite dimensional systems followed in parallel to those for finite dimensional systems in the 1980's. This means that the ability to design a finite dimensional controller for bounded additive and multiplicative uncertainty[86] has existed for awhile. Much of the modern literature for robust control of time delay systems is focused on incremental improvements in reducing the conservativeness of robust controllers or ways to implement infinite dimensional controllers. A recent summary is given in the monograph by Zhong.[79] The most

common approach is through an extension of Lyapunov theory.[87] A good introduction to this topic is found in the survey by Niculescu et al.[88] Most of the work in this area came out of the former Soviet Union and is not available in English; however, Kolmanovskiĭ and Myshkis[89] contains an excellent summary of these works which covers application to optimal control and estimation.

More advanced yet simpler controllers are still needed since optimal and robust controllers can be difficult to design and implement. The idea of pole placement is very powerful and attractive but the existence of an infinite number of eigenvalues makes this idea complicated. Older techniques like finite spectrum assignment only had a finite number of eigenvalues to relocate because they hide the time delay. Continuous pole placement[90] is a technique that considers all the eigenvalues and controls the placement of the right most eigenvalue in the complex plane, called the spectral abscissa. Extensions of these idea lead to the development of the stability radii[91] as a measure of robustness to bounded additive uncertainty.

What is nice about these pole placement techniques is that stronger relationships exist between the physics of the system and the location of the eigenvalues than an arbitrary system norm. This allows for training physical intuition on how feedback control of combustion instabilities affects the combustor behavior which can then be reapplied to more mathematically complex optimal and robust controllers. The importance of this cannot be understated. In the combustion instability community the engineer designing and implementing the control system is unlikely to be a control engineer by discipline nor strongly versed in the appropriate mathematics that field requires. As a result, the design rules for good control design which tend to be very mathematical in nature need to be translated to physic based design rules.

1.5 Fundamental Limitations of Feedback Control

Studies of factors that limit control effectiveness have focused on explaining the origins of unwanted combustion dynamics during the presence of control; this does not actually address what the peak performance level of a feedback control system can be, only what happens as that level is approached. Furthermore, all of these studies, except for Banaszuk et al.,[65] are actually surmountable barriers to control performance due to control design based upon incomplete thermo-acoustic modeling. Additionally, if a controller is not optimal with respect to a quantifiable metric then making claims about performance limits are not meaningful. A detailed study aimed at understanding the actual limits to control effectiveness is the sole objective of this thesis. The direct engineering application of these results will allow combustors to be designed with improved controllability and stabilizability properties which enable the use of new combustor designs with a wider operability envelope.

Experimental evidence seem to indicate that time delays and combustion noise have a leading role to play in limiting control effectiveness; however, these effects are not typically included in thermo-acoustic models used for feedback control of combustion instabilities. This thesis focuses on self-excited, noise driven, combustors that are likely to be seen in current and future aircraft engines and ground power applications. As a result, the thermo-acoustic model needed will require multiple independent time delays of arbitrary size in the system state and control input while including a stochastic driving function. All of the mathematical preliminaries for stochastic and infinite dimensional systems in Hilbert spaces will be introduced as needed to analyze time delays and noise simultaneously. A thermo-acoustic model must also carefully balance between mathematical solvability and physical realizability. Understanding of what is currently analyzable in time delay systems will aid the process of making simplifying assumptions in thermo-acoustic modeling in Chapter 2.

Investigating the factors that limits control effectiveness requires the ability to benchmark the performance of a combustor before and after the application of feedback control. To date, a successful prediction of control system performance applied to a combustor has not been made. Chapter 3 of this thesis describes a probabilistic approach to deliver the system response as a probability density function (pdf) and the means to solve for its statistics. The pdf approach is physical satisfying but it is not the most natural framework for a control engineer. Furthermore, the pdf approach is computationally not well suited for designs studies. An alternative operator-theoretic approach is introduced in the same chapter which describes the system response in terms of spectra. Linking these two very different frameworks will allow a cross pollination of ideas from combustion and control theory which can be used to describe behavioral trends of combustion instabilities under the influence of feedback control. The factors that limit control effectiveness can be investigated once the new analysis tools developed in Chapter 3 show that the improved thermo-acoustic model in Chapter 2 can reproduce some of the combustion dynamics discussed in this introductory chapter that is currently irreproducible.

Equipped with proper mathematical tools, Chapter 4 looks at how to design a control system for an infinite dimensional system by using the full extended state space. Both the mathematical and physical limitations of control performance are investigated with emphasis placed upon the concepts of β-exponential stabilizability and sensitivity integral constraints. Solving the LQR problem for the thermo-acoustic model in this thesis yields a linear functional control law. In practice this control law has some implementation issues and deficiencies about how it is constrained. Understanding these limitations reveals the role that RHCP poles and zeros play in limiting control effectiveness. The implications that this has for combustor design and future research is discussed and then expand upon in Chapter 5.

CHAPTER 2

THERMO-ACOUSTIC MODELING

In Chapter 1 the history of combustion instabilities and their control was reviewed to demonstrate that there are a number of observed behaviors in combustion instability control experiments that are not reproducible in current thermo-acoustic models. Combustion instabilities were also shown to have multiple causes that can behave very differently based upon subtle changes in combustor geometry and operating conditions. What is important about these observations is that a thermo-acoustic modeler cannot derive a universal thermo-acoustic model. As a result, much more emphasis needs to be placed on the process of modeling to maximize the physical consistency of any derived thermo-acoustic model. This chapter presents such a modeling process applied to self-excited, noise driven, combustors. At first, the required physic models are discussed individually to gather together all the assumptions that a thermo-acoustic model has to inherit. Afterwards, the interactions between physical models are considered to allow the derivation of an appropriate wave equation describing combustion instabilities in combustors. Spatial averaging is then used to break the wave equation into a coupled set of oscillator equations. Once this is completed, a proper definition of state is provided to give a mathematical framework to interpret the governing equations. This will set the stage for later chapters in this thesis for the development of analysis tools to interpret thermo-acoustic behavior which can then be used to explore the factors that limit control effectiveness.

2.1 Modeling Process

The process of thermo-acoustic modeling has inherited much from the process of aeroacoustic modeling to the point that combustion instability models are often treated as

a duct acoustics problem with a volumetric heat release source term. While this is technically true, the danger behind this mentality is that the volumetric heat release source term is treated as a plug in model for the same recycled wave equation. Since volumetric heat release modeling is still in its infancy, these models have a large number of assumptions and uncertainties associated with them which may violate assumptions in the wave equation being recycled. This creates subtle physical consistency problems that often go unnoticed, especially for thermo-acoustic models designed for combustion instability control systems because they integrate several distinct engineering fields that do not have a historical record of working together. Having a good modeling process can go a long way in minimizing, but not eliminating, physical consistency errors in thermo-acoustic models. Furthermore, finding physical inconsistencies requires the modeler to backtrack and iterate on a previous step in the modeling process. A good process can minimize the amount of engineering hours that go into model creation. The process used for thermo-acoustic modeling in this thesis is illustrated in Figure 2-1 below.

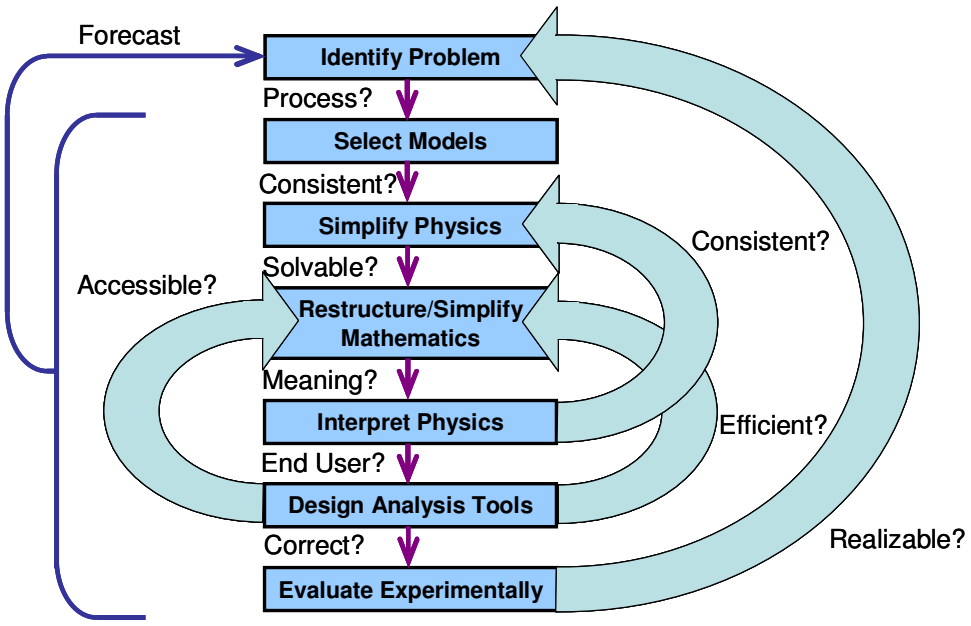

Figure 2-1: Illustration of the modeling process used in this thesis.

Explaining why identifying the physical problem to be solved is a first step in modeling is self-evident; however, selecting a framework by how this should be done is much more subtle and has ramifications for future steps in the modeling process. This requires some mathematical foresight. Different engineering fields have grown up in different mathematical environments. As a result, when working on a closed loop model the different physical models it uses will have to be brought into a compatible mathematical framework. The selection of an ideal mathematical framework requires some foresight into the different possible forms the final closed loop model can take and which ones are analytically tractable. Furthermore, the mathematical framework will dictate which physical processes are either explicitly or implicitly expressed. This has ramifications in the next step in the modeling process which involves selecting the appropriate individual models for each physical processes of interest.

Each independent physical model required for the final closed loop model will have a set of associated assumptions that go with it. For the closed loop model to be physical realizable, and hence, experimentally validatable, all of the individual physical models must have the same set of assumptions. A sufficient condition that guarantees physical realizability is applying the smallest superset of assumptions to all physical models which inherently restrict the range of validity of the closed loop model. Physical consistency requires this, but this can only be satisfied if all of the used models are derived from first principles. When physical models are either phenomenological or empirical in nature then physical consistency cannot be guaranteed. In this case the modeler needs to make appropriate engineering judgments, usually based on experimental evidence, to minimize the severity of unintentional physical inconsistencies.

Once a model is as physically consistent as possible, attention can be turned to making the model mathematically useful. This can vary from making the model susceptible to a particular analysis technique to making the model amendable to physical insight. The process of making mathematical simplifications can lead to new sources of

physical inconsistencies. For every mathematical simplification an equivalent physical assumption or constraint exists that gives the same results. That physical assumption or constraint must be compatible with all of the previously used assumptions. Furthermore, that new assumption or constraint must be applied to every individual model used for a physical process to maintain the physical consistency of the closed loop model. This necessitates an iterative process where mathematical simplifications requires the deconstruction of a closed loop model to modify the individual models for the required physical processes and then rebuilding the close loop model to check if the new mathematical form is acceptable.

Ultimately, what makes a model useful is how it can be used to develop new analysis tools that help in the design process. For a model to successfully proliferate into active use it should describe new and relevant physical processes that is of concern to the end user that previous models could not reproduce while not requiring a steep mathematical learning curve to use it. Clearly, deciding if a mathematical form is acceptable has a strong dependence on what type of engineer the end user will be because different engineering fields have their own set of mathematical predispositions. A thermo-acoustic model for feedback control requires juggling the competing preferences of the combustion, acoustic, and control engineer. This creates an accessibility problem.

Addressing accessibility must compete with the need to address the efficiency of the model. The introduction of new mathematics may be merited if it can collapse several calculations into one streamlined process, has numerical benefits, or if the limits of a previous mathematical framework has been reached. What is interesting about the idea of efficiency is that it reveals that two aspects exist to the accessibility problem: is the model accessible to the development of new design tools and is the result from those design tools accessible? Not every engineer will need to use a design tool for a given model but every engineer should be able to understand the results from that design tool. This means that the modeler can think of the accessibility problem as a mathematical

translation problem in the results and focus on efficiency when it comes to the design of new analysis tools.

As shown by the modeling process illustrated by Figure 2-1, this design process requires a restructuring and simplification of the mathematical structure of the model to put it into a convenient form for manipulations, but this reintroduces the physical consistency problem from earlier modeling steps. Poor modeling choices will lead to a large number of time consuming iterations as assumptions are made and then retracted. Using mathematical foresight in previous steps can alleviate the number of iterations required by eliminating known dead ends. Linear infinite dimensional system theory builds the foundation for how to handle time delay systems. Most of the mathematical preliminaries will be covered in Chapter 3 while developing analysis tools; however, a certain subset will be cursorily introduced in this chapter as needed so that this idea of mathematical foresight will seem less nebulous and more rigorous when applied.

Taking the time to consider all of the procedural issues associated with modeling, which are designed to meticulously ensure physical consistency, allows a validating experiment to be physically realizable. This means that the results of an experiment and model predictions are comparing the same thing. Assuming that the experiment is performed correctly, discrepancies in the results tell the modeler that the physics was oversimplified and the model needs to be revisited to relax some modeling assumptions. Unfortunately, progress in experimental and theoretical work has often advanced independently of each other which prevent proper validation studies. The first step to addressing this shortcoming is developing a thermo-acoustic model that can reproduce unexplained behavior from previous feedback control experiments on combustion instabilities so that proper thermo-acoustic model validation experiments can be designed.

2.2 Formulation

According to the modeling process illustrated by Figure 2-1 the first step to developing a thermo-acoustic model is to understand what physical processes need to be modeled and how they interact with each other. Understanding how the processes interact is vital to maintaining physical consistency in a closed loop model. Some processes are more likely to inherit assumptions from other processes or bequest assumptions upon other processes. This creates a preferential order in what physical process to begin mathematically modeling. Generally, as physical processes become more complex they need more assumptions to be mathematically manageable and conducive to physical insight.

A self-excited noise driven combustor with feedback control naturally presents itself as a more complex case of a stable combustor. Building a diagram to show how the physical processes interact such as Figure 2-2 can start with this simpler problem. From a control theory perspective every model should start with a plant transfer matrix that maps some type of input into an output. In the duct acoustics limit the plant transfer matrix should describe the combustor acoustic response in the absence of unsteady combustion. This separates the response of the combustor physics from the response of the combustion physics; a very important distinction.

Combustion instabilities manifest themselves as pressure and velocity oscillations which imply that pressure and velocity would make good output functions for the plant transfer matrix. An input function would be anything that provokes the combustor into making sound such as combustion noise or a volumetric heat release perturbation. When volumetric heat release perturbations are self-sustaining then the combustor is self-excited. This implies that this process should appear as a feedback loop in a diagram illustrating how the physical processes interact with each other. The combustor output drives the volumetric heat release perturbations which in turn drives the combustor response. A control system will behave similarly since it provides a user imposed

volumetric heat release perturbation, but the feedback loop will require additional transfer matrices because volumetric heat release perturbations are controlled indirectly. These perturbations will come from an actuator which needs to receive command signals derived from a control law acting on information about the system behavior. This can range from the filtered response of a sensor to elaborate information provided by a state estimator. When all of these processes are weaved together the feedback diagram of Figure 2-2 results. In this diagram the combustor responds to combustion noise and two feedback loops. The positive interior feedback loop shows the effect of the self-excitation and is generally destabilizing while the negative control feedback loop fights to stabilize the system response.

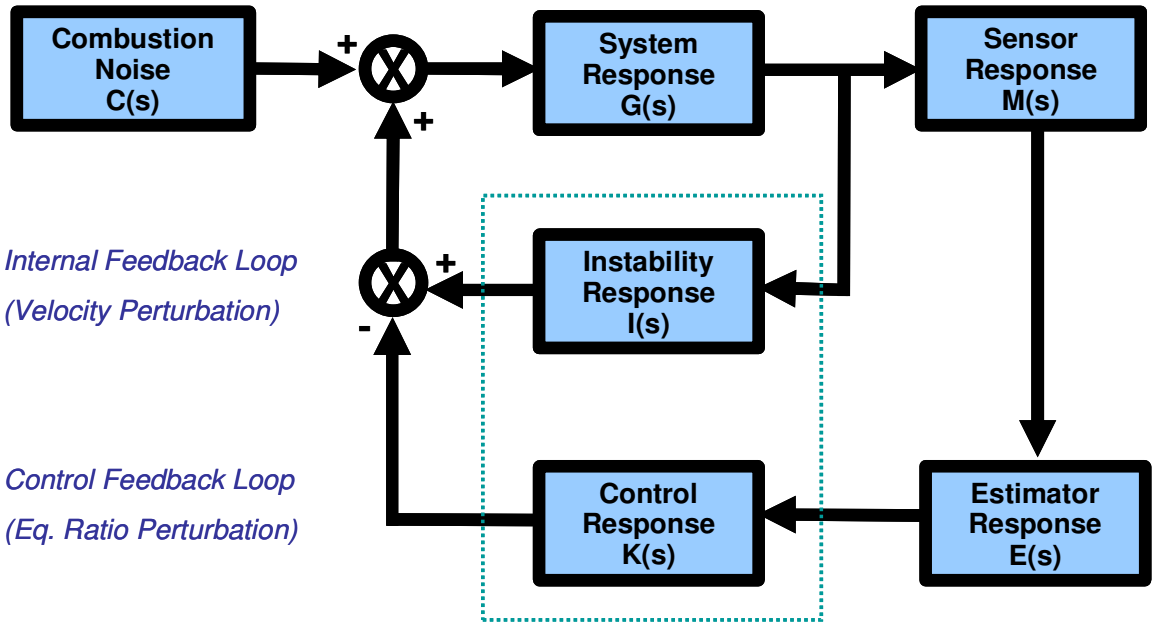

Figure 2-2: Feedback diagram of a self-exited noise driven combustor with feedback control.

With the aid of the feedback diagram from Figure 2-2 the order of which physical process to model mathematically can be determined. Processes that are indifferent to modeling order should be done when and if needed to make the thermo-acoustic model as general as possible. Examples of this include the control actuator and sensor. A process

can also be indifferent to modeling order if it is poorly understood, such as combustion noise. The lack of physical processes feeding into it should not be taken to mean that they do not exist. Consequently, the assumptions conferred by combustion noise upon other physical processes are unknown which is why the order in which a combustion noise model is implemented does not matter.

Of the processes that have to be modeled and are understood the ones that mostly inherit assumptions should be done last. The combustor response has the most processes feeding into it which means that the combustion modeling needs to be done prior to the acoustic modeling. Both volumetric heat release perturbation models, marked by the dashed box in the feedback diagram from Figure 2-2, feed into the combustor response and to each other indirectly. This means that they need to be developed simultaneously. Once the combustion modeling is completed the combustor acoustics can be modeled followed by everything else. With the modeling order determined the question of how to put the physicals models in a mathematical framework can now be addressed.

2.3 Methodology

The feedback diagram from Figure 2-2 shows all of the physical processes needed to describe the thermo-acoustic behavior of self-excited, noise driven, combustors with feedback control. Constructing a closed loop model to understand combustion instability behavior requires the selection of a mathematical framework which defines how the governing physics express themselves and constrain what is analytically tractable. All of this relates back to the problem of ensuring mathematical and physical consistency mentioned in §2.1, which can be alleviated by applying the idea of mathematical foresight illustrated by the modeling process in Figure 2-1. Two overarching steps exist that require the selection of different mathematical tools: the derivation of a set of governing equations that describe how the individual acoustic modes interact with each

other, and how to analyze those equations to learn about the factors that limit control effectiveness.

In aeroacoustics several different ways exists to express an equation governing the propagation of sound in the presence of combustion.[92] Historically, the combustion instability community has preferred to use the acoustic wave equation derived through a perturbation method because it allows for drawing parallels from preexisting results in classical acoustics. The wave equation describes the behavior of perturbations in the flow field of the combustor but does not describe their contributions to individual acoustic modes. A modal decomposition can be done either in the frequency or time domain.

One way of isolating the individual acoustic modes is to assume a form of the temporal response in the complex domain and solve for its frequency. Tutorials of this technique is given by Dowling and Stow.[93] The idea is that the wave equation can be integrated across the flame to derive a jump condition. Substituting the assumed form of the solution into the jump condition results in a nonlinear transcendental equation, an exponential polynomial,[94] describing the resonant combustion instability frequency.[95] This equation must be solved numerically with a root finder which creates a set of analytical problems. Root finding in exponential polynomials can be extremely sensitive to rounding errors.[96] Additionally, an initial guess is required which is usually based on the classical acoustic resonance frequency. Exponential polynomials have an infinite number of roots. This means that the characteristic response will excite an infinite number of frequencies, but this analysis will only recover a single frequency for an acoustic mode which may not be the correct dominant frequency response due to frequency correction effects from mean flow, boundary conditions, and volumetric heat release perturbations. As a result this method cannot capture the entire temporal response of a given spatial mode.

An alternative method of working with the wave equation is using the Galerkin expansion methods which has been heavily advocated by Culick[8] in the combustion instability community. The strength of this method is that it is based on Hilbert space theory which gives it a cleaner interpretation and the ability to handle a wide breadth of mathematical problems; however, the price paid for this clarity is increased mathematical bookkeeping in the modeling process. In this approach the perturbations are projected onto an infinite dimensional set of orthonormal spatial basis functions which will have to be truncated to allow for numerical analysis. Orthonormality ensures that projections are monotonically increasing in accuracy as the dimension of the projector is increased. Unfortunately, an orthonormal basis can be a bit of a hindrance when working with nonnormal systems because their eigenfunctions are not orthogonal. This creates modal coupling in the dynamics of the projected system. In combustors modal coupling comes from mean flow effects, boundary conditions, and volumetric heat release perturbations. When truncation is used in these thermo-acoustic models the modal coupling that allows acoustic energy to transfer to more dissipative higher order modes are ignored. As a result, truncated models under predict stability. One common approach to alleviate these errors, particularly in the turbulence community,[97] is to add artificial dissipation. A different approach has been adopted by the combustion instability community that relies upon keeping enough spatial mode shapes beyond those of interest to accurately reproduce their temporal behavior. Annaswammy et. al.[63] showed that common thermo-acoustic models used for feedback control may need approximately two or three more mode shapes than the modes being controlled to accurately reproduce phase information in the combustor response. This makes drawing physical insight from the reduced order model harder and creates an increased numerical burden.

The clarity of the Galerkin expansion, despite its other shortcomings, is desirable since a major objective of this thesis is to enable better collaboration between theory and experimentation. Furthermore, its time domain formulation allows a larger breadth of

control theory to be applied to understand the effects of time delays and system noise on combustion instability behavior. Several different ways exist to structure the mathematical representation of time delay systems. The two representations being used for this thesis will be properly introduced later in this thesis: functional differential equations and abstract operator equations. Both of these representations are natural extensions of linear system theory for finite dimensional systems and hence reduce the accessibility barrier discussed in §2.1 and illustrated by the modeling process in Figure 2-1. A third representation views time delay systems as differential equations over rings of operators. This approach requires a strong knowledge of algebra that is typically outside the education of combustion and acoustic engineers which creates an accessibility problem. Additional details on the different mathematical frameworks available for modeling time delay systems are given in the monograph by Niculescu.[98]

2.4 Combustion Modeling

The feedback diagrams from Figure 2-2 in the previous section details all the physical processes which needs individual models. Following the modeling process outlined in Figure 2-1, the next step is the collection of individual models and ensuring that they all use the same set of physically consistent assumptions. Combustion modeling is a logical starting point because it is the most poorly understood physical process that need to be modeled and hence it will have the largest number of assumptions associated with it. Up to this point, the modeling of the feedback diagram from Figure 2-2 has been fairly generic in the sense that the combustor design has not been specified. Understanding the differences between commonly used combustor designs will elucidate the gap between the combustion models that the combustion instabilities community needs versus the models that are actually available. Pertinent details needed to describe the flame behavior include how the flame is stabilized and the degree of premixing between the reactants. Three combustor types of interest exist for this thesis due to their

susceptibility to combustion instabilities: lean, premixed (LPM); lean, premixed prevaporized (LPP); and lean direct injection (LDI). Each of these combustors have flames at lean equivalence ratios which means that the ratio of the actual fuel to air ratio over the fuel to air ratio required for complete combustion is less than one.

LPM and LPP combustors share many common design features such as a premixing duct that feeds the resulting lean gaseous mixture into the combustor chamber. In a LPM combustor a gaseous fuel, usually natural gas, is homogeneously mixed with air. Similarly, in a LPP combustor a liquid fuel, usually Jet-A or a similar military grade, is vaporized and homogeneously mixed with air. The premixing duct is usually connected to a dump chamber with the premixed fuel air mixture flowing through a swirler. Flame stabilization takes place through a central toroidal recirculation zone and is aided by corner recirculation zones. Both of these combustor designs are widely used in industry, particularly for ground and marine power applications such as the GE LM6000.[99]

LDI combustors are currently considered by NASA[100] as a candidate for a next-generation low NO_x combustor design, particularly for aircraft engines. Market demands for improvements in thermal efficiency has steadily driven the pressure ratio in aircraft engines upwards.[101] This greatly reduces the autoignition delay time and increases the propensity of flashback. Together, these problems turn premixing at high pressure into a safety hazard. LDI combustors circumvent this by using a large grid of small swirlers that have a fuel injector embedded in their centerline to create a sheet of localized recirculation zones to stabilize the flame. In the recirculation zones high shear rates and turbulence intensities exist which enhance mixing directly in the flame holding region of the combustion chamber. This allows lean partially premixed combustion to occur. The similarities between LPM, LPP, and LDI combustor engine architecture suggest that a common model archetype for volumetric heat release perturbations and combustion noise models may be possible.

2.4.1 Volumetric Heat Release Perturbation Models

A useful visual tool in organizing volumetric heat release perturbation models is the Borghi diagram in Figure 2-3 which categorizes premixed combustion regimes as a function of the ratio of the largest turbulent length scale to the flame thickness on the abscissa and the ratio of turbulent velocity perturbations to the laminar flame speed, S_L, on the ordinate.[102] Different authors delineate combustion regimes by different criteria and as a result many different variations of the Borghi diagram exists with different names for combustion regimes with slightly different boundaries;[103] however, the concept of organizing premixed flames by their flame structure remains the same. By itself, the flame structure is insufficient information to define a volumetric heat release perturbation model. Additional information on the how the flame is stabilized and its shape is also needed. With that said, the Borghi diagram is still useful because the flame structure imposes a mathematical structure on the problem such that the same analysis tool works throughout a given combustion regime. As a result, volumetric heat release perturbation models tend to cluster together by combustion regimes.

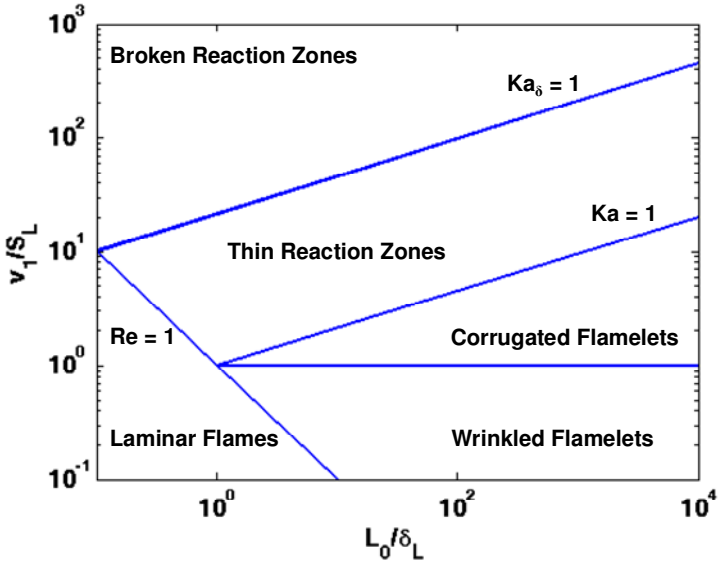

Figure 2-3: Borghi diagram depicting possible combustion regimes.

Each combustion regime has an incomplete collection of flow or mixture perturbations models developed for it that is either of empirical or first principles origin. Some of these models also possess phenomenological extensions. Ideally, volumetric heat release perturbation models derived from first principles should be used so that the predicted closed loop response of Figure 2-2 can be experimentally verified. At the same time the volumetric heat release perturbation model should be selected from a combustion regime that is commonly encountered in gas turbine combustors. Unfortunately, these goals are very close to being mutually exclusive. Gas turbine combustors tend to be closer to the corrugated flamelet and thin reaction sheet regimes which are the hardest to model mathematically. Corrugated flames are difficult because wrinkles in the flame start to fold in on themselves and break off into separate flamelets. The thin reaction sheet regime is even more difficult since flow disturbances are capable of penetrating the preheat zone of a flame which affects the chemical kinetics.

All of the other combustion regimes in the Borghi diagram have available first principles volumetric heat release perturbation models. As a result, volumetric heat release perturbation models from nearby combustion regimes tend to be phenomenological extensions of first principles models in order to include effects such as heat release saturation due to flow reversal.[104] Modeling perturbations in the volumetric heat release rate depends upon perturbation in the flame area, flame speed, and the heat of reaction.[105] Flame area perturbation models in the laminar flame and wrinkled flamelet regime are based upon the G-equation[106] which describes the instantaneous flame front as a thin boundary between the products and the reactants. A commonly assumed flame shape is an axisymmetric conical flame, see Figure 2-4, with a flame stabilization point prescribed as a boundary condition. The G-equation is perturbed using a two parameter expansion, which will be discussed in more detail in the next section. Its solution is substituted into a two parameter expansion for the expression for the volumetric heat release rate to derive a volumetric heat release perturbation model.

When volumetric heat release perturbation models are in the frequency domain they are called flame transfer functions (FTF) where the non-dimensional frequency used is the flame Strouhal number, *St*, which is the ratio of the flame length to the disturbance wavelength. Physically, the Strouhal number is important because it tells the modeler if the flame is compact, $O(St) << 1$, with respect to disturbances.

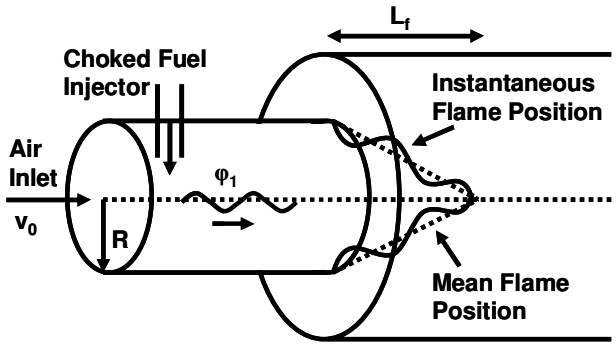

Figure 2-4: Model geometry for an axisymmetric conical flame.

The first theoretical derived FTF was for a laminar premixed flame with respect to acoustic velocity perturbations in Poiseuille flow.[64] An improvement to include the modeling of arbitrary flame angles for axisymmetric conical flames was derived and experimentally evaluated by Ducruix et al.[107] They found that their model was acceptable for $St < 6$. Eventually, this experiment was shown to be contaminated by advected velocity perturbations and that the addition of a honeycomb could reproduce this FTF for $St < 40$.[108] Similar collaborations between theory and experiment work on FTFs also occurred for V-flames[109] and swirl stabilized flames.[110] Recent emphasis has been placed on understanding the contributions of nonlinearities in the G-equation to finite amplitude and higher *St* effects.[111]

Development of FTFs due to equivalence ratio perturbation has lagged that of velocity perturbations. Unlike velocity perturbations which only affect the flame area, equivalence ratio perturbations also affect the flame speed and the heat of reaction which

complicates the theory. On the experimental side a high frequency response fuel actuator is needed and the combustor needs to be isolated from velocity perturbations. Currently, theoretical and experimental models do not exist for the same combustor configuration. Theoretical models are confined to axisymmetric conical flames while linear experiments exist for LDI combustors.[112] The only current theoretical FTF is from Cho and Lieuwen[105] with a later extension looking at flame stretch and finite amplitude effects .[113]

Since only one flame configuration is available for equivalence ratio perturbation modeling this automatically selects which acoustic velocity perturbation model has to be used to ensure physical consistency. This allows for a gathering of common assumptions that all the other physical models needed to obey to complete the feedback diagram from Figure 2-2, particularly the acoustics covered in the next section. Besides fixing the flame configuration, and hence the combustor geometry, the closed loop model will have to be restricted to one dimension. The assumption that perturbations in the equivalence ratio occur at constant density is also used and is claimed to be valid when the Mach number M satisfies $O(M^2) << 1$,[105] which imposes a low Mach number assumption.

Another common assumption made in thermo-acoustic modeling is that St is small; however, this can be problematic and this thesis will not make this assumption. Time delays are sensitive to what order derivative they belong to in the governing equations. Abrupt nonphysical changes in the combustor behavior occur if a time delay ever shows up in the highest order derivative and this should be a red flag to any thermo-acoustic modeler that something is wrong with the model. Unfortunately, reduced order low St models can change the derivative order. Although the point of a reduced order model is mathematical simplicity, often at the expense of accuracy at high frequencies, a minimum amount of information needs to be preserved about the structure of a transfer function at high frequencies. This fact should not be taken to mean that low St models are incorrect; instead, increased care and caution should be applied when using

them in closed loop transfer functions. A more rigorous introduction to the mathematical behavior of time delay systems is provided in the next chapter.

The full *St* FTF's used in this thesis, which have never been used in a complete closed loop thermo-acoustic analysis before, are described by Eq. (2.1) for acoustic velocity perturbations, v_1, and Eq. (2.2) for equivalence ratio perturbations at the flame base, $\varphi_{b,1}$, below. Mean variables are denoted by the subscript 0 while their perturbations are denoted by the subscript 1.

$$\frac{\partial^2}{\partial t^2}\left(\frac{q'''_{v,1}}{q'''_0}\right)=\frac{2}{S_{L,0}\tau_V}\sqrt{\frac{\beta^2-1}{\beta^2}}\left(\frac{\partial v_1(x,t)}{\partial t}-\frac{v_1(x,t)-v_1(x,t-\tau_V)}{\tau_V}\right)\delta(x-x_f) \tag{2.1}$$

$$\begin{aligned}\frac{\partial^2}{\partial t^2}\left(\frac{q'''_{\phi,1}}{q'''_0}\right)=&\left(2\beta^2\frac{n_H+n_S}{\tau_V}\frac{\partial\phi_{b,1}(x,t)}{\partial t}-2\beta^2\frac{(1+\beta^2)n_S+\beta^2 n_H}{\tau_V^2}\phi_{b,1}(x,t)\right.\\&\left.2\beta^4\frac{(\beta^2-1)n_H+\beta^2 n_S}{\tau_V^2(\beta^2-1)}\phi_{b,1}\left(x,t-\frac{\tau_V}{\beta^2}\right)-\frac{2\beta^2 n_S}{\tau_V^2(\beta^2-1)}\phi_{b,1}(x,t-\tau_V)\right)\delta(x-x_f)\end{aligned} \tag{2.2}$$

In the volumetric heat release response the magnitude of the time delay, τ_V, is governed by the flame geometry variables defined in Figure 2-4. A scaling factor, β, represents how much longer the flame front is compared to the flame length L_f. Two terms representing the sensitivity to heat of reaction with equivalence ratio, n_H, and another for flame speed, n_S, appear in the FTF for equivalence ratio modulation. Relations between these variables are clarified below.

$$\tau_V=\frac{\beta^2 L_f}{v_0} \tag{2.3}$$

$$n_H=\frac{d}{d\phi}\left(\frac{\Delta h_R}{\Delta h_{R,0}}\right)\Bigg|_{\phi_0} \tag{2.4}$$

$$n_S=\frac{d}{d\phi}\left(\frac{S_L}{S_{L,0}}\right)\Bigg|_{\phi_0} \tag{2.5}$$

For the combustion regime for which Eq. (2.1) and Eq. (2.2) are valid the heat release takes place in a flame sheet. To enforce this fact each FTF is multiplied by a Dirac delta function, δ, evaluated at the position of mean heat release, x_f. This is a particularly important variable that is calculated by finding the position of an imaginary plane that bisects the cone the flame sheet forms such that both halves have equal surface area.

$$x_f = \frac{\sqrt{2}-1}{\sqrt{2}} L_f \tag{2.6}$$

Additionally, each FTF has been normalized by the mean volumetric heat release rate which can be approximated by Eq. (2.7). The numerator give the mean heat release rate which depends upon the density, ρ, the heat of reaction, h_R, the laminar flame speed, S_L, and the area of the flame, S_f, while the denominator represents the volume of the combustor based upon its length, L, and its cross sectional area, S_{comb}.

$$q_0''' \approx \frac{\rho_0 h_R S_{L,0} S_f}{S_{comb} L} \tag{2.7}$$

Control engineers do not have direct control of the equivalence ratio at the flame position that the volumetric heat release perturbation model (2.2) depends upon. Practical concerns on actuator placement, denoted by x_a, require the fuel actuator to be placed upstream of the flame to protect it from high temperatures and allow time for injected fuel to mix with the airstream. As a result, perturbations in the equivalence ratio field needs to be rewritten as a function of the control input representing the equivalence ratio perturbation at the position of the fuel actuator. By modeling the equivalence ratio field as being advected downstream by the mean flow field, which neglects dispersion[19] effects, the equivalence ratio volumetric heat release perturbation model can be written as a single valued function of the control input. Mathematically, this is expressed as a spatial dependent delay in the control input.

$$\frac{\partial^2}{\partial t^2}\left(\frac{q'''_{\phi,1}}{q'''_0}\right)=\left(2\beta^4\frac{\left(\beta^2-1\right)n_H+\beta^2 n_S}{\tau_V^2\left(\beta^2-1\right)}u\left(t-\frac{x-x_a}{v_0}-\frac{\tau_V}{\beta^2}\right)\right.$$
$$+2\beta^2\frac{n_H+n_S}{\tau_V}\frac{\partial}{\partial t}u\left(t-\frac{x-x_a}{v_0}\right)-2\beta^2\frac{\left(1+\beta^2\right)n_S+\beta^2 n_H}{\tau_V^2}u\left(t-\frac{x-x_a}{v_0}\right) \qquad (2.8)$$
$$\left.-\frac{2\beta^2 n_S}{\tau_V^2\left(\beta^2-1\right)}u\left(t-\frac{x-x_a}{v_0}-\tau_V\right)\right)\delta\left(x-x_f\right)$$

The easiest way to evaluate the coefficients in Eq. (2.8) is to use correlation functions. These relations usually come from experimental data or numerical computation and are valid for a range of input temperatures, pressures, and equivalence ratios based upon reactant composition. This thesis will rely upon correlations for methane-air flames because it is the combination of fuel and oxidizer that is most studied. Methane is also the predominate gas in natural gas which is a major fuel source in ground power gas turbines. The correlation for laminar flame speed as a function of equivalence ratio, φ, temperature, T, and pressure, p, comes from Abu-Orf and Cant.[114]

$$S_L\left(\phi,T,p\right)=0.6079\phi^{-2.554}e^{-7.31(\phi-1.23)^2}\left(\frac{T}{300K}\right)^2\left(\frac{p}{1atm}\right)^{-0.5}\left(m/s\right) \qquad (2.9)$$

Finding a correlation for the heat of reaction is much more difficult. Instead, an equilibrium solver such as Gaseq can be used to find the properties of interest at the appropriate operating conditions. For all calculation in this thesis the combustor operating condition is taken at 18 atmospheres, 575 K, and at an equivalence ratio of 0.65 to simulate the operation of a modern natural gas powered gas turbine combustor.

$$n_S\left(\phi=0.65,T=575K,p=18atm\right)\approx 4.55 \qquad (2.10)$$

$$n_H\left(\phi=0.65,T=575K,p=18atm\right)\approx 1.57 \qquad (2.11)$$

Full details on these calculations are covered in Appendix C.

2.4.2 Combustion Noise Modeling

Historically, combustion noise sources have been broken into two categories: direct and indirect combustion noise.[115] Indirect combustion noise is caused by acceleration of entropy waves that is typically associated with a nozzle at the combustor boundary. This thesis will assume that sufficient dispersion exists in the combustor such that any entropy wave produced by the flame is fully dissipated by the time it reaches the boundary. Direct combustion noise is due to unsteady volumetric expansion at the flame induced by the volumetric heat release rate.

The stochastic component of direct combustion noise throughout this thesis will be referred to as combustion noise. In the feedback diagram from Figure 2-2 the direct combustion noise sources are the volumetric heat release perturbation models in the feedback loops, modeled with a known deterministic response, and the driving force, with an unknown stochastic behavior. Combustion noise essentially behaves as a catchall for unmodeled behavior. A better physical grasp of what combustion noise is can be gleamed by further exploring their origins. Stochastic behavior can come from the boundary conditions due to turbulent flow at the combustor inlet from the compressor. Generation of stochastic behavior can also come from interactions within the flow field. Another source of stochastic sound generation may be from a neglected heat release perturbation model such as an advected velocity perturbation model. Sound can also be scattered in a stochastic fashion at the flame front due to random wrinkling. All together, these stochastic sources can be daunting to model as a lumped source term; however, pertinent information about their behavior can be gathered by asking the right questions. Particularly, what is its probability density function (pdf), correlation function, and how does it appear in the governing equations?

A stochastic source term can be either additive or multiplicative, sometimes called parametric, in the governing equations depending if it is multiplied by a state variable. In the feedback diagram from Figure 2-2 the combustion noise is illustrated as an additive

source. Mathematically, this is desirable because multiplicative noise can cause the stability boundaries and performance trends to be a function of the noise strength.[116] Coming up with a physical reason for additivity of combustion noise is impeded by the dearth of work on this subject. A noteworthy contribution on this topic comes from the Ph.D thesis of Burnley[117] who looked at how stochastic sources come into being from mean flow and gas dynamic interactions. This is done via a canonical decomposition originally from Chu and Kovásznay[118] to break fluctuations into their acoustic, vortical, and entropic components. Any non-acoustic terms in the wave equation is treated as stochastic source, a process that created additive and multiplicative noise.

Additive and multiplicative noise have the same order of magnitude in their amplitude but since multiplicative noise multiples a state variable such as pressure or velocity it means that the complete term has a lower order of magnitude than the amplitude of the multiplicative noise by itself; therefore multiplicative noise should be neglected before neglecting additive noise. The justification to neglect these multiplicative noise terms follows from their small amplitude with respect to the other terms in the wave equation. Since indirect noise was neglected by assuming a strong dispersion process, the entropic component of the stochastic sources can be neglected leaving the vortical component behind. As the ratio of turbulent velocity perturbations to the laminar flame speed decreases the vortical component of the stochastic sources become weaker. This is accomplished by moving down the abscissa of the Borghi diagram, Figure 2-3, into the laminar and wrinkled flamelet regime which are exactly the regimes being investigated in this thesis. In these regimes the multiplicative noise due to mean flow and gas dynamics interactions can be neglected. Arguments based on Burnley's[117] modeling does not exhaust the neglection of all different possible sources of multiplicative noise; however, the same line of logic based on the combustion regime can still be useful. For example, heat release perturbations due to vorticity and sound scattering from a random flame front are weaker in the laminar and wrinkled flamelet

regimes compared to other available combustion regimes. Together, these ideas seem to suggest that modeling combustion noise as an additive source is permissible.

Additional logic based arguments can provide further details about the behavior of stochastic sources. Clavin et al.[119] argued that combustion noise due to turbulence should be Gaussian based upon the central limit theorem since the aggravate effect of turbulence is coming from the sum of statistically independent turbulent structures. This does not include every possible source of combustion; however, analysis of experimental data[120] where linear acoustics is valid indicate that this is true. Technically, experiments measure the system output such as the pressure and not the combustion noise. Since the pressure is Gaussian the combustion noise can also be shown to be Gaussian by considering the mathematical structure of the linear acoustic response of the combustor in a Gaussian Hilbert space.[121] Such a system with Gaussian output must have Gaussian input which implies that combustion noise must be Gaussian.

Working backwards from experimental data is also helpful for trying to deduce how combustion noise is correlated to itself. Rajaram et al.[122] found that the sound pressure level (SPL) of a turbulent Bunsen flame resembles a damped oscillator in shape but with non-integer slopes. In the high frequency limit this slope varied between -2.2 and -3.6 which is in decent agreement with analysis,[123] despite a turbulence intensity mismatch in test conditions compared to theoretical assumptions, giving a slope of -2.5. This is important because the SPL of the combustor response is the SPL of the combustion noise multiplied by a transfer function. The slope of a damped oscillator in the high frequency limit is -2 which means the combustion noise has a slope between -0.2 and -1.6. Having an integer slope in a combustion noise model is mathematically desirable because it can be constructed through linear operators acting on white noise. As a result the closest available correlation models can be white noise or an Ornstein-Uhlenbeck process[124] which is just white noise run through a first order low pass filter.

Taken altogether, these heuristic arguments suggest the use of an additive Gaussian colored or white noise model for combustion noise. Since this is not an analytic model the region of validity is unknown which creates some problems in ensuring physical consistency between the individual physical processes in the feedback diagram from Figure 2-2. The best that can be done is to use conservative arguments to get a lower bound on the region of validity which this subsection has done by placing it inside a subset of the laminar and wrinkled flamelet regime. Further improvements will require new research. Some key pieces of information are still missing from this model such as the variance of the combustion noise and the cutoff frequency of its spectra.

One final issue in using stochastic processes in differential equations is that their answer is dependent upon what quadrature rule is used.[125] In stochastic calculus[126] two main type of integrals exist: the Itô integral which uses a left end point quadrature rule and the Stratonovich integral which uses a midpoint quadrature rule. The physical interpretation of these integrals is given by van Kämpen[127] who related the non-anticipating Itô integral to noise sources external to the system being modeled while the anticipating Stratonovich integral is related to noise sources internal to the system being modeled. Since combustion noise is neglected and unmodeled dynamics inside the combustor it must be viewed via the Stratonovich interpretation. Most of the time this distinction will not matter because in linear stochastic systems additive white noise is commutative,[128] but it is an important distinction that needs to be made if someone builds upon the work in this thesis to add nonlinearities or multiplicative noise.

2.5 Wave Equation

The derivation of a wave equation in this section follows the work of Dowling and Stow,[93] but with increased commentary on understanding the ramifications of assumptions that go into deriving a wave equation. For notational convenience the substantial derivative D/Dt (2.12) is used throughout this section.

$$\frac{D}{Dt}(\cdot)=\left(\frac{\partial}{\partial t}+v\cdot\nabla\right)(\cdot) \tag{2.12}$$

Four equations, listed below, are needed to derive the wave equation: conservation of mass (2.13), conservation of momentum (2.14), conservation of energy (2.15), and a state relation (2.16).

$$\frac{D\rho}{Dt}+\rho\nabla\cdot v=0 \tag{2.13}$$

$$\rho\frac{Dv}{Dt}+\nabla p=0 \tag{2.14}$$

$$\rho\frac{D\left(e+\frac{1}{2}(v\cdot v)^2\right)}{Dt}+\nabla\cdot pv=q''' \tag{2.15}$$

$$p=\rho RT \tag{2.16}$$

These four equations already have a number of assumptions built into them. The momentum and energy equation, Eq. (2.14) and Eq. (2.15) respectively, has neglected the effects of viscosity and heat conduction. Simple analysis[129] shows that the absorption coefficient due to these effects do not become important until frequencies on the order of *MHz* while the highest frequency combustion instabilities seen in practice are on the order of *kHz*. Furthermore, these sound waves would have to travel distances of the order of *km* to see appreciable absorption effects while the largest combustor are of the order of *m*. For similar reasons, other nonlinear effects such as acoustic boundary layers, molecular relaxation, gravitational potential energy, and buoyant forces are also neglected.

Of the assumptions currently made the use of the ideal gas law, Eq. (2.16), as a state relation has the most questionable applicability due to the use of liquid fuels such as Jet-A. Marble[130] shows that in a two-phase flow with a droplet cloud an effective ideal gas formulation can be used. More complicated fluid dynamics would require volumetric

heat release perturbation models that do not exist yet, as detailed in the previous section. As a result, the wave equation being derived needs to inherit the ideal gas assumption to ensure compatibility with combustion modeling. Eventually, the ideal gas law will provide a route to rewrite the internal energy, e, in Eq. (2.15) as a function of pressure, p, and density, ρ.

The first step to simplifying the energy equation (2.15) is to remove the explicit dependence on the kinetic energy by expanding the substantial derivative of the total energy.

$$\rho \frac{De}{Dt} + v \cdot \rho \frac{Dv}{Dt} = -\nabla \cdot pv + q''' \tag{2.17}$$

This allows the substitution of the momentum equation (2.14) into Eq. (2.17).

$$\rho \frac{D(e)}{Dt} = -p\nabla \cdot v + q''' \tag{2.18}$$

Removing the divergence of velocity from Eq. (2.18) will take a few more intermediate steps. In particular, several thermodynamic relations will be required.

Ideal gas turbine combustion is an isobaric process which makes working with the enthalpy preferable to working with the internal energy because it avoids the explicit calculation of work done by the flow. The easiest way to implement this is to add $\pm p/\rho$ inside the substantial derivative for the internal energy in Eq. (2.18) and separate the enthalpy from the remaining terms by recalling that the definition of enthalpy is $h = e + p/\rho$.

$$\rho \frac{Dh}{Dt} = \frac{Dp}{Dt} - \frac{p}{\rho}\frac{D\rho}{Dt} - p\nabla \cdot v + q''' \tag{2.19}$$

Hidden within Eq. (2.19) is the expression of the continuity equation (2.13) which allows for the removal of the velocity divergence term.

$$\rho \frac{Dh}{Dt} = \frac{Dp}{Dt} + q''' \tag{2.20}$$

Further simplification of Eq. (2.20) can be realized by using a *T-ds* relation.

$$dh = Tds + \frac{1}{\rho}dp \tag{2.21}$$

Substitution of Eq. (2.21) into Eq. (2.20) gives an equation for the entropy, *s*.

$$\rho T \frac{Ds}{Dt} = q''' \tag{2.22}$$

An entropy equation is helpful because it allows for a very simple relationship between entropy, density and pressure via the evaluation of the exact differential.

$$d\rho(p,s) = \left.\frac{\partial\rho}{\partial p}\right|_s dp + \left.\frac{\partial\rho}{\partial s}\right|_p ds = \frac{1}{c^2}dp - \frac{\rho}{c_p}ds \tag{2.23}$$

The first partial derivative in Eq. (2.23) comes from the definition of the speed of sound, *c*, while the second partial derivative takes a few intermediate steps to derive. It comes from taking the path integral of Eq. (2.21) and taking the partial derivative of the resulting equation with respect to entropy at constant pressure while assuming ideal gas behavior.

All the equations derived so far in this section are for total quantities. The governing equations need to be decomposed to show the perturbations explicitly since combustion instabilities are pressure and velocity perturbations. This can be done using a two parameter expansion where each variable is broken down into a stationary mean component, denoted by the subscript 0, and a fluctuating component, denoted by the subscript 1. A two parameter expansion is one of the simplest perturbation methods available. More refined perturbation methods exist, which can be attested by the monograph by Holmes;[131] however, the selected volumetric heat release perturbation models were derived using a two parameter expansion. For the sake of consistency, and potentially compatibility, the wave equation should be derived using the same two parameter expansion method.

Proper perturbation analysis requires grouping each set of terms in the governing equations by their order of magnitude. In this analysis all perturbed variables are assumed to scale with the acoustic Mach number, ε, the ratio of the velocity perturbation amplitude to the speed of sound. The acoustic Mach number needs to be smaller than the Mach number; otherwise the flow field would experience periodic flow reversal resulting in a heat release saturation nonlinearity in the combustion process.[104] These terms can be grouped using Landau notation.

$$\mathrm{O}(1) > \mathrm{O}(M) > \mathrm{O}(\varepsilon) > \mathrm{O}(M^2) > \mathrm{O}(M\varepsilon)\ldots \tag{2.24}$$

Most of the thermo-acoustic models used for feedback control of combustion instabilities, discussed in Chapter 1, strive to be of $O(M\varepsilon)$ because the effects of linear acoustic damping come from Mach number effects at the combustor boundaries; therefore, all terms up to $O(M\varepsilon)$ need to be kept. With the ordering scheme established by Eq. (2.24), the continuity (2.13), momentum (2.14), and entropy (2.22) equations can now be perturbed.

$$\frac{D_0\rho_1}{Dt} + \rho_0\nabla\cdot v_1 + \underbrace{\rho_1\nabla\cdot v_0 + v_1\cdot\nabla\rho_0}_{Homogeneous} + \underbrace{\rho_1\nabla\cdot v_1 + v_1\cdot\nabla\rho_1}_{Second\ \ Order} + \underbrace{\frac{D_0\rho_0}{Dt} + \rho_0\nabla\cdot v_0}_{Mean\ \ Flow\ \ Equation} = 0 \tag{2.25}$$

$$\begin{aligned}
&\rho_0 T_0\frac{D_0 s_1}{Dt} + \underbrace{\rho_1 T_0\frac{D_0 s_1}{Dt} + \rho_0 T_1\frac{D_0 s_1}{Dt} + \rho_1 T_1\frac{D_0 s_0}{Dt} + \rho_0 T_0 v_1\cdot\nabla s_1}_{Second\ \ Order} \\
&+ \underbrace{\rho_1 T_1\frac{D_0 s_1}{Dt} + \rho_0 T_1 v_1\cdot\nabla s_1 + \rho_1 T_0 v_1\cdot\nabla s_1}_{Third\ \ Order} + \underbrace{\rho_1 T_1 u_1\cdot\nabla s_1}_{Fourth\ \ Order} \\
&+ \underbrace{\left(\rho_0 T_0 v_1 + \rho_0 T_1 v_1 + \rho_1 T_0 v_1 + \rho_1 T_1 v_1 + \rho_0 T_1 v_0 + \rho_1 T_0 v_0\right)\cdot\nabla s_0}_{Homogeneous} \\
&+ \underbrace{\left(\rho_0 T_1 + \rho_1 T_0\right)\frac{\partial s_0}{\partial t}}_{Stationary} + \underbrace{\rho_0 T_0\frac{D_0 s_0}{Dt} - q_0''' = q_1'''}_{Mean\ \ Flow\ \ Equation}
\end{aligned} \tag{2.26}$$

$$\rho_0 \frac{D_0 v_1}{Dt} + \nabla p_1 + \underbrace{\left(\rho_1 v_0 + \rho_0 v_1 + \rho_1 v_1\right) \cdot \nabla v_0}_{Homogeneous} + \underbrace{\rho_1 \frac{D_0 v_1}{Dt} + \rho_0 v_1 \cdot \nabla v_1}_{Second\ \ Order}$$
$$+ \underbrace{\rho_1 v_1 \cdot \nabla v_1}_{Third\ \ Order} + \underbrace{\rho_1 \frac{\partial v_0}{\partial t}}_{Stationary} + \underbrace{\rho_0 \frac{D_0 v_0}{Dt}}_{Mean\ \ Flow\ \ Equation} + \nabla p_0 = 0 \tag{2.27}$$

The perturbed continuity (2.25), entropy (2.26), and momentum equations (2.27) both have terms underlined giving the reason why they should be neglected. A consistence perturbation analysis needs to automatically satisfy the equations given by all lower order perturbations analysis. As a result, the $O(1)$ equation can be neglected. Stationary terms drop out because the time derivative of a time invariant term must be zero. Some terms can be neglected for multiple reasons such as being a higher order term or being zero from the assumption of homogeneous mean flow.

Physically, the assumption of homogeneous mean flow is peculiar because a jump in thermodynamic properties exist across a flame front as well as in the mean flow velocity. Understanding the ramifications of assuming homogeneous mean flow first requires a detour on why such an assumption is mathematically desirable. Mathematical foresight has already established that the wave equation will be analyzed by spatially averaging a Galerkin expansion. Inhomogeneous mean flow makes the spatial averaging process cumbersome and obfuscates the drawing of physical insight from the spatial averaged governing equations, especially since the focus of this thesis, from a mathematical point of view, is the effects of time delays and stochastic forcing. The spatial averaging process will change the coefficients in front of preexisting terms in the Galerkin expansion but it will not change the type of the functional differential equation yielded.

Justifying the assumption of homogeneous mean flow now rests upon finding a physical constraint that ensures inhomogeneous mean flow has a negligible contribution to the coefficients in the governing equations after spatial averaging. When the combustor volume predominately consists of a single state then the spatial average will

approach that state. If the flame position is constrained to be close to the combustor inlet then the assumption of homogeneous mean flow using the flow field properties downstream of the flame is justifiable. This assumption is valid for an LDI combustor because the flame is stabilized in a small volume close to the injection plane.[132] In LPP combustors the flames are larger[133] and can violate the homogeneous mean flow assumption, particularly in aircraft engines. LPP combustors in ground power applications are longer than their aircraft engine counterparts such that the flames could take up a reasonably small volume to still apply the assumption of homogeneous mean flow. For the actual flame geometry being considered in this thesis, an axisymmetric conical flame, this assumption means the position of mean heat release has to be close to the combustor inlet. This assumption can also place constraints on the magnitude of the time delays from disturbances that originate within the combustor; however, nothing in this formulation prevents a disturbance from originating outside of the combustor. A fuel actuator could be placed in the premixing duct leading to the combustor in a LPP system.

Since the ramifications of all simplifying assumptions are now understood, the task of deriving the wave equation can now focus on removing the dependence of velocity from the governing equations. This requires a few intermediate expressions: the mean substantial derivative of the perturbed continuity equation (2.25) and the divergence of the perturbed momentum equation (2.27).

$$\frac{D_0^2\rho_1}{Dt} + \rho_0\frac{D_0}{Dt}\left(\nabla\cdot v_1\right) + \underbrace{\frac{\partial\rho_0}{\partial t}}_{Stationary}\nabla\cdot v_1 + \underbrace{\left(v_0\cdot\nabla\rho_0\right)}_{Homogeneous}\nabla\cdot v_1 = 0 \tag{2.28}$$

$$\rho_0\frac{D_0}{Dt}\left(\nabla\cdot v_1\right) + \nabla^2 p_1 + \underbrace{\frac{D_0 v_1}{Dt}}_{Homogeneous}\cdot\nabla\rho_0 = 0 \tag{2.29}$$

The mean second order substantial derivative can be simplified when fully expanded; however, it is convenient to continue using this compact notation for one more step. A wave type equation can be derived by substituting Eq. (2.29) into Eq. (2.28).

$$\frac{D_0^2 \rho_1}{Dt} - \nabla^2 p_1 = 0 \tag{2.30}$$

Removing the dependence on density in Eq. (2.30) can be accomplished by using the definition of an exact differential of the density for an ideal gas (2.23).

$$\frac{D_0^2 p_1}{Dt} - c_0^2 \nabla^2 p_1 = \frac{\rho_0 c_0^2}{c_p} \frac{D_0^2 s_1}{Dt} \tag{2.31}$$

Finally, the perturbed entropy equation (2.26) can be substituted into Eq. (2.31). This is a good time to fully expand the mean substantial derivative.

$$\begin{aligned} &\frac{\partial^2 p_1}{\partial t^2} + 2v_0 \cdot \frac{\partial \nabla p_1}{\partial t} - c_0^2 \nabla^2 p_1 + \underbrace{v_0 \cdot \nabla \left(v_0 \cdot \nabla p_1 \right)}_{Second\ \ Order} + \underbrace{\frac{\partial v_0}{\partial t} \cdot \nabla p_1}_{Stationary} \\ &= \left(\gamma - 1 \right) \frac{\partial q_1'''}{\partial t} + \left(\gamma - 1 \right) v_0 \cdot \nabla q_1''' \end{aligned} \tag{2.32}$$

Simplifying Eq. (2.32) results in the wave equation.

$$\underbrace{\frac{\partial^2 p_1}{\partial t^2} + 2v_0 \cdot \frac{\partial \nabla p_1}{\partial t} - c_0^2 \nabla^2 p_1}_{Wave\ \ Operator} = \underbrace{\left(\gamma - 1 \right) \frac{\partial q_1'''}{\partial t} + \left(\gamma - 1 \right) v_0 \cdot \nabla q_1'''}_{Heat\ \ Release\ \ Source\ \ Terms} \tag{2.33}$$

On the left hand side of the wave equation (2.33) is the standard wave operator which gives the mean flow wave equation from acoustics. The right hand side contains the volumetric heat release source terms which depends on the temporal and spatial rate of change of the perturbations in the volumetric heat release rate. If the homogeneous flow assumption was relaxed then the right hand side would also include a large number of sound scattering terms due to inhomogeneity. In preparation for performing a Galerkin expansion in the next section the volumetric heat release perturbation terms can be explicitly divided according to their physical origin: acoustic velocity perturbations, equivalence ratio perturbations, and combustion noise.

$$q_1''' = q_{v,1}''' + q_{\phi,1}''' + q_{stoc}''' \tag{2.34}$$

Each individual volumetric heat release perturbation term corresponds to a physical process needed in the closed loop thermo-acoustic model in Figure 2-2. The

wave operator in Eq. (2.33) represents the combustor acoustics and is the system plant. It is self-excited by velocity perturbations (2.1) from the first term on the right hand side of Eq. (2.34), stabilized by feedback control using equivalence ratio modulations (2.8) from the second term, and stochastically driven by combustion noise from the third term.

$$\begin{aligned}
&\frac{\partial^2}{\partial t^2}\left(\frac{\partial^2}{\partial t^2}p_1(x,t)+2v_0\frac{\partial\nabla}{\partial t}p_1(x,t)-c_0^2\nabla^2 p_1(x,t)\right)=2(\gamma-1)q_0'''\\
&*\left[\frac{1}{S_{L,0}\tau_V}\sqrt{\frac{\beta^2-1}{\beta^2}}\left(\frac{\partial^2 v_1(x,t)}{\partial t^2}-\frac{1}{\tau_V}\left(\frac{\partial v_1(x,t)}{\partial t}-\frac{\partial v_1(x,t-\tau_V)}{\partial t}\right)\right)\delta(x-x_f)\right.\\
&+\frac{v_0}{S_{L,0}\tau_V}\sqrt{\frac{\beta^2-1}{\beta^2}}\left(\frac{\partial\nabla v_1(x,t)}{\partial t}-\frac{\nabla v_1(x,t)-\nabla v_1(x,t-\tau_V)}{\tau_V}\right)\delta(x-x_f)\\
&+\nabla\delta(x-x_f)\left(\frac{v_0}{S_{L,0}\tau_V}\sqrt{\frac{\beta^2-1}{\beta^2}}\left(\frac{\partial v_1(x,t)}{\partial t}-\frac{v_1(x,t)-v_1(x,t-\tau_V)}{\tau_V}\right)\right.\\
&+\beta^4 v_0\frac{(\beta^2-1)n_H+\beta^2 n_S}{\tau_V^2(\beta^2-1)}u\left(t-\frac{x-x_a}{v_0}-\frac{\tau_V}{\beta^2}\right)+\beta^2 v_0\frac{n_H+n_S}{\tau_V}\frac{\partial}{\partial t}u\left(t-\frac{x-x_a}{v_0}\right)\\
&\left.\left.-\beta^2 v_0\frac{(1+\beta^2)n_S+\beta^2 n_H}{\tau_V^2}u\left(t-\frac{x-x_a}{v_0}\right)-\frac{\beta^2 n_S}{\tau_V^2(\beta^2-1)}v_0 u\left(t-\frac{x-x_a}{v_0}-\tau_V\right)\right)\right]\\
&+Noise(x,t)
\end{aligned}\tag{2.35}$$

For convenience Eq. (2.35) shows all of its arguments explicitly. It has been collapsed to its one dimensional form as required by the assumptions inherited from the volumetric heat release perturbation models used. Two time derivatives have been taken on both sides of Eq. (2.35) since the heat release dynamics are second order in time; otherwise, the wave equation (2.35) would take the form of a partial functional integro-differential equation.

Great care has been taken to neglect terms in the wave equation (2.35) for mathematical simplicity and to keep the equation valid to $O(M\varepsilon)$; however, the volumetric heat release perturbation terms have been left untouched in this process. Part of the reason behind this is that hidden mean flow velocity dependences exist in the mean volumetric heat release rate and from evaluating its spatial gradient. This will not be

evident until the wave equation is non-dimensionalized in the next section. Volumetric heat release perturbations due to velocity perturbations will end up contributing $O(\varepsilon)$ and $O(M\varepsilon)$ terms while the order of magnitude of the equivalence ratio perturbations are unquantifiable because the control input gain cannot be known *a priori* to the design of the controller. If the gain ends up being large then all the terms will have to be kept while some of the terms may be negligible if the gain is small. All of the control input terms have to be kept to guarantee accuracy to $O(M\varepsilon)$.

2.6 Spatial Averaging

The Galerkin expansion is a technique used to isolate the modal responses of state variables in a governing equation by expressing them as a function of an orthogonal basis. With the standard Galerkin expansion these orthogonal basis also have to satisfy the boundary conditions which is very restricting; however, modified Galerkin expansion methods introduced by Culick[8] can adjust to nonstandard boundary conditions. A Fourier basis makes a good selection for an orthogonal basis because the spatial modes shapes of a duct in the longitudinal direction are trigonometric functions in the classical acoustic limit. An additional benefit of this selection is that the question of if the Galerkin expansion exists becomes a question of the existence of a Fourier series which is well studied.[134] This is actually a larger basis than is required. The odd or even Fourier basis will suffice because the space of interest, $[0,L]$, can be written as an odd or even wave in $(-\infty,\infty)$. Different selections will give different answers in $(-\infty,\infty)$ but will converge in $(0,L)$. As a result, basis selection should focus upon the rate of convergence and minimizing Gibbs phenomenon at the combustor boundaries.

An actual combustor will have boundaries that behave like a rigid wall and hence have velocity nodes and pressure antinodes close to the boundaries. This occurs because the inlet and outlet of a combustor tend to have a choked flow at low Mach numbers.[16] The natural choice for a spatial basis function becomes the set of cosine functions.

$$\psi_n(x) = \sqrt{2}\cos(k_n x) \tag{2.36}$$

$$k_n = \frac{\pi n}{L} \tag{2.37}$$

A useful fact about this basis is that each element satisfies the Helmholtz equation below.

$$\nabla^2 \psi_n + k_n^2 \psi_n = 0 \tag{2.38}$$

Some care needs to be taken when comparing results from published work on combustion instabilities because the prevalence of Rijke tubes which have a pressure release type boundary condition at the outlet. As a result, the definition of the wave number (2.37) used to define the spatial basis function (2.36) can be different.

The selection of a spatial basis allows the state variables of pressure, velocity, and density to be expanded in the equations below. They are defined in such a way so that the spatial basis functions and their temporal response are dimensionless. Each state variable has a natural mean quantity to use for non-dimensionalization. Velocity perturbations have two choices, but the speed of sound is a superior choice over the mean flow velocity because this thesis is looking at the acoustic response of the combustor.

$$p_1(x,t) = p_0 \sum_{m=1}^{\infty} \eta_m(t)\psi_m(x) \tag{2.39}$$

$$v_1(x,t) = c_0 L \sum_{m=1}^{\infty} \chi_m(t)\nabla\psi_m(x) \tag{2.40}$$

$$\rho_1(x,t) = \rho_0 \sum_{m=1}^{\infty} \vartheta_m(t)\psi_m(x) \tag{2.41}$$

Associated with every spatial basis for each of the state variables is a temporal response. Spatial averaging can be used to derive a constitutive relation between the different temporal responses of each state variable. These relationships will end up being explicit for all temporal responses because of the assumption of homogeneous mean flow. A relationship between η_n and χ_n is found by substituting in Eq. (2.39) and Eq. (2.40) into the perturbed momentum equation (2.27). Similarly, a relationship

between χ_n and ϑ_n is found by substituting in Eq. (2.40) and Eq. (2.41) into the perturbed continuity equation (2.25).

$$\begin{aligned}&\rho_0 c_0 L\sum_{m=1}^{\infty}\dot{\chi}_m(t)\nabla\psi_m(x)-\rho_0 v_0 c_0 L\sum_{m=1}^{\infty}k_m^2\chi_m(t)\psi_m(x)\\&+p_0\sum_{m=1}^{\infty}\eta_m(t)\nabla\psi_m(x)=0\end{aligned}\tag{2.42}$$

$$\rho_0\sum_{m=1}^{\infty}\dot{\vartheta}_m(t)\psi_m(x)+v_0\rho_0\sum_{m=1}^{\infty}\vartheta_m(t)\nabla\psi_m(x)-\rho_0 c_0 L\sum_{m=1}^{\infty}k_m^2\chi_m(t)\psi_m(x)=0\tag{2.43}$$

To spatially average Eq. (2.42) and Eq. (2.43) they need to be multiplied by a spatial mode shape, $\nabla\psi_n$ and ψ_n respectively, and averaged over the combustor volume. This operation is actually using the inner product to perform a projection on an element of the spatial basis. If the other combination of ψ_n and $\nabla\psi_n$ is used then the answer is zero because spatial averaging would be projecting into the half of the Fourier basis not being used.

$$\rho_0 c_0 L\dot{\chi}_n(t)+p_0\eta_n(t)=0\tag{2.44}$$

$$\dot{\vartheta}_n(t)-c_0 L k_n^2\chi_n(t)=0\tag{2.45}$$

Some published works on combustion instabilities like to use a constitutive relationship for velocity and pressure based upon classical acoustics. This is called the linearized Galerkin method[135] and the use of this technique is problematic. Dowling[95] showed that large discrepancies can exist in the predicted frequency response of the linearized Galerkin method compared to more exact techniques but could not explain why it existed. Two reasons can be offered for this discrepancy. First, it assumes a small volumetric heat release perturbation term; however, an order of magnitude analyze of the velocity perturbation model (2.1) shows that it is $O(1)$. Sometimes this objection does not bear out in practice because the order of magnitude of the acoustic response from a volumetric heat release rate perturbation can be lower than the actually order of magnitude in the governing equations.[136] The second objection is always true: it changes

the order of the highest order derivative containing a time delay in it. As warned in §2.4.1 a modeling error of this type can produced nonphysical behavior in closed loop transfer functions. This thesis will continue to use the standard Galerkin method to avoid these effects.

When using spatial averaging the dependence on the spatial variable in the governing equations drop out, but the boundary conditions also depend on the spatial variable. To enforce a boundary condition with spatial averaging the volume integrals that the technique uses need to be converted to surface integrals with an outward normal direction *n*. The trick to doing this is to find an operation to perform on Eq. (2.35) so that Green's second identity can be applied.

$$\begin{aligned}&\iiint_V \left[p_1(x,t)\nabla^2\psi_n(x) - \psi_n(x)\nabla^2 p_1(x,t)\right] dV \\ &= \iint_S \left[p_1(x,t)\nabla\psi_n(x) - \psi_n(x)\nabla p_1(x,t)\right]\cdot \vec{n} dS\end{aligned} \tag{2.46}$$

Spatial averaging expression (2.47) gives the form needed to apply boundary conditions.

$$\frac{\partial^2 p_1(x,t)}{\partial t^2} * \text{Eq.(2.38)} + \frac{\psi_n(x)}{c_0^2} * \text{Eq.(2.35)} \tag{2.47}$$

For convenience of exposition certain terms have been broken into groups defined by brackets.

$$\begin{aligned}&\left[\frac{\partial^2}{\partial t^2} p_1(x,t)\nabla^2\psi_n(x) - \psi_n(x)\frac{\partial^2\nabla^2}{\partial t^2} p_1(x,t)\right] \\ &+\left[\frac{\psi_n(x)}{c_0^2}\frac{\partial^4}{\partial t^4} p_1(x,t) + 2v_0\frac{\psi_n(x)}{c_0^2}\frac{\partial^3\nabla}{\partial t^3} p_1(x,t) + k_n^2\frac{\partial^2}{\partial t^2} p_1(x,t)\psi_n(x)\right] \\ &= F_V(x,t) + F_\phi(x,t) + Noise(x,t)\end{aligned} \tag{2.48}$$

$$F_V(x,t) = 2(\gamma-1)q_0'''\frac{\psi_n(x)}{c_0^2}\left[\left(\left(\frac{\partial^2 v_1(x,t)}{\partial t^2} - \frac{1}{\tau_V}\left(\frac{\partial v_1(x,t)}{\partial t} - \frac{\partial v_1(x,t-\tau_V)}{\partial t}\right)\right)\right.\right.$$
$$\left.+v_0\left(\frac{\partial \nabla v_1(x,t)}{\partial t} - \frac{\nabla v_1(x,t) - \nabla v_1(x,t-\tau_V)}{\tau_V}\right)\right)\delta(x-x_f) \qquad (2.49)$$
$$\left.+v_0\left(\frac{\partial v_1(x,t)}{\partial t} - \frac{v_1(x,t) - v_1(x,t-\tau_V)}{\tau_V}\right)\nabla\delta(x-x_f)\right]\frac{1}{S_{L,0}\tau_V}\sqrt{\frac{\beta^2-1}{\beta^2}}$$

$$F_\phi(x,t) = 2(\gamma-1)q_0'''\frac{\psi_n(x)}{c_0^2}\left[\beta^4 v_0\frac{(\beta^2-1)n_H + \beta^2 n_S}{\tau_V^2(\beta^2-1)}u\left(t - \frac{x-x_a}{v_0} - \frac{\tau_V}{\beta^2}\right)\right.$$
$$+\beta^2 v_0\frac{n_H + n_S}{\tau_V}\frac{\partial}{\partial t}u\left(t - \frac{x-x_a}{v_0}\right) - \beta^2 v_0\frac{(1+\beta^2)n_S + \beta^2 n_H}{\tau_V^2}u\left(t - \frac{x-x_a}{v_0}\right) \qquad (2.50)$$
$$\left.-\frac{\beta^2 n_S}{\tau_V^2(\beta^2-1)}v_0 u\left(t - \frac{x-x_a}{v_0} - \tau_V\right)\right]\nabla\delta(x-x_f)$$

The volume integral of the first set of terms in brackets on the left hand side of Eq. (2.48) matches the volume integral in Green's second identity (2.46). Technically, this identity requires the state variables to be twice continuously differentiable; a requirement it inherits from the divergence theorem from which it is derived. This creates a problem with discontinuities at the flame front. Farasset[137] showed that the divergence theorem will work with piecewise continuous functions as long as the derivative is treated as a generalized or distributional derivative. The gradient in the Dirac delta function in the volumetric heat release perturbation models have already been treated as a distributional derivative so this assumption will provide no additional constraints.

Typically, a boundary condition in acoustics is defined by the impedance *Z* or the reflection coefficient in the frequency domain. Impedance describes the scaling and phase difference between pressure and velocity perturbations in the outward normal direction from the control volume at the boundary while the reflection coefficient

describes the scaling and phase difference between incident pressure waves with their reflection.

$$Z(x,\omega) = \frac{p_a(x,\omega)}{v_a(x,\omega)\cdot\vec{n}} \tag{2.51}$$

An important point to make about the ratio in Eq. (2.51) is that they are for the acoustic component of pressure and velocity. Chu and Kovásznay[118] showed in the linear regime fluctuations in the pressure are predominantly acoustic but the velocity perturbations can have acoustic and vortical components. Experimentally determined impedances reported in the literature do not always separate out the vortical component. Fortuitously, a theoretically derived nozzle impedance is available from Marble and Candel.[16] They show that the reflection coefficient for a compact nozzle is real and that finite length effects are needed to add an imaginary component. Unfortunately, the expression is only simple in the case of a compact nozzle; otherwise, the impedance has to be solved through an implicit equation. Even if the impedance was analytically tractable it will have to be modified to account for acoustic damping from neglected higher order modes. As a result, this thesis will consider a generic boundary condition by looking at a Laurent series expansion of the impedance in frequency.

$$\frac{Z(x,\omega)}{\rho_0 c_0} = \frac{C_0(x)}{\omega^2} + \frac{C_1(x)}{i\omega} + C_2(x) + \ldots \tag{2.52}$$

Converting Eq. (2.52) into the time domain gives the easiest expression to implement in the surface integral (2.46) that needs to be evaluated.

$$\frac{\partial^2}{\partial t^2} p_1(x,t) = \rho_0 c_0 \sum_{i=0}^{\infty} C_i(x) \frac{\partial^i v_1(x,t)}{\partial t^i} \tag{2.53}$$

In this thesis the terms kept are those that do not change the order of the highest derivative or add an integral for analytical convenience. This imposes limits on the range of frequencies that Eq. (2.52) is valid.

Returning back to the surface integral (2.46), the first term will always evaluate to zero because the antinodes of the projected mode shapes (2.36) are located at the combustor boundaries; therefore, the boundary condition (2.53) only needs to be substituted into the second term. Another repercussion from the form of the projected mode shapes is that half of the terms of coming from the gradient of pressure will also evaluate to zero.

$$\begin{aligned}&\iint_S\left[\frac{\partial^2}{\partial t^2}p_1(x,t)\nabla\psi_n(x)-\psi_n(x)\frac{\partial^2\nabla}{\partial t^2}p_1(x,t)\right]\cdot\vec{n}dS=\\&\iint_S\left[-\psi_n(x)\rho_0c_0\left(\sum_{i=0}^{\infty}\nabla C_i(x)\frac{\partial^{i+2}v_1(x,t)}{\partial t^{i+2}}+C_i(x)\frac{\partial^i\nabla v_1(x,t)}{\partial t^i}\right)\right.\\&\left.+p_1(x,t)\nabla\psi_n(x)\right]dS\cdot\vec{n}\end{aligned}\tag{2.54}$$

To see this explicitly the surface integral in Eq. (2.54) needs to be broken into separate integrals for the inlet and the outlet. A third surface integral should also be included for the walls of the combustor but because of the assumption of one dimensional flow that integral would evaluate to zero. Even in the one dimensional setting the velocity still needs to be viewed as a vector because the dot product of the velocity vector with the outward normal vector causes a sign change in the surface integral for the inlet.

$$\begin{aligned}&\iint_{S(x=0)}\left[\frac{\partial^2}{\partial t^2}p_1(x,t)\nabla\psi_n(x)-\psi_n(x)\frac{\partial^2\nabla}{\partial t^2}p_1(x,t)\right]\cdot\vec{n}dS\\&+\iint_{S(x=L)}\left[\frac{\partial^2}{\partial t^2}p_1(x,t)\nabla\psi_n(x)-\psi_n(x)\frac{\partial^2\nabla}{\partial t^2}p_1(x,t)\right]\cdot\vec{n}dS\\&=2\rho_0c_0^2LS_{noz}\left(\sum_{i=0}^{\infty}\sum_{m=1}^{\infty}\left(C_i(L)(-1)^{n+m}-C_i(0)\right)k_m^2\frac{\partial^i\chi_m(t)}{\partial t^i}\right)\end{aligned}\tag{2.55}$$

For convenience the cross sectional area for the inlet and outlet, S_{noz}, has been assumed to be the same in Eq. (2.55). Inspection of Eq. (2.55) shows that the boundary conditions are a source of modal coupling.

Evaluating the volume integral of the second set of terms in brackets on the left hand side of Eq. (2.48) is much more straightforward.

$$\iiint_V \left[\frac{\psi_n(x)}{c_0^2} \frac{\partial^4}{\partial t^4} p_1(x,t) + 2v_0 \frac{\psi_n(x)}{c_0^2} \frac{\partial^3 \nabla}{\partial t^3} p_1(x,t) + k_n^2 \frac{\partial^2}{\partial t^2} p_1(x,t) \psi_n(x) \right] dV = S_{comb} L p_0 \left[\frac{1}{c_0^2} \dddot{\eta}_n(t) + k_n^2 \ddot{\eta}_n(t) \right] \tag{2.56}$$

Equation (2.56) may seems peculiar upon first inspection because it starts with three terms on the left hand side but ends up with two terms on the right hand side. This occurs because the only term with a contribution from the mean flow field is zero, but this does not mean that the mean flow does not influence the acoustics in an unbounded domain; it just means that the spatial averaged contribution of mean flow to the acoustics in an unbounded domain is zero. In the spatially averaged equations mean flow still makes itself felt from the volumetric heat release perturbation models and in the acoustic impedance.

On the right hand side of Eq. (2.48) are terms involving the Dirac delta function and its derivative. Evaluating an integral with a derivative of the Dirac delta function can be determined by using integration by parts. This results in some interesting behavior in the velocity perturbation heat release model because it starts with three grouping of terms and collapses into two grouping of terms after spatial averaging.

$$\iiint_V F_V(x,t)\, dV = 2q_0''' S_{comb} \frac{(\gamma-1)L}{S_{L,0} c_0 \tau_V} \int_0^L \sum_{m=1}^{\infty} \left[\left(\ddot{\chi}_m(t) - \frac{1}{\tau_V} \left(\dot{\chi}_m(t) - \dot{\chi}_m(t-\tau_V) \right) \right) \psi_n(x) \nabla \psi_m(x) - v_0 \left(\dot{\chi}_m(t) - \frac{\chi_m(t) - \chi_m(t-\tau_V)}{\tau_V} \right) \nabla \psi_n(x) \nabla \psi_m(x) \right] \sqrt{\frac{\beta^2 - 1}{\beta^2}} \delta(x - x_f)\, dx \tag{2.57}$$

When using integration by parts on the third grouping of terms on the left hand side of Eq. (2.57) the product rule needs to be used. One of two terms that results from the product rule perfectly cancels the second grouping of terms on the left hand side of Eq. (2.57). The volume integral of the remaining terms in Eq. (2.57) has not been fully

evaluated on the right hand side in order to maintain dimensional consistency. Once non-dimensionalization is introduced this integral will be fully evaluated.

Working with equivalence ratio heat release perturbation model also requires using integration by parts to work with the gradient of the Dirac delta function.

$$\begin{aligned}\iiint_V F_\phi(x,t)\,dV = \frac{S_{comb}\,2(\gamma-1)q_0'''}{c_0^2}\int_0^L \Bigg[& -\frac{\beta^2 n_S}{\tau_V^2(\beta^2-1)}\frac{\partial}{\partial t}u\left(t-\frac{x-x_a}{v_0}-\tau_V\right)\psi_n(x) \\ & +\beta^4\frac{(\beta^2-1)n_H+\beta^2 n_S}{\tau_V^2(\beta^2-1)}\frac{\partial}{\partial t}u\left(t-\frac{x-x_a}{v_0}-\frac{\tau_V}{\beta^2}\right)\psi_n(x) \\ & +\beta^2\left(\frac{n_H+n_S}{\tau_V}\frac{\partial^2}{\partial t^2}u\left(t-\frac{x-x_a}{v_0}\right)-\frac{(1+\beta^2)n_S+\beta^2 n_H}{\tau_V^2}\frac{\partial}{\partial t}u\left(t-\frac{x-x_a}{v_0}\right)\right)\psi_n(x) \\ & +\left(\frac{\beta^2 v_0 n_S}{\tau_V^2(\beta^2-1)}u\left(t-\frac{x-x_a}{v_0}-\tau_V\right)-\beta^2 v_0\frac{(n_H+n_S)}{\tau_V}\frac{\partial}{\partial t}u\left(t-\frac{x-x_a}{v_0}\right)\right)\nabla\psi_n(x) \\ & +\beta^2 v_0\frac{(1+\beta^2)n_S+\beta^2 n_H}{\tau_V^2}u\left(t-\frac{x-x_a}{v_0}\right)\nabla\psi_n(x) \\ & -\beta^4 v_0\frac{(\beta^2-1)n_H+\beta^2 n_S}{\tau_V^2(\beta^2-1)}u\left(t-\frac{x-x_a}{v_0}-\frac{\tau_V}{\beta^2}\right)\nabla\psi_n(x)\Bigg]\delta(x-x_f)\,dx\end{aligned} \tag{2.58}$$

Once again, the volume integral in Eq. (2.58) has not been fully evaluated on the right hand side in order to maintain dimensional consistency. The control input that appears in Eq. (2.58) does not show itself in the traditional form because it has time delays and time derivatives acting on it. An important time delay representing the advection time between the fuel actuator and the flame front, τ_A, will show itself when the integrals and the right hand side of Eq. (2.58) are fully evaluated.

$$\tau_A = \frac{x_f - x_a}{v_0} \tag{2.59}$$

With the Galerkin expansion finished Eq. (2.48) can be fully expanded by combining Eq. (2.55) through Eq. (2.58). Now is a good time to introduce some

non-dimensional variables for time and space. Throughout the rest of this thesis a prime superscript will denote non-dimensional groupings.

$$t' = \frac{c_0 t}{2L} \tag{2.60}$$

$$x' = \frac{x}{L} \tag{2.61}$$

In Eq. (2.60) time has been normalized by the period of the fundamental mode in the classical acoustic limit while the spatial coordinate (2.61) has been normalized by the length of the combustor.

Before non-dimensionalizing Eq. (2.48) the equation should be rewritten as a function of a single state variable. Currently, it is a function of both the temporal response of the pressure and velocity; however, they can be converted between each other by using the proper constitutive relation (2.44). Pressure is the state variable of greatest interest but mathematical reasons exists for why an equation in velocity is preferable. An equation in pressure would end up being a functional integro-differential equation. Integrals would also appear in an expression for the acoustic energy which is undesirable from a control theory point of view; therefore, the work in this thesis will be easier to build upon if it uses a velocity equation.

Inspection of the non-dimensional equation for the velocity temporal response shows that it is an infinite set of coupled oscillators. In particular, it is a system of linear stochastic retarded delay differential equations with time delayed feedback.

$$\begin{aligned} &\chi_n^{(5)}(t') + \omega_n'^2 \ddot{\chi}_n(t') + \left(\sum_{i=0}^{5} \sum_{m=1}^{\infty} C_{i,n,m} \frac{\partial^i \chi_m(t')}{\partial t'^i} \right) = \\ &F_V'(t') + F_\phi'(t') + \sigma_n \xi_n(t') \end{aligned} \tag{2.62}$$

$$\begin{aligned} F_V'(t') = -\frac{n_C}{\tau_V'} \sum_{m=1}^{\infty} \Bigg[&\left(\ddot{\chi}_m(t') - \frac{1}{\tau_V'} \left(\dot{\chi}_m(t') - \dot{\chi}_m(t' - \tau_V') \right) \right) \psi_n(x_f') \nabla' \psi_m(x_f') \\ &-2M \left(\dot{\chi}_m(t') - \frac{\chi_m(t') - \chi_m(t' - \tau_V')}{\tau_V'} \right) \nabla' \psi_n(x_f') \nabla' \psi_m(x_f') \Bigg] \end{aligned} \tag{2.63}$$

$$
\begin{aligned}
F'_{\phi}(t') = -M\frac{n_C\beta^2}{\tau'_V}\Bigg[& -\frac{n_S}{\tau'_V\left(\beta^2-1\right)}\frac{\partial}{\partial t'}u\left(t'-\tau'_A-\tau'_V\right)\psi_n\left(x'_f\right) \\
& +\beta^2\frac{\left(\beta^2-1\right)n_H+\beta^2 n_S}{\tau'_V\left(\beta^2-1\right)}\frac{\partial}{\partial t'}u\left(t'-\tau'_A-\frac{\tau'_V}{\beta^2}\right)\psi_n\left(x'_f\right) \\
& +\left(\left(n_H+n_S\right)\frac{\partial^2}{\partial t'^2}u\left(t'-\tau'_A\right)-\frac{\left(1+\beta^2\right)n_S+\beta^2 n_H}{\tau'_V}\frac{\partial}{\partial t'}u\left(t'-\tau'_A\right)\right)\psi_n\left(x'_f\right) \\
& +2\left(\frac{Mn_S}{\tau'_V\left(\beta^2-1\right)}u\left(t'-\tau'_A-\tau'_V\right)-M\left(n_H+n_S\right)\frac{\partial}{\partial t'}u\left(t'-\tau'_A\right)\right)\nabla'\psi_n\left(x'_f\right) \\
& +2M\frac{\left(1+\beta^2\right)n_S+\beta^2 n_H}{\tau'_V}u\left(t'-\tau'_A\right)\nabla'\psi_n\left(x'_f\right) \\
& -2\beta^2 M\frac{\left(\beta^2-1\right)n_H+\beta^2 n_S}{\tau'_V\left(\beta^2-1\right)}u\left(t'-\tau'_A-\frac{\tau'_V}{\beta^2}\right)\nabla'\psi_n\left(x'_f\right)\Bigg]
\end{aligned}
\tag{2.64}
$$

For convenience the non-dimensional volumetric heat release perturbations have been collected together based upon if they belong to the internal (2.63) or external feedback loop (2.64) in Figure 2-2 while several common non-dimensional groupings in Eq. (2.62) are redefined as new non-dimensional parameters. The combustion noise is also explicitly written as the product of a unit variance process and a scaling constant.

$$
n_C = \left(8\frac{\Delta T}{T_0}\frac{S_{noz}}{S_{comb}}\right) \tag{2.65}
$$

$$
\omega'_n = 2\pi n \tag{2.66}
$$

$$
C_{i,n,m} = -4\frac{S_{noz}}{S_{comb}}\left(\frac{c_0}{2L}\right)^{i-2}\left(C_i(L)(-1)^{n+m}-C_i(0)\right)\omega'^2_m \tag{2.67}
$$

At certain junctures within this thesis Eq. (2.62) will be more amendable to analysis if it is in state space form.

$$
\begin{aligned}
\dot{\vec{x}}\left(t'\right) = {} & A_0\vec{x}\left(t'\right)+A_1\vec{x}\left(t'-\tau'_V\right)+B_1\vec{u}\left(t'-\tau'_A\right) \\
& +B_2\vec{u}\left(t'-\tau'_A-\frac{\tau'_V}{\beta^2}\right)+B_3\vec{u}\left(t'-\tau'_A-\tau'_V\right)+\Omega\vec{\xi}\left(t'\right)
\end{aligned}
\tag{2.68}
$$

$$\vec{x}(t') = \left[\chi_1(t') \quad \dots \quad \chi_n(t') \mid \quad \dots \quad \mid \ddot{\chi}_1(t') \quad \dots \quad \ddot{\chi}_n(t') \right]^T \tag{2.69}$$

$$\vec{u}(t') = \left[u(t') \quad \dot{u}(t') \quad \ddot{u}(t') \right]^T \tag{2.70}$$

$$\vec{\xi}(t') = \left[\xi_1(t') \quad \dots \quad \xi_n(t') \right]^T \tag{2.71}$$

$$A_0 = \begin{bmatrix} 0_n & I_n & 0_n & 0_n & 0_n \\ 0_n & 0_n & I_n & 0_n & 0_n \\ 0_n & 0_n & 0_n & I_n & 0_n \\ 0_n & 0_n & 0_n & 0_n & I_n \\ -\tilde{C}_0 - 2\frac{M}{\tau_V'}\tilde{S}_2 & -\tilde{C}_1 + \frac{1}{\tau_V'}\tilde{S}_1 + 2M\tilde{S}_2 & -\tilde{C}_2 - \tilde{S}_1 & -\tilde{C}_3 - I_n\tilde{W} & -\tilde{C}_4 \end{bmatrix} \tag{2.72}$$

$$\tilde{C}_i = \begin{bmatrix} C_{i,1,1} & C_{i,1,2} & \cdots \\ C_{i,2,1} & C_{i,2,2} & \ddots \\ \vdots & \ddots & \ddots \end{bmatrix} \tag{2.73}$$

$$\tilde{W} = \left[\omega_1'^2 \quad \omega_2'^2 \quad \cdots \quad \omega_n'^2 \right]^T \tag{2.74}$$

$$\tilde{S}_1 = \frac{n_C}{\tau_V'} \begin{bmatrix} \psi_1(x_f') \\ \vdots \\ \psi_n(x_f') \end{bmatrix} \begin{bmatrix} \nabla'\psi_1(x_f') \\ \vdots \\ \nabla'\psi_n(x_f') \end{bmatrix}^T \tag{2.75}$$

$$\tilde{S}_2 = \frac{n_C}{\tau_V'} \begin{bmatrix} \nabla'\psi_1(x_f') \\ \vdots \\ \nabla'\psi_n(x_f') \end{bmatrix} \begin{bmatrix} \nabla'\psi_1(x_f') \\ \vdots \\ \nabla'\psi_n(x_f') \end{bmatrix}^T \tag{2.76}$$

$$\tilde{S}_3 = M\beta^2 \frac{n_C}{\tau_V'} \begin{bmatrix} \psi_1(x_f') \\ \vdots \\ \psi_n(x_f') \end{bmatrix} \tag{2.77}$$

$$\tilde{S}_4 = M\beta^2 \frac{n_C}{\tau_V'} \begin{bmatrix} \nabla'\psi_1(x_f') \\ \vdots \\ \nabla'\psi_n(x_f') \end{bmatrix} \tag{2.78}$$

$$A_1 = \begin{bmatrix} 0_n & 0_n & 0_n & 0_n & 0_n \\ 0_n & 0_n & 0_n & 0_n & 0_n \\ 0_n & 0_n & 0_n & 0_n & 0_n \\ 0_n & 0_n & 0_n & 0_n & 0_n \\ 2\frac{M}{\tau_V'}\tilde{S}_2 & -\frac{1}{\tau_V'}\tilde{S}_1 & 0_n & 0_n & 0_n \end{bmatrix} \tag{2.79}$$

$$B_1 = \begin{bmatrix} 0_{nx1} & 0_{nx1} & 0_{nx1} \\ 0_{nx1} & 0_{nx1} & 0_{nx1} \\ 0_{nx1} & 0_{nx1} & 0_{nx1} \\ 0_{nx1} & 0_{nx1} & 0_{nx1} \\ \frac{\left(1+\beta^2\right)n_S + \beta^2 n_H}{\tau_V'}\left(\tilde{S}_3 - 2M\tilde{S}_4\right) & 2\left(n_H + n_S\right)M\frac{n_C}{\tau_V'}\tilde{S}_4 & -\left(n_H + n_S\right)\tilde{S}_3 \end{bmatrix} \tag{2.80}$$

$$B_2 = \begin{bmatrix} 0_{nx1} & 0_{nx1} & 0_{nx1} \\ 0_{nx1} & 0_{nx1} & 0_{nx1} \\ 0_{nx1} & 0_{nx1} & 0_{nx1} \\ 0_{nx1} & 0_{nx1} & 0_{nx1} \\ 2\beta^2 M\frac{\left(\beta^2-1\right)n_H + \beta^2 n_S}{\tau_V'\left(\beta^2-1\right)}\tilde{S}_4 & -\beta^2\frac{\left(\beta^2-1\right)n_H + \beta^2 n_S}{\tau_V'\left(\beta^2-1\right)}\tilde{S}_3 & 0_{nx1} \end{bmatrix} \tag{2.81}$$

$$B_3 = \begin{bmatrix} 0_{nx1} & 0_{nx1} & 0_{nx1} \\ 0_{nx1} & 0_{nx1} & 0_{nx1} \\ 0_{nx1} & 0_{nx1} & 0_{nx1} \\ 0_{nx1} & 0_{nx1} & 0_{nx1} \\ -2\frac{Mn_S}{\tau_V'\left(\beta^2-1\right)}\tilde{S}_4 & \frac{n_S}{\tau_V'\left(\beta^2-1\right)}\tilde{S}_3 & 0_{nx1} \end{bmatrix} \tag{2.82}$$

$$\Omega = \begin{bmatrix} 0_n & 0_n & 0_n & 0_n & \begin{bmatrix} \sigma_1 & 0 & \cdots \\ 0 & \sigma_2 & \ddots \\ \vdots & \ddots & \ddots \end{bmatrix}^T \end{bmatrix} \tag{2.83}$$

2.7 Sensors and Actuators

So far the wave equation has been split into a coupled set of spatially averaged time delayed stochastic oscillators. In terms of the modeling process illustrated in

Figure 2-1 the governing equations have been mathematically simplified to increase their solvability while trying to preserve their physical consistency. The next step is to begin developing analysis design tools but before that can be done the system inputs and outputs in Figure 2-2 need to be defined. Ideally, the sensor should measure a linear functional of the state variables. Similarly, the actuator should act on a linear functional of the state variables. This ensures that the design tools developed are easily accessible and does not require modification of the governing equations. Insight on what to choose for a sensor/actuator combination and how to incorporate then into an input-output model can be gleamed from looking at the historic progression of sensor/actuator pairs used in the feedback control of combustion instabilities.

When feedback control of combustion instabilities was a young discipline the state of development of sensors and actuators for applications in gas turbine combustors was immature. As a result, early experiments relied heavily on sensors and actuators from the automotive industry.[138] Since then increased interest has developed for improving gas turbine sensors and actuators to understand and suppress a plethora of problems,[139] of which combustion instabilities are a subset. This lead to a wider selection of possible sensors tailored for gas turbine engines and fuel actuators with improved bandwidth and authority. Most improvements in sensor development have been done with an eye towards improving diagnostic capabilities but not every diagnostic sensor is a suitable choice for a control sensor.

A control sensor should be noninvasive; it should not interfere with how the system is operating nor force a major redesign to incorporate it. In gas turbine combustors a control sensor needs to be light weight and low volume, particularly in aircraft engines. Additionally, the control sensor needs to be able to withstand high temperatures and pressures. Collectively, these restraints prevent the use of sensors that measure velocity and other laser based means of measurement because they are too bulky and costly. Other sensors such as ion probes and fiber optics are measuring phenomena

associated with heat release, but this is not a function of the state variables and would require more explicit modeling of chemical kinetics. In the thermo-acoustic model used in this thesis the effects of chemical kinetics are hidden within the mean volumetric heat release rate and associated sensitivities in the volumetric heat release perturbation models introduced in §2.4.1. By process of elimination the only remaining physical quantity of interest that is a state variable is the pressure.

Most feedback control systems for combustion instabilities rely upon microphones measuring the sound radiated from the combustion chamber, a practice that dates back to Heckl's thesis.[34] A microphone is impractical beyond the laboratory setting because it cannot withstand the high pressure and temperatures of a combustor and takes the pressure measurement outside of the modeled domain. An ideal sensor should measure the pressure at a given location in the combustor, x_s, and may be contaminated by sensor noise, ξ_s, as shown in Eq. (2.84).

$$y(t) = p_0 \sum_{m=1}^{\infty} \eta_m(t) \psi_m(x_s) + \sigma_s \xi_s(t) \tag{2.84}$$

Pressure transducers come much closer to this ideal and have seen successful implementation in industry. While pressure transducers can withstand elevated temperatures typical flame temperature still exceeds what a pressure transducer can withstand. In practice, combustors are modified with stand-off tubes so that the pressure transducer can operate in a lower temperature environment, but this introduces frequency distortion effects such that Eq. (2.84) is not what is actually being measured.[140] A stand-off tube has its own resonance frequency which can introduce low frequency dynamics. For actual experiments the sensor output should probably be band-pass filtered.

Choosing a fuel actuator is much easier because the dominating criterion is the required bandwidth and authority of the actuator. The first feedback control experiments[35] using equivalence ratio modulation had on-off automotive fuel injectors

with a bandwidth of approximately 150 *Hz*. Besides distorting the waveform into approximately a square wave, these early actuators can have a hard time matching the frequency of the combustion instability. In gas turbine power applications combustion instabilities can range from the low tens of hertz to a few hundred hertz while the fundamental longitudinal instability can easily be half a kilohertz in an aircraft engine. This means fuel actuator bandwidth is a critical issue and can be a particularly severe constraint on control system operation especially when higher harmonics are present in the SPL. Modern fuel actuators are now approaching this range. Siemens[40] used a direct-drive valve with a bandwidth of approximately 450 *Hz* while GaTech[141] and Goodrich[142] have both developed actuators that can reach 1 *kHz*. The price paid for high bandwidth is low actuation amplitudes. Fortunately, most experimental work shows equivalence ratio modulations only need to be a few percent of the mean equivalence ratio, although exceptions exist when limit cycles are present such as in dump combustors.[143] UTRC developed a high authority spinning valve for this circumstance.[144]

A mismatch will always exist between what the sensors and actuators are supposed to do versus what they actually do. Increasing the complexity of the thermo-acoustic modeling can incorporate these effects but this conflict with the modeling goal of mathematical simplicity for analytical tractability and drawing physical insight into the system behavior. The difference between real and ideal components can be cast as a problem in constrained and unconstrained control. When control design is constrained certain behaviors in the state space are forbidden when designing the control law to match shortcomings in the modeling. For example, a bandwidth constraint on a fuel actuator translates into enforcing a gain of zero in the control law transfer function for frequencies above the actuator cutoff frequency. In the next chapter of this thesis the focus will be placed upon understanding the behavior of the unconstrained problem because mastery of the ideal feedback control of combustion instabilities is a prerequisite for understanding real systems.

2.8 Definitions of State

Before moving into how to analyze the governing equations (2.68) a more fundamental question of how to interpret these equations needs to be investigated. Akin to ordinary differential equations an initial state needs to be specified so that the future behavior is completely defined for all time, provided that all future inputs are known. For the non-mathematician this translates into asking: what is the minimum amount of information, called the state, which is needed to uniquely determine the system's future behavior? This is not a trivial question because it requires understanding the mathematical properties of the state. In turn, this has profound implications for how the governing equations (2.68) are analyzed because it defines the space of the system response.

The initial state for ordinary differential equations is the finite dimensional Euclidean space of real numbers, $\mathbb{R}^n$, because only information about the present is needed to predict the future. Time delay systems are more complicated because information about the past is needed in addition to information about the present to predict the future. Furthermore, the information needed about the past changes with time such that the state is not just a collection of state behavior at individual points in time but instead is a continuum of state behavior in time. This simple fact gives time delay systems their infinite dimensionality.

Early work in time delay system by Bellman and Cooke[80] and Hale and Lunel[81] used the space of continuous functions, $C([-\tau_{max},0],\mathbb{R}^n)$, which is a Banach space. While such a formulation is sufficient to study stability, the space of continuous functions is not a Hilbert space, and hence, denies the control engineer the use of the inner product needed for geometric interpretations. The additional simplicity induced in mathematical proofs by the inner products helps address the accessibility problem introduced in §2.1 concerning the exchange of information between acoustic, combustion, and control

engineers. Typically, of these three types of engineers, only the control engineer is likely to have the functional analysis background to analyze the behavior of Banach spaces.

The completion of a Banach space will result in a Hilbert space. Coleman and Mitzel[145] purposed using the completion of the space of continuous functions to study differential delay equations which yields the Lebesgue space of square-integrable functions $\mathbb{L}^2([-\tau_{max},0],\mathbb{R}^n)$. Even this choice of state space would prove awkward in formulating the Cauchy problem and the optimal control problem. The weights on the cost function used in optimal control tend to be evaluated only in the present. Delfour and Mitter[146] proposed adding this point to the state space by using the Cartesian product of two Hilbert spaces: $\mathbb{M}^2([-\tau_{max},0],\mathbb{R}^n) = \mathbb{R}^n \times \mathbb{L}^2([-\tau_{max},0],\mathbb{R}^n)$, which is aptly named the product space approach.

This idea of adding a point to a Lebesgue space was conceived multiple times independently in slightly different contexts;[83] however, the notation introduced by Delfour and Mitter[146] was the one to survive. Part of the inspiration leading to this came from Lions[147] who set up partial differential equations as an abstract operator equation. Using the product space approach, a time delay system takes the form of an abstract operator differential equation. Eventually this would lead to a general framework for infinite dimensional linear systems theory.[84] The same tools under a similar methodology of thought used for linear partial differential equations can be used for linear delay systems.

By itself, the product space approach allows the control engineer to analyze and synthesize controllers for a large class of time delay systems, but complications arise when time delays are in the system input. To put this class of delay systems into the product space framework the form of the controller must be known *a priori*. Clearly, this forbids the use of the product space approach for controller synthesis when input delays exists. Ichikawa[148] addressed this by adding the control input history to the product space which creates the extended state space $\mathbb{M}^2([-\tau_1,0],\mathbb{R}^n) \times \mathbb{L}^2([-\tau_2,0],\mathbb{R}^n)$. Intuitively, this

makes sense. As control is applied the system has not yet responded to a period of previously applied controls. By the time the system reacts to the present control input it has already responded to all previous control inputs; therefore, the previous control input needs to be taken into account for control synthesis.

This thesis will switch between the product space and the extended state space approach as convenient depending if control analysis or synthesis is required. Additional definitions of state exist as well as further extensions of the extended state space concept. The monograph by Bensoussan et al.[83] provide a healthy sampling of these, but they are not needed for the contents of this thesis. In the next chapter a set of analysis tools will be formulated for the thermo-acoustic model derived in this chapter with the goal of reproducing some of the unexplained behaviors discussed in Chapter 1. Definitions of state will prove to be crucial to interpreting the results of these new analysis tools.

CHAPTER 3

SYSTEM PERFORMANCE

Predictions made by thermo-acoustic models have not been historically successful in predicting system performance prior to running an experiment. In Chapter 2 an increased emphasis on physical realizability and mathematical analyzability in thermo-acoustic modeling was made in an attempt to increase model fidelity. The next step in this process, dictated by Figure 2-1, is to develop new analysis tools that can handle arbitrarily large time delays and compare the results of these analyses to pre-existing experimental data. Once the new thermo-acoustic model is verified to be an improvement this thesis will be ready to look at the factors that limit control effectiveness in the next chapter. To accomplish this task this chapter develops two sets of tools using probability density functions (pdf) and spectral methods. Having pdf's of physical quantities is more natural for the combustion engineer to use because this set of mathematical tools overlaps with what an engineer with a background in turbulent flows would use. Unfortunately, limits exist for what is easily analyzable with pdf's. Spectral methods can cover a larger set of problems with less effort and matches the mathematical tool set a control engineer would possess. A key goal of this chapter is to create enough overlap between these two methods to give the combustion engineer access to stronger mathematical tools and give the control engineer access to stronger physical insight of thermo-acoustic behavior. Additionally, these tools are applied to explain trends in the performance of controlled and uncontrolled self-excited, noise driven, combustors.

3.1 Prototype Equations

In many ways trying to find an exact closed form analytic solution to an infinite set of linearly coupled stochastic delay differential equations is a fruitless undertaking.

The mathematical system of interest contains an infinite number of oscillators which are individually infinite dimensional due to the presence of time delays. Furthermore, the mathematical theory for these systems is incomplete and an active area of research.[46] Analysis will need to be coupled with numerical methods for an engineer to make meaningful progress; however, this impedes the ability to draw meaningful physical insight and may force the application of additional assumptions to make the thermo-acoustic model fit within a framework where the available mathematical tools work. This means certain arguments will have to be based on analogy. Looking at prototype equations that are as close as possible to the governing equations but solvable is useful in building mathematical and physical intuition to make responsible simplifying assumptions and to aid the interpretation of results. The objective of this section is to relate the eigenvalues of the deterministic systems to the statistics that describe stochastic behavior.

Mathematicians like to distinguish between weak and strong solutions in stochastic systems.[128] A strong solution is the actual path the output process takes but this is unknowable in practice because the exact path-wise realization of the driving noise process is never available. Instead, a weak solution, the pdf, is used which allows for any possible realization of the driving noise process. This means that a good prototype equation will be solvable for the pdf of the system response and its statistics. Looking at linear stochastic first and second order differential equations without time delays is a good starting point because some infinite dimensional system can be thought of as an infinite set of coupled finite dimensional oscillators.

The simplest possible stochastic differential equation is the Langevin's equation,[149] associated with the Ornstein-Uhlenbeck process,[124] where $W(t)$ is a Wiener process.[125]

$$dX(t) = -\frac{1}{\tau_{rel}} X(t)\,dt + \sigma dW(t) \tag{3.1}$$

On the right hand side of Eq. (3.1) the first term is deterministic and called the drift term while the second term is stochastic and called the diffusion term. In this equation the relaxation time, τ_{rel}, determines the eigenvalue of the deterministic system, $-1/\tau_{rel}$, and the cutoff frequency in the power spectrum, $1/2\pi\tau_{rel}$, which gives the process its characteristic low-pass filter behavior scaled by the standard deviation of the noise process, σ. Since this is a linear system driven by a Gaussian process the state process, $X(t)$, is also Gaussian process.[121] All that is needed to define the stochastic system response are the time history of the mean and variance of the state.

Solving for the first two moments of $X(t)$ starting from a stationary position, X_0, requires solving the expectation of $X(t)$ in Langevin's equation (3.1) and an equation for $X^2(t)$. Forming the stochastic differential equation for the second moment requires an application of the stochastic chain rule, also known as Itô's formula.[128] The resulting equations are easily solvable because they are linear differential equations.

$$\left\langle X(t)\right\rangle = X_0 e^{-\frac{t}{\tau_{rel}}} \tag{3.2}$$

$$Var\left(X(t)\right) = \frac{\sigma\tau_{rel}}{2}\left(1 - e^{\frac{-2t}{\tau_{rel}}}\right) \tag{3.3}$$

Inspection of the mean (3.2) and variance (3.3) show that decreasing the relaxation time causes shorter transient responses, improves the steady state response, and moves the eigenvalue of the deterministic system deeper into the left hand complex plane (LHCP).

A stochastically driven second order damped oscillator is the simplest prototype equation to analyze to develop an understanding of how a complex conjugate pair of eigenvalues affects stochastic behavior

$$d\vec{X}(t) = \begin{bmatrix} 0 & 1 \\ -\omega^2 & -2\zeta\omega \end{bmatrix}\vec{X}(t)\,dt + \begin{bmatrix} 0 \\ \sigma \end{bmatrix} dW(t) \tag{3.4}$$

Equation (3.4) was first solved by Stratonovich[150] using the Fokker-Planck equation[151] which describes the evolution of the pdf of a Markovian, or memoryless, process.

Looking at Eq. (3.4) in an amplitude phase space is physically more appealing because it behaves like an oscillator. This transformation, given below, comes from Kryloff and Bogoliuboff,[152] but the explanation of its rationale will have to wait until the next section.

$$\vec{X}(t) = \begin{bmatrix} R(t)\sin\theta(t) \\ \omega R(t)\cos\theta(t) \end{bmatrix} \tag{3.5}$$

The steady state joint pdf for amplitude, $R(t)$, and total phase, $\theta(t)$, was solved by Stratonovich using the method of stochastic averaging.[153] A full transient response is also available from Solomos and Spanos;[154] however, discussion in this thesis will only require the steady state solution.

$$f_{ss}(R,\theta) = \frac{1}{2\pi}\frac{R}{\sigma_{ray}^2} e^{-\frac{R^2}{2\sigma_{ray}^2}} \tag{3.6}$$

$$\sigma_{ray} = \sqrt{\frac{\sigma^2}{4\zeta\omega^3}} \tag{3.7}$$

In this steady state limit amplitude and phase behave as independent random variables in with their marginal pdf respectively a Rayleigh and a circular uniform pdf. Everything about the system response can be distilled into the Rayleigh parameter, σ_{ray} (3.7), which is the mode of the amplitude. Damped harmonic oscillators (3.4) also have a relaxation time, $1/\zeta\omega$, which plays a similar role as in Langevin's equation (3.1) in improving the system response as the relaxation time is decreased. Another useful parameter is the DC offset (response at zero frequency) in the power spectrum which scales to ω^{-4}. When the DC offset decreases so too does the Rayleigh parameter.

The relaxation time and the DC offset in the power spectrum directly affect the eigenvalues of the deterministic version of Eq. (3.4): $-\zeta\omega \pm i\omega\sqrt{(1-\zeta^2)}$. As the relaxation time decreases the eigenvalues are pushed farther in the LHCP as long as the oscillator remains under-damped. Decreasing the DC offset in the power spectrum also pushes the eigenvalues deeper into the LHCP while increasing the damped natural frequency. From

a control prospective increasing the frequency can be undesirable, despite its helpful influence on the Rayleigh parameter, because a higher bandwidth actuator is required and higher frequency combustion instability responses are more damaging to the combustor liner. The lesson that can be inferred from Langevin's equation (3.1) and the damped second order oscillator (3.4) is that performance in linear stochastic systems is related to how far the eigenvalues are in the LHCP, at least for memoryless systems.

When time delays are added to a system the output process is no longer Markovian which prevents the use of the Fokker-Planck method. Furthermore, the statistics of a stochastic delay differential equation can only be solved in increments in time equal to the smallest time delay. This is called the method of steps.[80] A time delayed version of Langevin's equation[155] is the only known stochastic delay differential equation that has a closed form steady state solution for its statistics.

$$dX(t) = aX(t)dt + bX(t-\tau)dt + \sigma dW(t) \tag{3.8}$$

$$d\langle X(t)\rangle = a\langle X(t)\rangle dt + b\langle X(t-\tau)\rangle dt \tag{3.9}$$

$$d\langle X^2(t)\rangle = 2a\langle X^2(t)\rangle dt + 2b\langle X(t)X(t-\tau)\rangle dt + \sigma^2 dt \tag{3.10}$$

Clever exploitation of steady state symmetry properties yields an ordinary differential equation on the interval $[0,\tau]$ for the steady state covariance function which is easily solvable.[155] The solution, given below, is valid only when the mean response of Eq. (3.8) is exponentially stable.

$$Var_{ss}(X(t)) = \begin{cases} \sigma^2 \dfrac{b\sinh(d\tau) - d}{2d(a + b\cosh(d\tau))} & |b| < -a \\ \sigma^2 \dfrac{b\tau - 1}{4b} & b = a \\ \sigma^2 \dfrac{b\sin(d\tau) - d}{2d(a + b\cos(d\tau))} & b < -|a| \end{cases} \tag{3.11}$$

$$d^2 = |a^2 - b^2| \tag{3.12}$$

Before looking at trends in the variance the region of stability of the mean response (3.9) is needed. Fortuitously, the deterministic equation (3.9) has been heavily studied and the region of stability, S, is well known.[156]

$$\mathrm{S} = \left\{ (a\tau, b\tau) : b\tau < a\tau \quad \& \quad b\tau > C_0 \right\} \tag{3.13}$$

$$C_0 = \left\{ (a\tau, b\tau) = \left(\kappa \cot(\kappa), -\kappa \csc(\kappa) \right) \forall \kappa \in [-\pi, \pi] \right\} \tag{3.14}$$

A contour plot of the inverse of the variance of Eq. (3.8) for the fixed product $\sigma\tau$ is shown in Figure 3-1. As the system parameters are moved deeper into the region of stability the variance decreases. This is accomplished by decreasing $a\tau$ and $|b\tau|$.

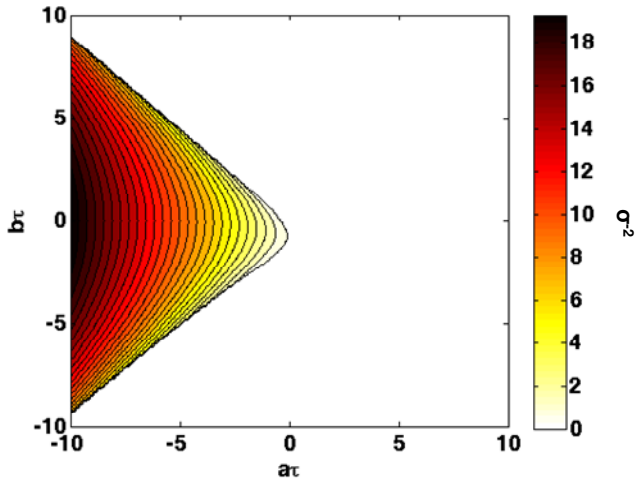

Figure 3-1: Contour plot for the inverse of the variance of the delayed Langevin's equation at στ = 1.

Trying to compare trends in the variance to the behavior of the eigenvalues of Eq. (3.8) is very difficult because an exact explicit analytical expression of all the eigenvalues for any differential delay equation does not currently exist; although, methodologies do exist to determine when eigenvalues cross the imaginary axis in the complex plane as equation parameters are varied.[157] Numerical routines offer an efficient way to understand the spectra of time delay systems. The governing equations can be viewed as an abstract operator differential equation. By using a finite dimensional

approximation of the infinitesimal generator standard eigenvalue analysis tool can be applied to the resulting high dimensional ordinary differential equation. More complete details about how this works is found in Appendix A. Another point of consternation is how to know what to look for in the infinite number of eigenvalues that reveal meaningful performance trends and is easily extractable. In the previous prototype equations understanding the relaxation time was very important. This suggests that the rightmost eigenvalue in the complex plane, or the spectral abscissa, might be a good candidate for comparison with the variance.

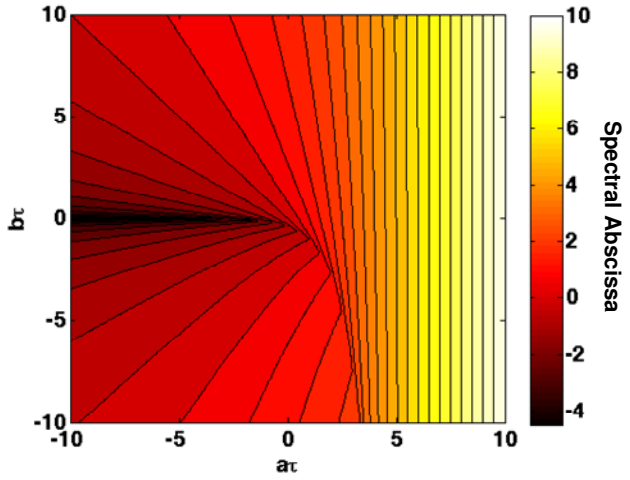

Figure 3-2: Contour plot for the spectral abscissa of the delayed Langevin's equation.

A contour plot of the spectral abscissa of Eq. (3.8) using a pseudospectral method[85] is shown in Figure 3-2. Just like in Figure 3-1, the spectral abscissa is decreasing as the system parameters are moved deeper in the region of stability by decreasing $a\tau$ and $|b\tau|$. The trends in the spectral abscissa agree with the trends in the variance but they do not agree on what trend is best. Figure 3-1 indicates that the best performance gains come from decreasing $a\tau$ while Figure 3-2 suggests that this comes from decreasing $|b\tau|$. Clearly, the spectral abscissa is a decent figure of merit but should not be used as a direct substitute for the variance.

Spectral abscissa should be viewed as a measure of stability margin instead of performance. A very explicit example of comes from comparing the spectral abscissa and the Rayleigh parameter of the second order damped oscillator driven by noise (3.4). The spectral abscissa is $-\zeta\omega$ while the Rayleigh parameter (3.7) depends upon $\zeta\omega^3$. As a result, there is a collection of values for the damping coefficient and natural frequency that yields the same spectral abscissa but very different Rayleigh parameters. Only if the natural frequency is held fixed in this example can the spectral abscissa be viewed as an indicator or performance instead of stability margin.

Studying a more complicated prototype equation will require numerical methods for both the variance and the eigenvalues which lead to diminishing returns for trying to draw physical and mathematical incite. The easiest thing to look at is the stability boundary. Hsu and Bhatt[158] studied the damped harmonic oscillator with time delay in both the frequency and damping term. In their equations time has been normalized such that the magnitude of the time delay is one.

$$\ddot{X}(t) + 2\zeta\omega\dot{X}(t) + \omega^2 X(t) + c_n X^{(n)}(t-1) = 0 \tag{3.15}$$

Generally, increasing the damping coefficient widens the stability boundaries while increasing the magnitude of the coefficient in front of the time delay term is destabilizing. A change in the frequency causes oscillatory changes in the stability boundaries.

3.2 Probability Density Function Response

Analytical work that views combustion instabilities through a probabilistic lens is very rare. Part of the reason for this is that the theory for combustion noise is so incomplete that the community's focus has been placed on understanding the source terms instead of their effect on the acoustics in the combustor. Burnley[117] is the first person to look at the pdf response of combustion instabilities, but the results are purely numerical because the effects of nonlinear acoustics was included in the thermo-acoustic model used. Numerically simulating a linear stochastic differential equation[128] until it

reaches a steady state just to get one data point needed for the construction of a pdf is not the most efficient use of computational resources. If the response pdf type is known then much faster methods are available to solve for that statistics instead using the non-unitary Fourier transform.

$$\mathcal{F}\left[f(t)\right]=\int_{-\infty}^{\infty} f(t)\exp(jvt)\,dt \qquad \mathcal{F}^{-1}\left[f(v)\right]=\frac{1}{2\pi}\int_{-\infty}^{\infty} f(v)\exp(-jvt)\,dv \tag{3.16}$$

The covariance matrix Σ of a process can be solved directly by taking the inverse Fourier transform of the power spectral density matrix Φ (Wiener-Khinchin Theorem).[159]

$$\sum=\mathcal{F}^{-1}\Phi \tag{3.17}$$

This approach is used by UTRC[59] to look at experimental data of a combustor driven by combustion noise. An earlier analytical investigation from Crawford and Lieuwen[160] uses the thermo-acoustic model from Chapter 2 of this thesis in the limit of no mean flow and truncated to one mode shape to look at performance trends. All the work in this subsection is the generalization of this previous work to the full thermo-acoustic model in this thesis.

Using the same arguments as in §2.4.2 the output of linear system with Gaussian input must be Gaussian. This transforms the problem of solving for the pdf response of the thermo-acoustic model (2.62) into one of solving for its statistics. The steady state mean of a stable linear autonomous system is always zero; therefore, only the variance needs to be solved to fully define the output pdf. Time can be saved from unnecessary calculations by knowing when the variance is stable. Appendix B shows for a linear stochastic system that exponential stability in the mean implies the existence of a steady state variance. An alternative proof is provided by Liu.[116]

Taking the non-unitary Fourier transform of the thermo-acoustic model (2.62) creates a transfer function between the n velocity temporal responses and n noise inputs. For compactness the control input has been assumed to be an arbitrary functional of the state and the matrix notation from §2.6 is reused.

$$\hat{A}(\upsilon)\hat{\vec{\chi}}(\upsilon)=\hat{\Omega}(\upsilon)\hat{\vec{\xi}}(\upsilon) \tag{3.18}$$

$$\hat{\vec{\chi}}(\upsilon)=\mathcal{F}\left[\chi_1(t') \quad \ldots \quad \chi_n(t')\right]^T \tag{3.19}$$

$$\hat{\vec{\xi}}(\upsilon)=\mathcal{F}\vec{\xi}(t') \tag{3.20}$$

$$\begin{aligned}\hat{A}(\upsilon)=&\left(i\upsilon^5\right)I_n-\left[0_n \quad 0_n \quad 0_n \quad 0_n \quad I_n\right]\left[A_0-e^{-i\upsilon\tau_V'}A_1\right]\begin{bmatrix} I_n \\ i\upsilon I_n \\ -\upsilon^2 I_n \\ -i\upsilon^3 I_n \\ \upsilon^4 I_n \end{bmatrix} \\ &-\left[0_n \quad 0_n \quad 0_n \quad 0_n \quad I_n\right]\left[e^{-i\upsilon\tau_A'}B_1+e^{-i\upsilon\left(\tau_A'+\frac{\tau_V'}{\beta^2}\right)}B_2+e^{-i\upsilon(\tau_A'+\tau_V')}B_3\right]\begin{bmatrix} 1 \\ i\upsilon \\ -\upsilon^2 \end{bmatrix}K(\upsilon)\end{aligned} \tag{3.21}$$

$$\hat{\Omega}(\upsilon)=\left[0_n \quad 0_n \quad 0_n \quad 0_n \quad I_n\right]\Omega \tag{3.22}$$

If Eq. (3.18) is multiplied by its complex conjugate, denoted by $(\cdot)^*$, then the resulting equation is a transfer matrix of the power spectrum of the noise, provided by the user, to the power spectrum of the velocity temporal response.

$$\Phi_{\chi\chi}(\upsilon)=\hat{A}^{-1}(\upsilon)\Phi_{\Omega\Omega}(\upsilon)\hat{A}^{-*}(\upsilon)=\hat{A}^{-1}(\upsilon)\hat{\Omega}(\upsilon)\Phi_{\xi\xi}(\upsilon)\hat{\Omega}^*(\upsilon)\hat{A}^{-*}(\upsilon) \tag{3.23}$$

Building a pdf for the pressure response (2.44) will also require information about the derivatives of χ_n. This suggests that a joint pdf for χ_n and its derivative for all modes shapes would be a good cornerstone for deriving new pdfs of interest. For future convenience, the derivative of χ_n will be normalized by ω'_n, because it simplifies future analysis when working in the amplitude-phase probability space.

Augmenting the power spectrum in Eq. (3.23) to account for the additional variables just mentioned can be done by just applying the definition of the Fourier transform of a derivative. The new random variables X_n and Y_n are χ_n and their normalized derivative respectively while the vector Z will refer to the collection of all of these variables.

$$\Phi_{ZZ}(\upsilon) = F_Z(\upsilon)\Phi_{\chi\chi}(\upsilon)F_Z^*(\upsilon) \tag{3.24}$$

$$F_Z(\upsilon) = \begin{bmatrix} 1 & \frac{i\upsilon}{2\pi} & 0 & 0 & \cdots & 0 & 0 \\ 0 & 0 & 1 & \frac{i\upsilon}{2\pi * 2} & \cdots & 0 & 0 \\ \vdots & \vdots & \vdots & \vdots & \ddots & \vdots & \vdots \\ 0 & 0 & 0 & 0 & \cdots & 1 & \frac{i\upsilon}{2\pi n} \end{bmatrix}^T \tag{3.25}$$

$$Z = \begin{bmatrix} X_1 & Y_1 & \ldots & X_n & Y_n \end{bmatrix}^T \tag{3.26}$$

Taking the inverse Fourier transform of Eq. (3.24) yields the covariance function. To define a joint pdf only the covariance matrix is needed. This makes taking the inverse Fourier transform an integral over the power spectrum. Half the terms in the power spectrum are symmetric while the other half is anti-symmetric which makes half the terms in the covariance matrix zero. All of the terms that are zero are covariances between X_n and Y_m for all n and m.

$$\Sigma_{ZZ} = \begin{bmatrix} \Sigma_{(1,1)} & \Sigma_{(1,2)} & \cdots \\ \Sigma_{(2,1)} & \Sigma_{(2,2)} & \cdots \\ \vdots & \vdots & \ddots \end{bmatrix} \tag{3.27}$$

$$\Sigma_{(n,m)} = \begin{bmatrix} \sigma_{(x,n,m)}^2 & 0 \\ 0 & \sigma_{(y,n,m)}^2 \end{bmatrix} \tag{3.28}$$

Since the covariance matrix needs to be symmetric $\Sigma_{(n,m)}$ must equal $\Sigma_{(m,n)}$. Once the covariance matrix is known the joint pdf of Z can be written as a multivariate Gaussian.

$$f(Z) = \frac{1}{2\pi\sqrt{\det \Sigma_{ZZ}}} \exp\left(-\frac{1}{2} Z^T \Sigma_{ZZ}^{-1} Z\right) \tag{3.29}$$

Analytic inversion of the Fourier transform in Eq. (3.24) has only been done in the limit of no mean flow without heat release. This limit will recover the equation for a stochastically driven second order damped oscillator (3.4). In practice, the covariance

matrix (3.27) will have to be solved using numerical integration via adaptive quadrature on an infinite interval. Unfortunately, the integrands that come from Eq. (3.24) are badly behaved because they are fractions with quasi-polynomials of trigonometric functions in the denominator. Quasi-polynomials create aperiodic undulations in the power spectrum which can confuse numerical schemes into placing quadratures in suboptimal locations if the amplitude of the undulations is large enough. Adaptive Gaussian quadrature[161] is the closest numerical scheme in terms of integrand structure that will work but even that has difficulties because it was made for oscillatory integrals that behave periodically instead of aperiodically. This problem becomes more pronounced as the magnitude of the time delay is increased and higher order mode shapes are investigated. Despite these problems, adaptive Gaussian quadrature is still orders of magnitude faster than numerically construction the response pdf.

Due to these numerically problems this thesis will only calculate the pdf response in the limit of one projected mode shape, although analytical work throughout this thesis will try to incorporate any arbitrary number of projected mode shapes. Even in this limit the power spectral density matrix is quite complex.

$$\Phi_{ZZ}(\upsilon)=\begin{bmatrix} \dfrac{\Phi_{\Omega\Omega}(\upsilon)}{D(\upsilon)D^{*}(\upsilon)} & 0 \\ 0 & \dfrac{\upsilon^{2}}{4\pi^{2}}\dfrac{\Phi_{\Omega\Omega}(\upsilon)}{D(\upsilon)D^{*}(\upsilon)} \end{bmatrix} \tag{3.30}$$

$$\begin{aligned} D(\upsilon)=\Bigg[&(i\upsilon)^{5}+C_{4}(i\upsilon)^{4}+\left(\omega'^{2}+C_{3}\right)(i\upsilon)^{3}+\left(C_{2}+\tilde{S}_{1}\right)(i\upsilon)^{2}+ \\ &\left(C_{1}-\frac{1}{\tau'_{V}}\tilde{S}_{1}-2M\tilde{S}_{2}\right)(i\upsilon)+\left(C_{0}+2\frac{M}{\tau'_{V}}\tilde{S}_{2}\right)-2\frac{M}{\tau'}\tilde{S}_{2}\,\mathrm{e}^{-(i\upsilon)\tau'_{V}}+\frac{1}{\tau'_{V}}\tilde{S}_{1}(i\upsilon)\mathrm{e}^{-(i\upsilon)\tau'_{V}}\Bigg] \end{aligned} \tag{3.31}$$

This power spectral density matrix (3.30) is for velocity but in experiments pressure is much more likely to be measured. The conversion between these two power spectra is not trivial because the constitutive relation (2.44) derived in the previous chapter to convert between pressure and velocity temporal responses is not valid. Spatial averaging

does not commute with quadratic operations; a term may spatially average to zero but it still has nonzero energy. To capture this behavior a constitutive relation between the squares of the pressure and velocity temporal responses is needed. The correct quadratic constitutive relation results from squaring the perturbed momentum equation (2.27) and then spatially averaging the result.

$$\frac{1}{4}\left(\sum_{m=1}^{\infty}\omega_m'^2\frac{\dot{\chi}_m^2(t')}{\omega_m'^2}+M^2\sum_{m=1}^{\infty}\omega_m'^2\chi_m^2(t')\right)=\frac{p_0^2}{\rho_0^2c_0^4}\sum_{m=1}^{\infty}\eta_m^2(t') \tag{3.32}$$

In the limit of one projected mode shape the power spectral density for the pressure looks similar to a scaled power spectral density for the derivative of χ_n.

$$\Phi_{\eta\eta}(\upsilon)=\frac{1}{4}\frac{\rho_0^2c_0^4}{p_0^2}\left(\upsilon^2+M^2\omega_1'^2\right)\frac{\Phi_{\Omega\Omega}(\upsilon)}{D(\upsilon)} \tag{3.33}$$

An $O(M^2\varepsilon^2)$ correction is the main difference from the quadratic constitutive relation (3.32) at low frequencies. Without this correction the power spectral density for the pressure looks nonphysical as the frequency response approaches zero with a nonzero slope. This is not seen in experiments. A calculated pressure spectrum example is shown in Figure 3-3 which looks almost indistinguishable from the spectrum for a fifth order oscillator. This occurs because the time delays show up in low frequency terms only (3.31) and are dominated by the combustor dynamic terms. Additionally, the combustor dynamic terms that have the same frequency scaling still have higher gains multiplying them compared to the volumetric heat release perturbation terms. If the frequency scaling is stronger or the gains higher more pronounced undulations will be present in the pressure spectrum which is more likely if feedback control is added because it acts on higher frequency terms. For the uncontrolled case the primary factor controlling the shape of the pressure spectrum in Figure 3-3 are the boundary conditions.

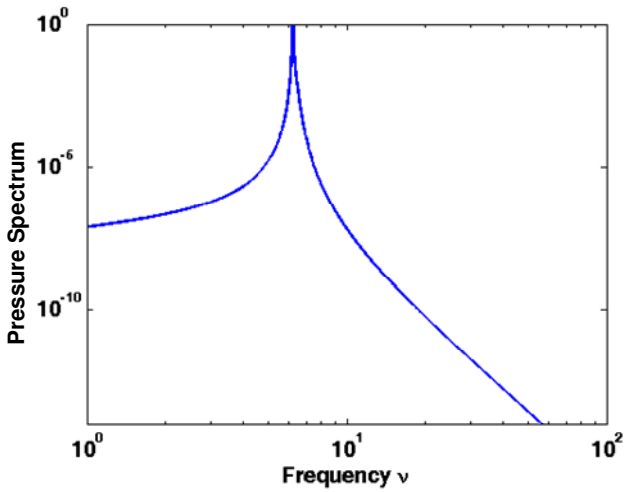

Figure 3-3: Example of the pressure spectrum of case 1 in Appendix D.

Despite the fact that no undulations are present from time delays in Figure 3-3 does not mean that the volumetric heat release perturbations does not affect the pressure spectrum. The velocity perturbation model (2.1) has terms that do not depend on time delay that are at least $O(M^{-1})$ greater in magnitude than its delayed terms. This effect is enough to give the volumetric heat release dynamics influence to shape the low frequency behavior of the pressure spectrum. In particular, the flame position of mean heat release x'_f (2.6) is the most sensitive component of the volumetric heat release perturbation model because it appears nonlinearly in the heat release dynamics and is determined by the Mach number, the time delay, and the flame shape parameter β.

3.3 Acoustic Energy PDF

Any design process requires figures of merit to benchmark one design from another. Ideally, these figures of merit should be physically meaningful and mathematically optimizable. The acoustic energy in the combustor is an excellent choice because the SPL and amplitudes of individually excited tones should scale with acoustic energy. Furthermore, acoustic energy is a semi-positive definite scalar that is quadratic in the state variables used in Eq. (2.62) which allows it to be used as part of a cost

function in $\mathcal{H}_2$ control design. Myers[162] solved for energy fluctuations in a homentropic flow up to $O(M\varepsilon^2)$. Acoustic energy is associated with terms that are second order in the acoustic Mach number.

$$E_2 = \frac{1}{2}\rho_0 v_1^2 + \frac{1}{2}\frac{p_1^2}{\rho_0 c_0^2} + v_0 \rho_1 v_1 \tag{3.34}$$

Energy fluctuations also exist that are first order in the acoustic Mach number but their contributions to the total energy time averages to zero.

In the classical acoustics limit the second order fluctuations in energy (3.34) simplifies to just the first two terms representing the acoustic kinetic and potential energy. The third term is a correction to the total acoustic energy due to advection. Spatially averaging the acoustic energy expression will help put it into a framework compatible with the previous section.

$$\begin{aligned} E_2 &= \frac{1}{2}\rho_0 c_0^2 L \int_0^L \left(\sum_{m=1}^{\infty} \chi_m(t) \nabla \psi_m(x) \right)^2 dx + \frac{p_0^2}{2\rho_0 c_0^2 L} \int_0^L \left(\sum_{m=1}^{\infty} \eta_m(t) \psi_m(x) \right)^2 dx \\ &+ v_0 \rho_0 c_0 L \int_0^L \left(\sum_{m=1}^{\infty} \vartheta_m(t) \psi_m(x) \right) \left(\sum_{m=1}^{\infty} \chi_m(t) \nabla \psi_m(x) \right) dx = \\ &\frac{1}{2}\rho_0 c_0^2 L^2 \sum_{m=1}^{\infty} k_m^2 \chi_m^2(t) + \frac{p_0^2}{2\rho_0 c_0^2} \sum_{m=1}^{\infty} \eta_m^2(t) \end{aligned} \tag{3.35}$$

Due to the assumption of homogeneous mean flow the advection of acoustic energy term has been spatially averaged to zero implying that the same amount of acoustic energy is being advected out of the combustor as there is coming into it. Hence, the spatially averaged acoustic energy appears to be the same as in the classical acoustics limit. This does not mean that advection is not contributing to the acoustics. The quadratic constitutive relation (3.32) between pressure and velocity has an $O(M^2\varepsilon^2)$ correction that accounts for the advection of acoustic energy which is very explicit when Eq. (3.32) is substituted into Eq. (3.35).

$$\frac{E_2}{\rho_0 c_0^2} = \frac{1}{8}\sum_{m=1}^{\infty} \omega_m'^2 \chi_m^2(t') + \frac{1}{8}\left(\sum_{m=1}^{\infty} \omega_m'^2 \frac{\dot{\chi}_m^2(t')}{\omega_m'^2} + M^2 \sum_{m=1}^{\infty} \omega_m'^2 \chi_m^2(t') \right) \tag{3.36}$$

Additionally, the expression for acoustic energy has been non-dimensionalized and rewritten in terms of the random variables X_n and Y_n defined in the previous section. To be consistent with Myers[162] this $O(M^2\varepsilon^2)$ correction needs to be dropped.

Acoustic energy (3.36) is a linear combination of squared Gaussian random variables. One way to visualize this is that equi-density contours of acoustic energy forms an ellipsoid in the probability space defined by Z (3.26). A useful precursor exercise is to consider the pdf of the square of a single Gaussian random variable with zero mean. This pdf belongs to the family of Gamma distributions[159] and is supported on the semi-infinite interval $[0,\infty)$.

$$G_x\left(\alpha=\frac{1}{2},\beta=2\sigma^2\right)=\frac{x^{\alpha-1}}{\Gamma(\alpha)\beta^{\alpha}}e^{-\frac{x}{\beta}} \tag{3.37}$$

Many distributions do not have the stability[163] property which means that linear combinations of random distributions in the same family do not belong to the same family of distributions as their individual components; the Gamma distribution is no exception.[164] Alouini et al.[165] solved this pdf for the general case of the sum of arbitrarily correlated Gamma distributed random variables, but this pdf is complicated and requires a recursive relation to define it. Even if Z is uncorrelated a recursion is still needed to define the pdf.[166] A marginal pdf for the acoustic energy of a single projected mode shape with the assumption that $\sigma_x^2=\sigma_y^2$ can be written as an exponential distribution.

$$f_x\left(\lambda=\frac{4}{\omega_m'^2\sigma^2}\right)=\lambda e^{-\lambda x} \tag{3.38}$$

Although the assumption on the variances may seem too constraining it is still useful to make because numerical results coming in §3.6 will show that this tends to be approximately true without control applied.

When working with the statistics of acoustic energy (3.36) the state variables are more easily viewed as powers of Gaussian random variables because Isserlis' theorem[167] allows for rapid evaluation of mixed moments.

$$\left\langle E_2' \right\rangle = \frac{1}{8}\left(\sum_{m=1}^{\infty} \omega_m'^2 \left(\sigma_{(x,m,m)}^{\ 2} + \sigma_{(y,m,m)}^{\ 2} \right) \right) \tag{3.39}$$

$$\begin{aligned} \left\langle E_2'^2 \right\rangle = \frac{1}{64} \sum_{m=1}^{\infty} \sum_{n=1}^{\infty} \omega_m'^2 \omega_n'^2 \Bigg[& \left(\sigma_{(x,m,m)}^{\ 2} \sigma_{(x,n,n)}^{\ 2} + 2\sigma_{(x,m,n)}^{\ 4} \right) \\ & + 2\sigma_{(x,m,m)}^{\ 2} \sigma_{(y,n,n)}^{\ 2} + \sigma_{(y,m,m)}^{\ 2} \sigma_{(y,n,n)}^{\ 2} + 2\sigma_{(y,m,n)}^{\ 4} \Bigg] \end{aligned} \tag{3.40}$$

Inspection of the mean acoustic energy (3.39) reveals that the result is independent of the correlation between the random variables of *Z*. Furthermore, the kinetic and potential energy of a projected mode shape scales with the variance of that mode by the same constant; therefore, the ratio of variances, σ_y^2/σ_x^2, reveals what component of acoustic energy is dominant. The ratio of the mean potential energy to the mean kinetic energy of a projected mode is actually a linear function of the ratio of variances.

$$\frac{\left\langle P.E. \right\rangle_m}{\left\langle K.E. \right\rangle_m} = \frac{\sigma_{(y,m,m)}^{\ 2}}{\sigma_{(x,m,m)}^{\ 2}} + \mathrm{O}\left(M^2\right) \tag{3.41}$$

If this ratio is less than 1 then the majority of acoustic energy in that projected mode shape is kinetic energy while potential energy is the majority when this ratio is greater than 1. Calculating the variance of the acoustic energy is a bit more involved but this can be done by recognizing that the variance of a random variable is just the square of the mean subtracted from the second moment.

$$Var\left(E_2'\right) = \frac{1}{32} \sum_{m=1}^{\infty} \sum_{n=1}^{\infty} \omega_m'^2 \omega_n'^2 \left[\sigma_{(x,m,n)}^{\ 4} + \sigma_{(y,m,n)}^{\ 4} \right] \tag{3.42}$$

From inspection of the variance of the acoustic energy (3.42) a strong dependence on the cross correlation can be seen.

3.4 Amplitude-Phase PDF

The detrimental effects of combustion instabilities are mainly a function of their frequency and amplitude, but the joint pdf derived for *Z* (3.29) gives the distribution of the instantaneous response and not its amplitude. A change of random variable to

amplitude and phase can be accomplished by using the Kryloff and Bogoliuboff[152] decomposition.

$$\chi_n(t') = R_n(t')\sin\left(\omega_n' t' + \phi_n(t')\right) = R_n(t')\sin\left(\theta_n(t')\right) \tag{3.43}$$

This decomposition of χ_n is over defined because it replaces one random variable, the instantaneous velocity, with two random variables, the velocity amplitude R_n and its phase φ_n, with respect to ω'_n, or total phase θ_n. As a result, the new random variables need to satisfy any additional, but arbitrary mathematical relation between them so that they are no longer over defined. Since this relation is arbitrary the intelligent choice is one that simplifies analysis. The derivative of χ_n should be a function of amplitude and phase and not its derivatives to keep analysis simple. A relation should be picked to remove these unwanted terms.

$$0 = \dot{R}_n(t')\sin\left(\theta_n(t')\right) + R_n(t')\dot{\phi}_n(t')\cos\left(\theta_n(t')\right) \tag{3.44}$$

$$\frac{\dot{\chi}_n(t')}{\omega_n'} = R_n(t')\cos\left(\theta_n(t')\right) \tag{3.45}$$

Equation (3.43) and (3.45) can be rewritten to explicitly solve for the velocity amplitude and total phase by adding their squares and dividing by each other respectively. For notational shorthand these new random variables will be collected in vector Z_{pol}.

$$R_n(t') = \sqrt{X_n^2(t') + Y_n^2(t')} \tag{3.46}$$

$$\theta_n(t') = \arctan\left(X_n(t')/Y_n(t')\right) \tag{3.47}$$

$$Z_{pol} = \begin{bmatrix} R_1 & \theta_1 & \dots & R_n & \theta_n \end{bmatrix}^T \tag{3.48}$$

To convert any pdf from one set of random variables to another the Jacobian of the transformation is needed.[159] This accounts for the change of area in the differential elements of the pdf when converting coordinates.

$$J\left(Z_{pol}\right)=\det\begin{bmatrix} J_{(1,1)} & J_{(1,2)} & \cdots & J_{(1,n)} \\ J_{(2,1)} & J_{(2,2)} & \cdots & J_{(2,n)} \\ \vdots & \vdots & \ddots & \vdots \\ J_{(n,1)} & J_{(n,2)} & \cdots & J_{(n,n)} \end{bmatrix}=\prod_{i=1}^{n} R_i \tag{3.49}$$

$$J_{(n,m)}\left(R_n,\theta_n\right)=\begin{bmatrix} \frac{\partial X_n}{\partial R_m} & \frac{\partial X_n}{\partial \theta_m} \\ \frac{\partial Y_n}{\partial R_m} & \frac{\partial Y_n}{\partial \theta_m} \end{bmatrix}=\begin{cases} \begin{bmatrix} \sin\left(\theta_n\right) & R_n\cos\left(\theta_n\right) \\ \cos\left(\theta_n\right) & -R_n\sin\left(\theta_n\right) \end{bmatrix} & n=m \\ \begin{bmatrix} 0 & 0 \\ 0 & 0 \end{bmatrix} & n\neq m \end{cases} \tag{3.50}$$

The phase-amplitude pdf is the pdf of the instantaneous velocity and its derivative (3.29) evaluated in terms of Z_{pol} and multiplied by the Jacobian of the transformation (3.49).

$$f\left(Z_{pol}\right)=J\left(Z_{pol}\right)f\left(Z\left(Z_{pol}\right)\right)=\frac{\prod_{i=1}^{n} R_i}{2\pi\sqrt{\det\Sigma}}\exp\left(-\frac{1}{2}Z^T\Sigma^{-1}Z\right) \tag{3.51}$$

A full expansion of the exponential in the joint pdf of Z_{pol} (3.51) is not practical due to the need to express the inverse of the covariance matrix; however, this covariance matrix has a simple form to invert when looking at the marginal pdf of velocity amplitude and phase for a single projected mode.

$$f\left(R_n,\theta_n\right)=\frac{R_n}{2\pi\,\sigma_{(x,n,n)}\,\sigma_{(y,n,n)}}\exp\left[\frac{-\left(\sigma^2_{(x,n,n)}\cos^2\theta_n+\sigma^2_{(y,n,n)}\sin^2\theta_n\right)R_n^2}{2\,\sigma^2_{(x,n,n)}\,\sigma^2_{(y,n,n)}}\right] \tag{3.52}$$

This marginal pdf (3.52) was originally derived by Hoyt[168] and is very close to the pdf for the damped harmonic oscillator (3.4) considered in §3.1. When the ratio of the variances is one this relation is recovered. Since this is closely related to the equi-partition of acoustic energy, understanding which form of acoustic energy is dominant creates a powerful lens into understanding how the marginal pdf deviates from the pdf of the damped harmonic oscillator. More explicit results and insight are possible if the marginal pdfs of amplitude and total phase are considered individually.

A marginal pdf of the total phase comes from integrating over the region of support for the velocity amplitude in Eq. (3.52).

$$f(\theta_n) = \frac{\sigma_{(x,n,n)}\,\sigma_{(y,n,n)}}{2\pi}\left(\sigma^2_{(x,n,n)}\cos^2(\theta_n) + \sigma^2_{(y,n,n)}\sin^2(\theta_n)\right)^{-1} \tag{3.53}$$

If the ratio of the variances is one then the marginal pdf of the total phase is a circular uniform distribution as expected. In Figure 3-4 the total phase pdf is plotted for the cases where the acoustic kinetic energy and acoustic potential energy are individually the majority of the total acoustic energy in the combustor. Deviations from the equi-partition of acoustic energy create regions of preferential total phase. When more acoustic kinetic energy is present than acoustic potential energy the total phase prefers to avoid regions that are multiples of π. This increases the probability that $|sin(\theta_n)|$ is as large as possible while ensuring that $|cos(\theta_n)|$ is as small as possible. In turn, this implies that the fluctuations in velocity (3.43) are larger than the fluctuations in pressure, related to Eq. (3.45), as expected. Similarly, the situation is reversed when more acoustic potential energy exists than acoustic kinetic energy resulting in the total phase preferring regions that are multiples of π.

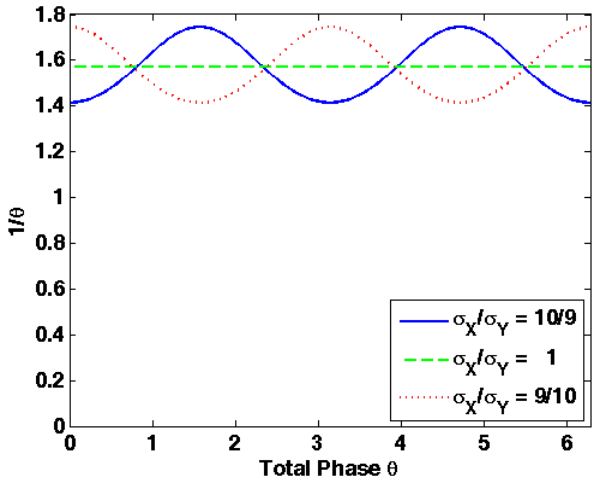

Figure 3-4: Total phase pdf for varying ratios of acoustic kinetic energy to acoustic potential energy.

Integrating Eq. (3.52) over the region of support for the total phase yields a Hoyt distribution, although more recent literature refers to this pdf as a Nakagami-q distribution.[169]

$$H_{R_n}\left(q=\frac{\underset{(y,n,n)}{\sigma}}{\underset{(x,n,n)}{\sigma}}, w=\underset{(x,n,n)}{\sigma^2}+\underset{(y,n,n)}{\sigma^2}\right)=\frac{\left(1+q^2\right)}{qw}R_n e^{-\frac{\left(1+q^2\right)^2 R_n^2}{4q^2 w}} I_0\left(\frac{\left(1-q^4\right)R_n^2}{4q^2 w}\right) \tag{3.54}$$

The Hoyt distribution (3.54) is the product of a zeroth order modified Bessel function of the first kind, I_0, and an exponential function. Two parameters fully describe this pdf: the shape parameter q is determined by the amount of deviation in the equi-partition of acoustic energy while the spread parameter w is determined by the total acoustic energy in that mode. An interesting feature of the Hoyt distribution is that it has inverted symmetry with respect to the shape parameter. In other words, the distribution given by Eq. (3.54) is exactly the same if q is replaced by $1/q$. The dominant form of acoustic energy can only be gleamed from the phase pdf (3.53).

Exploring the statistics of the velocity pdf can be very insightful. In these expressions E represents the complete elliptical integral of the second kind.

$$\left\langle R_n\right\rangle=\sqrt{\frac{2}{\pi}}\underset{(x,n,n)}{\sigma}E\left(1-\frac{\underset{(y,n,n)}{\sigma^2}}{\underset{(x,n,n)}{\sigma^2}}\right)=\sqrt{\frac{2w}{\pi\left(1+q^2\right)}}E\left(1-q^2\right) \tag{3.55}$$

$$\left\langle R_n^2\right\rangle=\underset{(x,n,n)}{\sigma^2}+\underset{(y,n,n)}{\sigma^2}=w \tag{3.56}$$

$$E(m)=\int_0^{\frac{\pi}{2}}\sqrt{1-m\sin^2\theta}\,d\theta \tag{3.57}$$

If the magnitude of the argument of $E(m)$ is greater than one then the returned value is a complex number which is physically invalid; therefore, the ratio of the variances must be positive as expected. Another useful statistical figure of merit is the coefficient of variation, c_v, which describes the amount of dispersion in a pdf.

$$c_v\left(R_n\right)=\frac{\sqrt{Var\left(R_n\right)}}{\left\langle R_n\right\rangle}=\frac{\sqrt{\frac{\pi}{2}\left(1+q^2\right)-E^2\left(1-q^2\right)}}{E\left(1-q^2\right)} \tag{3.58}$$

As this coefficient increases the velocity amplitude will deviate from its mean more often. This makes c_v an excellent indicator of amplitude breathing, introduced in §1.3, where it is noted as being associated with induced combustion dynamics from the implementation of feedback control. Understanding the trends in c_v shown in Figure 3-5 is a logical first step in determining if amplitude breathing is a cause of limited control effectiveness or a repercussion of it.

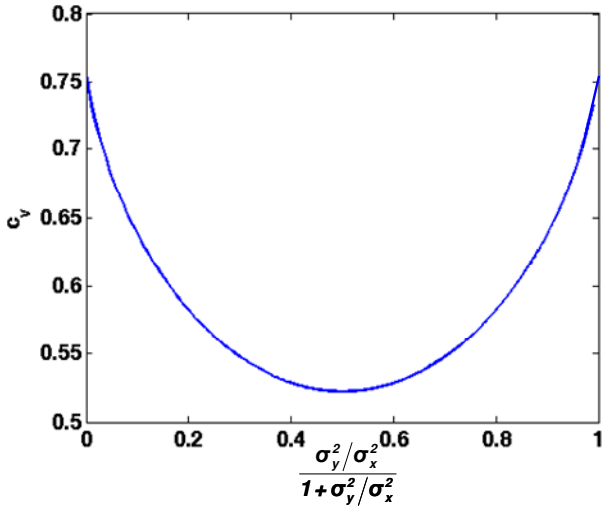

Figure 3-5: Coefficient of variation in the velocity amplitude as a function of the ratio between acoustic potential energy and acoustic kinetic energy.

In Figure 3-5 the abscissa has been normalized such that it belongs to the set [0,1] instead of [0,∞). The coefficient of variance is minimal, with a value of $\sqrt{(4/\pi-1)}$, when the ratio of the variances is one, corresponding to one half in the normalized coordinate, and reaches a maximum value of $\sqrt{(\pi/2-1)}$ at the boundary points. Clearly, Figure 3-5 is symmetric and monotonically increasing as deviations from equi-partition of energy increases. This suggests that the key to understanding why feedback control can cause

amplitude breathing will require an understanding to what happens to the ratio of acoustic potential energy to acoustic kinetic energy as control is applied. Unfortunately, this is difficult to analyze in general with an unspecified mathematical structure for the control law.

3.5 Exponential Polynomials

Back in §3.1 the spectral abscissa was suggested as an alternative way of looking at system performance, but the details about how to do this for time delay system was glossed over despite the fact that the solution to the time delayed Langevin's equation (3.8) was given. Developing insight into what governs the spectra of time delay systems first requires understanding some general properties of the characteristic equation, found by taking the determinate of the Laplace transform of the time delay system. The characteristic equation is a member of the general class of functions called exponential polynomials.

$$\sum_{i=0}^{m}\sum_{j=0}^{n} a_{ij} s^i e^{-s\tau_j} \tag{3.59}$$

In expression (3.59) the coefficient a_{ij} are real numbers and the sequence $\{\tau_j\}$ is monotonically increasing.

Several excellent monographs already exist on this subject by Bellman and Cooke,[80] Niculescu,[98] and Michiels and Niculescu[170] which this section will rely upon heavily. Depending on the values of the coefficients a_{ij} and τ_j an exponential polynomial (3.59) can describe a retarded delay, an advanced delay, or a neutral delay differential equation. A retarded delay differential equation has only non-negative delays but they cannot be present in the highest order derivative. This means that $\tau_j \geq 0 \nvdash j$ & $a_{mj} = 0 \nvdash j > 0$. An advanced delay differential equation is similar to a retarded delay differential equation except that all the delays are non-positive. When $\exists j > 0 : a_{mj} \neq 0$ then the exponential polynomial describes a neutral delay equation. The thermo-acoustic

model being studied in this thesis (2.68) is a retarded delay differential equation; however, this does not mean that all of the transfer matrices possible in the feedback diagram from Figure 2-2 are also described by retard delay differential equations once a controller or estimator is added. As a result, understanding a little bit about each type of delay differential equation can go a long way in understanding system behavior.

Exponential polynomials are entire functions having an infinite number of roots. Imagine an enumeration of these roots such that they are ordered with increasing magnitude. When the magnitude increases these roots approach asymptotic lines in the complex plane.[80] These asymptotic structures are called root chains. Not all roots have to belong to a root chain but these roots will be finite in number. An example of the eigenvalues of the time delayed Langevin's equation (3.8) is shown in Figure 3-6. From inspection, the eigenvalues of the time delayed Langevin's equation follow a very distinct type of pattern. The key to understanding these patterns lie in what type of exponential polynomial describes a given root chain.

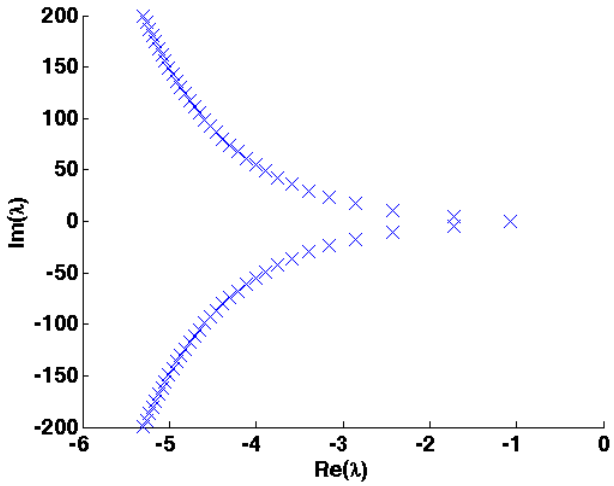

Figure 3-6: Eigenvalues of the time delayed Langevin's equation for aτ = -4 & bτ = 1.

For retarded delay differential equations as the magnitude of the eigenvalues increase without bound then the real part of the eigenvalues will also increase without

bound. This has some interesting repercussions. A vertical line exists in the complex plane such that all the eigenvalues are to the left of it. Furthermore, every vertical strip in the complex plane will have a finite number of eigenvalues. These two facts taken together mean that the number of eigenvalues in the right hand complex plane (RHCP) is also finite. Knowledge of how the eigenvalues vary as the parameters in an exponential polynomial (3.59) are changed is not generally known since the eigenvalues are calculated, not derived, but they do vary continuously with the parameters in the exponential polynomial, including the time delay.[170]

Advanced delay differential equations behave very similarly to retarded delay differential equations. A simple coordinate transformation of the time variable to negative time will convert an advanced delay differential equation to a retarded delay differential equation. As a result, all the trends are inverted. In the complex plane a vertical line exists such that all the eigenvalues are to the right of it and every vertical strip in the complex plane will have a finite number of eigenvalues; therefore, the number of eigenvalues in the left hand complex plane is also finite. This means that all advanced delay differential equations are unstable. The spectra of advanced delay differential equations will also vary continuously with respect to variation of parameters.

For neutral delay differential equations as the magnitude of the eigenvalues increase without bound the real part of the eigenvalues approaches a finite number; therefore, the set of the real part of all the eigenvalues are bounded. A vertical line exists in the complex plane such that all the eigenvalues are to the left of it, but a second vertical line exists such that all the eigenvalues are to the right of it. As a result, nothing definite can be said about the number of eigenvalues in a vertical strip or the eigenvalues in any half-plane. This has very interesting implications for stability. For example, all the eigenvalues must be in the left hand complex plane and be bounded away from the $j\omega$-axis to be stable. Furthermore, the eigenvalues do not have to vary continuously with respect to changes in the time delays;[171] however, an upper bound exists for all the values

the real part of the eigenvalues can take with infinitesimal perturbations. If this upper bound is negative then the neutral delay differential equation is said to be strongly stable. This implies that robustness is a very strong concern for neutral delay differential equations.

3.6 Combustor Performance Trends

The eigenvalues of the thermo-acoustic model (2.68) can now be investigated since the asymptotic behavior of eigenvalues of delay systems are better understood along with some of the implications that go along with them. Figure 3-7 shows the eigenvalues for the same case that corresponds to the pressure spectrum in Figure 3-3. Low magnitude eigenvalues deviate from the root chain in Figure 3-7, unlike Figure 3-6 which is actually an exceptional case. Not shown in Figure 3-7 are other root chains very deep in the left hand complex plane that begin to converge to a single root chain. This suggests that the eigenvalue behavior can be quite difficult to comprehend.

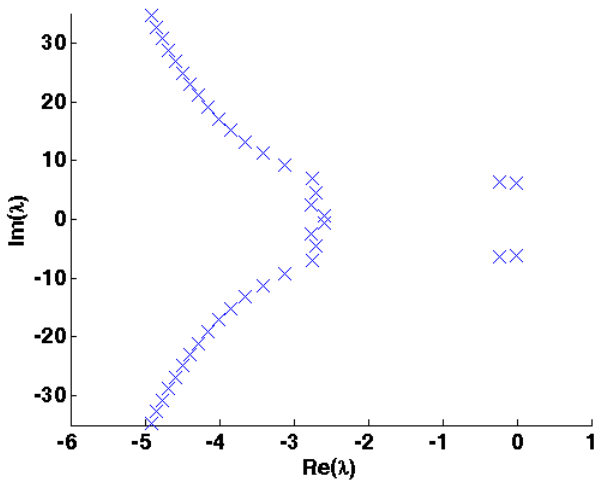

Figure 3-7: Eigenvalues for an uncontrolled self-excited, noise driven, combustor of case 1 in Appendix D.

A useful analogy is to think of the eigenvalues as belonging to a twined rope with frayed ends. When the magnitudes of the eigenvalues are large they all belong to the

asymptotic root chain like a rope. As the magnitude decreases the asymptotic root chain begins to break into other root chains like a twine rope unraveling. Finally, as the imaginary part of the eigenvalues approach zero they begin to scatter like a frayed piece of twine. The reason this is important is that the figure of merit chosen in §3.1, the spectral abscissa, tends to be one of these scattered eigenvalues at the beginning of a root chain. This behavior is what makes finding the spectral abscissa a numerical exercise since the location of specific eigenvalues cannot be explicitly solved. Despite this, the qualitative behavior of eigenvalues can be used to help understand performance trends in parameter maps for the thermo-acoustic model (2.68) being investigated.

Variations of the spectral abscissa are shown in Figure 3-8 as a function of the internal time delay and heat release gain. The spectral abscissa has a decaying periodic behavior as the time delay is increased. Figure 3-8 seems to suggest that for small enough gains the combustor is stable for all time delays. This property is called delay independent stability and has been proven for simpler mathematical models in thermo-acoustics.[98] Physically, the reason for the existence of delay independent stability has to due with the acoustic damping provided by the boundary conditions. As the boundary conditions are changed the location of the iso-contours also change but their shape remains qualitatively the same.

Earlier and less sophisticated 1-D flat flame stability models[172] predict that the combustor should switch periodically between being stable and unstable as the time delay is increased. In Figure 3-8 the combustor stability is increasing with time delay with a sloped asymptote marking the stability boundary. The sloped asymptote is due to the shape of the flame and in particular β. As the flame shape parameter is increased the cone defining the flame sheet flattens and causes the slope of the stability asymptote to decrease. At the same time the x'_f is pushed closer to a velocity node so that the volumetric heat release dynamics are weakened which pushes the stability asymptote

upwards. On the other end of this limit, long flames must be destabilizing because x'_f is pushed closer to a velocity anti-node.

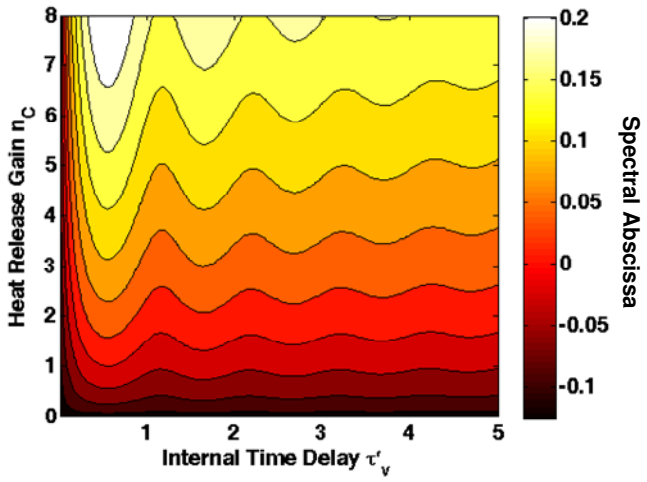

Figure 3-8: Spectral abscissa for an uncontrolled self-excited, noise driven, combustor of case 1 in Appendix D but allowed to vary as a function of n_C and τ'_V.

Explaining why stability increases with time delay is much more subtle. The shape of the flame sheet is fixed by β but not its surface area. Increasing the flame length, which is related to the internal time delay, for a fixed β will increase the flame surface area; however, this cannot be increased arbitrarily because defining these two parameters automatically define the area of the nozzle, which is the area of the base of the cone defining the flame sheet. In the boundary conditions the ratio of the nozzle area to the combustor area is a parameter which is held fixed; therefore, the only way for the time delay to increase the flame length is if the size of the combustor also grows. As this happens the volume of the combustor increases faster than the surface area of the flame sheet which guarantees that the mean volumetric heat release rate is decreasing as the time delay increases. This explains why the combustor stability increases. An important note to make here is that the advection time delay (2.59) in the control system can be changed without changing x'_f so that increasing this time delay will behave very differently than increasing the internal time delay as will be seen shortly.

Figure 3-8 properly defines the stability boundaries of the combustor. Since stability is a prerequisite to the existence of the Fourier transform the pdf tools developed earlier in this chapter can now be applied to the thermo-acoustic model and compared to Figure 3-8. This is done in Figure 3-9 by plotting iso-contours of the inverse mean amplitude as a function of heat release gain and internal time delay. When comparing Figure 3-9 to the appropriate region of Figure 3-8 the trends found are very similar and the iso-contours have the same shape and behavior. Matching between the trends of these two figures of merit is even better than what was found with the time delayed Langevin's equation. Obviously, minimizing the spectral abscissa is not equivalent to minimizing the mean amplitude response and vice versa. An example of this has already been discussed in §3.1 for second order systems. In higher order systems other eigenvalues can appear near the spectral abscissa and have a non-negligible effect on system performance. The thermo-acoustic model used in this thesis initial gets away with this oversight because the spectral abscissa is sufficiently far away from other eigenvalues as seen in Figure 3-7; however, this should not lull the design engineer into complacency. If the spectral abscissa is a flawed figure of merit then of what use is it?

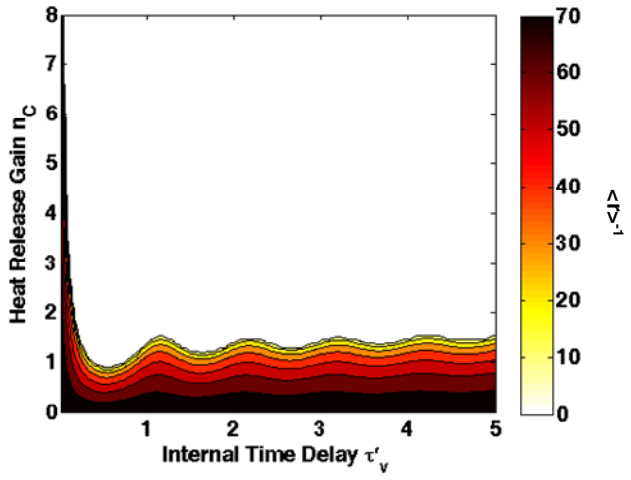

Figure 3-9: Inverse mean amplitude for an uncontrolled self-excited, noise driven, combustor of case 1 in Appendix D with $\sigma = 1$ but allowed to vary as a function of n_C and τ'_V.

The answer to this question goes back to the modeling process illustrated in Figure 2-1. Calculating the spectral abscissa is much more accessible and efficient then calculating the statistics of the response pdf. As fewer modes shapes are truncated and control introduces new time delays the computational time required to calculate pdf statistics increases much more rapidly than solving for the spectral abscissa to the point of being computationally infeasible for parameter mapping. Furthermore, the power spectral matrix (3.24) needs to be derived again for each change to the reduced order thermo-acoustic model being used. This makes pdf based methods harder to automate and hence make them less desirable to design engineers. Fortuitously, the spectral abscissa does get the performance trends correct so it can be used to narrow the parameter space before switching to the slower and more tedious statistical calculations.

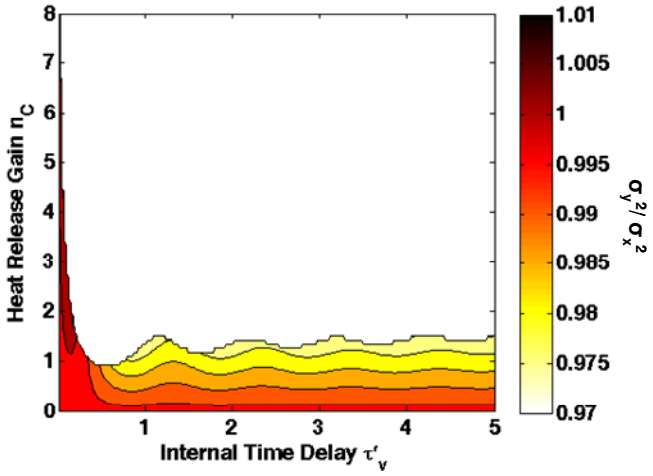

Figure 3-10: Ratio of potential to kinetic acoustic energy for an uncontrolled self-excited, noise driven, combustor of case 1 in Appendix D with $\sigma = 1$ but allowed to vary as a function of n_C and τ'_V.

Another design variable developed in §3.4, the coefficient of variation (3.58), can also be investigated in the same parameter space as the mean amplitude and the spectral abscissa. Figure 3-10 shows that this ratio varies by less than 3% which makes sense in the context of the previous discussion of Figure 3-3 on how the volumetric heat release dynamics influences the pressure spectrum. This translates into a negligible change in

the coefficient of variation which seems to paint a pessimistic case for feedback control causing amplitude breathing. Most likely, amplitude breathing is caused by nonlinear effects. For example, the experiment by Johnson et al.[57] used an unstable nonlinear observer[173] to track the dominant instability frequency which has to be reset periodically.

3.7 Temporal Modal Control

The idea of modal control has a long history in beam vibration,[174] particularly with the study of large flexible space structures.[175] Space structures are lightly damped and hence have high frequency dynamics and eigenvalues that must be modeled to accurately represent the system response which is very similar to the situation with time delay systems. One way to think of a time delay system is as a metaphorical beam in time. While abstract, this idea suggests the existence of an analogue for every analysis tool or methodology of thinking in the study of vibrations that can be recycled for time delay systems. Modal control concepts let the engineer use geometric thinking to train and develop physical insight. Such an idea is very powerful in the sense that it can explain the system response of time delay systems without resorting to convoluted calculations that may provide an answer to what the system is doing but provides no deeper understanding of why the system is behaving the way it desires.

Before proceeding some clarification is required on what is meant by modal control. In §2.5 the Galerkin expansion was used to expand the wave equation (2.33) into an infinite set of projected spatial mode shapes. These are not the modes being talked about in this section. Recall that the wave equation is infinite dimensional for two separate reasons; it is a distributed parameter system in space and time. Each individual projected spatial mode shape has an infinite dimensional temporal response due to the presence of time delays; hence, the temporal response can be decomposed as the collection of an infinite number of temporal modes shapes which each correspond to a

given eigenvalue. The attractiveness of temporal modal control is very apparent now since the spectral abscissa is represented by a single temporal mode shape.

Using spectral decomposition[176] each temporal mode shape can be viewed as an eigenvector. To facilitate discussion the product space $\mathcal{M}^2([-\tau_{max},0],\mathcal{R}^n)$ introduced in §2.8 is used. Equation (3.60) shows how a general time delay system can be written as an abstract operator equation using the product space formulation.

$$\begin{bmatrix} \dot{\vec{x}}(t') \\ \dot{\vec{x}}(t'+\bullet) \end{bmatrix} = \begin{bmatrix} \sum_{i=0}^{k} A_i \mathcal{S}(-\tau_i') \\ \mathcal{D} \end{bmatrix} \begin{bmatrix} \vec{x}(t') \\ \vec{x}(t'+\bullet) \end{bmatrix} = \mathcal{A} \begin{bmatrix} \vec{x}(t') \\ \vec{x}(t'+\bullet) \end{bmatrix} \tag{3.60}$$

In this notation $x(\bullet)$ denotes the past history of $x(r)\ \forall \tau'_k \le r < 0$. The past history of the system response is recovered by the differentiation operator $\mathcal{D}$ and the time delays needed to evaluate the system response in the present are replaced by the shift operator $\mathcal{S}(-\tau'_i)$.

$$\mathcal{S}(-\tau_i')\vec{x}(t') = \vec{x}(t'-\tau_i') \tag{3.61}$$

Together, these operators define the infinitesimal generator $\mathcal{A}$ that generates a strongly continuous semigroup describing the system response.

Changing the governing equations (2.68) into the abstract operator form (3.60) does not change the eigenvalues of the system. Numerically, the abstract operator form is the easier form to discretize as shown in Appendix A for approximating the eigenvalues of time delay systems. Finding the component of the eigenvector, $\mathcal{V}$, corresponding to the present is done by finding the nullspace of the characteristic matrix evaluated at the eigenvalues of the infinitesimal generator; this also has to be done numerically. The eigenvector component corresponding to the past is where spectral decomposition makes its utility known because the eigenfunction of the differentiation operator is an exponential function. This is always true for any linear functional differential equation and reveals significant detail about the temporal modal response. When spectral decomposition of Eq. (3.60) is completed it takes the form of Eq. (3.62).

$$\begin{bmatrix} \vec{x}(t') \\ \vec{x}(t'+\bullet) \end{bmatrix} = \sum_{i=1}^{\infty} \begin{bmatrix} \vec{c}_i \\ \vec{c}_i e^{\lambda_i(\bullet)} \end{bmatrix} = \sum_{i=1}^{\infty} \boldsymbol{v}_i \tag{3.62}$$

Making general comments about spectral decomposition is complicated by not knowing the vector of normalization constants; however, this is easy to calculate via inner products in the one dimensional case such as the time delayed Langevin's equation (3.8) and the solution is given below.

$$c_i = \left(1 + \frac{1}{2\,\mathrm{Re}(\lambda_i)} \left(1 - e^{-2\,\mathrm{Re}(\lambda_i)\tau} \right) \right)^{-\frac{1}{2}} \tag{3.63}$$

An inner product in the product or extended state space is just the sum of the inner products of the individual spaces. Another interesting calculation to perform is the inner product between two different temporal mode shapes because it gives information about the degree of orthogonality.

$$\left\langle \begin{bmatrix} c_i \\ c_i e^{\lambda_i(\bullet)} \end{bmatrix}, \begin{bmatrix} c_j \\ c_j e^{\lambda_j(\bullet)} \end{bmatrix} \right\rangle = c_i c_j \left(1 + \frac{1}{\lambda_i + \lambda_j^*} \left(1 + e^{-\left(\lambda_i + \lambda_j^*\right)\tau} \right) \right) \tag{3.64}$$

Working in an inner product space enables the use of geometry so that the angle between any two temporal modes can be calculated.

$$\cos\theta_{ij} = \frac{\left| \left\langle \boldsymbol{v}_i, \boldsymbol{v}_j \right\rangle \right|}{\left\| \boldsymbol{v}_i \right\| \left\| \boldsymbol{v}_j \right\|} \tag{3.65}$$

To illustrate the orthogonality of the time delayed Langevin's equation (3.8) Figure 3-11 enumerates all of the eigenvalues from Figure 3-6 by how deep they are in the LHCP and shows how of the angle between each of these temporal modes shapes with the temporal mode shape of the spectral abscissa, $\boldsymbol{v}_1$, changes.

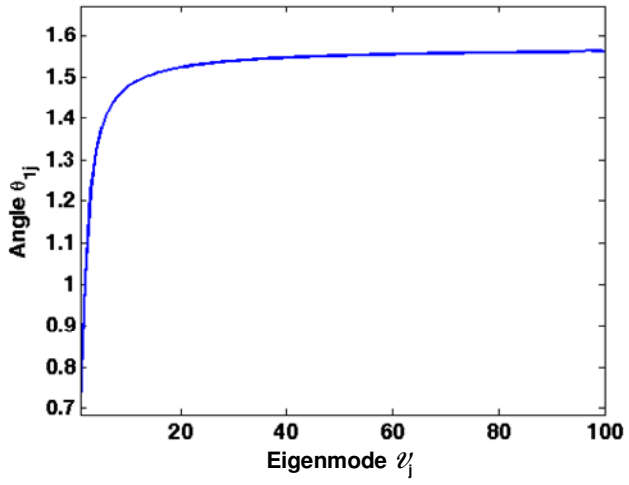

Figure 3-11: Angle between the temporal mode of the spectral abscissa and all other temporal modes enumerated by depth in LHCP of the time delayed Langevin's equation for aτ = -4 & bτ = 1.

The temporal mode shapes beyond the first ten complex conjugate pairs are nearly orthogonal to the temporal mode shape of the spectral abscissa, mainly due to the normalization constant shrinking rapidly as the mode number increases to compensate for the exponential growth in the temporal mode shape. This approximately corresponds to the eigenvalues to the left of the line defined by $Re(\lambda) = -4$ in Figure 3-6. For the mathematician, Figure 3-11 reveals a certain amount of nonnormality exists in the infinitesimal generator of this system; a fact that all time delay systems share. Nonnormal operators can have unpleasant transient response characteristics such as large peak overshoots.[177] In combustors this can lead to triggering as nonlinear dynamics become important.[178] Triggering in combustors with laminar premixed flames has been investigated by Subramanian and Sujith.[179] This particular issue is ignored in this thesis because of the emphasis on physical realizability and mathematical solvability as detailed in the previous chapter which prevents the use of nonlinear volumetric heat release perturbation models.

An aspect of nonnormality that can be addressed is its effect on the system robustness. When the parameters of a system are perturbed the location of the

eigenvalues will move. One way to investigate the propensity of eigenvalues to move is through pseudospectra. Multiple equivalent definitions of pseudospectra exist.[180]

$$\Lambda_\varepsilon(\mathcal{A}) = \left\{ s \in \mathbb{C} : \left\| (s\mathcal{I} - \mathcal{A})^{-1} \right\| \geq \varepsilon^{-1} \right\} \tag{3.66}$$

$$\Lambda_\varepsilon(\mathcal{A}) = \left\{ \exists \|\Delta\mathcal{A}\| \leq \varepsilon : s \in \Lambda(\mathcal{A} + \Delta\mathcal{A}) \in \mathbb{C} \right\} \tag{3.67}$$

The first definition shows that the pseudospectra is the value of the magnitude of the characteristic matrix, shown as a resolvent operator in Eq. (3.66). This happens to be the easiest way to calculate the pseudospectra but not the most intuitive way to think about it. In Eq. (3.67) contours of the ε-pseudospectra are revealed to contain the set of all possible eigenvalues of the infinitesimal generator with respect to perturbations less than ε; thereby creating a very powerful tool to visualize the robustness of the system.

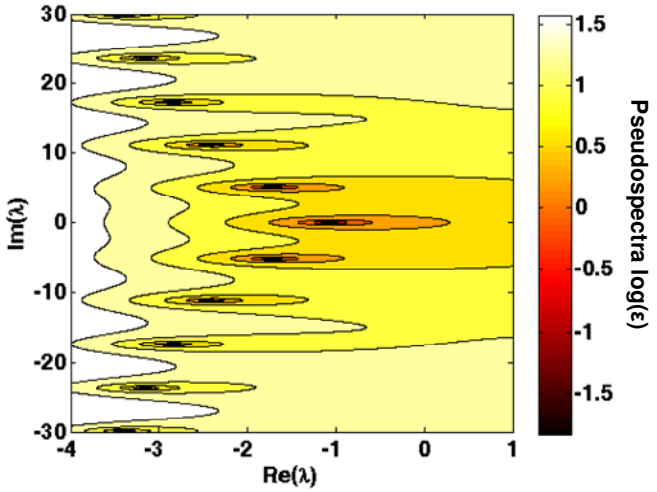

Figure 3-12: Logarithm of the pseudospectra of the time delayed Langevin's equation for aτ = -4 & bτ = 1.

A plot of the logarithm for the ε-pseudospectra of the time delayed Langevin's equation (3.8) is shown in Figure 3-12 which corresponds to the same conditions as Figure 3-6. The eigenvalues have a strong propensity to drift into the RHCP and does so for small perturbations. This suggests that significantly improving the performance of a

time delayed system without changing the maximum time delay will be difficult. Nothing in Figure 3-12 reveals if all the eigenvalues will move in the same direction. When these same concepts are applied to a self-excited combustor as in Figure 3-13 the sensitivity of the eigenvalue placement is even more pronounced. From a control system point of view the robustness of the system is a serious concern and needs to be addressed in addition to the system performance at the design point. While this result is pessimistic it is also conservative because the definition given for pseudospectra (3.67) is for unstructured uncertainty. The mathematically worst case scenario may not be physically realizable. Structured pseudospectra[170] concepts exist to enforce physical constraints but they require the thermo-acoustic modeler to be able to characterize the deficiency in their model. Thermo-acoustic modeling is still too immature to enable the use of this robust performance tool. Robustness will play an important role in understanding control effectiveness trends in combustors, particularly in the next chapter.

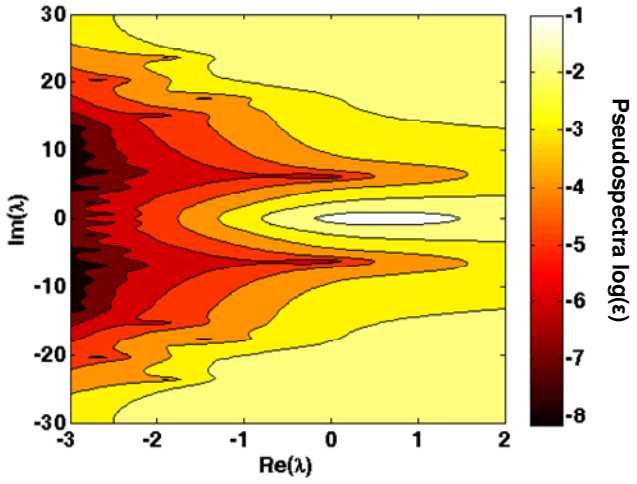

Figure 3-13: Logarithm of the pseudospectra for a controlled self-excited, noise driven, combustor of case 1 in Appendix D.

3.7.1 One Projected Spatial Mode Shape

Before considering the factors that limit control effectiveness a severe deficiency in present day thermo-acoustic models needs to be addressed: the simple fact that a controller's performance and trends have never been correctly predicted prior to the execution of an experiment. This means that an investigation of the limits of performance is premature until the behavior of very simple controllers can be predicted and collaborated with experimental data. One of the simplest controllers is a proportional delay compensator based upon pressure feedback. Artificial delays can also be added to the control law but these will be absorbed within the advection time delay. For ease of analysis the thermo-acoustic model will be truncated to one projected spatial mode shape in this subsection.

$$u(t') = k\dot{\chi}_1(t') \tag{3.68}$$

An example of a spectral abscissa contour map corresponding to Figure 3-7 and control law (3.68) is shown in Figure 3-14. When the control gain is held constant as the advection time delay is increased the spectral abscissa experiences a decaying exponential sinusoidal behavior. As a result, the controlled combustor has islands of stability that alternative between positive and negative gain with a period approximately equal to that of the fundamental period of the combustion instability. Improving the system performance with large advection delays is more difficult because the stability islands shrink which suggesting that increased robust performance issues exist. Figure 3-14 also shows that it is very easy to over drive the combustor with high gains in order to decrement system performance.

All of this behavior is very interesting but the real fundamental question here is why this happens? Typically, this is attributed to Rayleigh's criterion,[29] discussed in detail back in §1.3. While this is physically sound the standard mathematical analysis of Rayleigh's criterion are typical incorrect because they rely upon the method of harmonic

balance.[181] This method treats the system response as a harmonic function which clearly ignores the infinite dimensionality of the problem. Standard results yield alternating bands of equal width for stability and instability as a function of time delay. None of the interesting behavior and trends in Figure 3-14 is explained by this. Using Rayleigh Criterion is a dead end here, especially considering that the response of a time delay system cannot be generally written in explicit form. Clearly, an alternative framework is required.

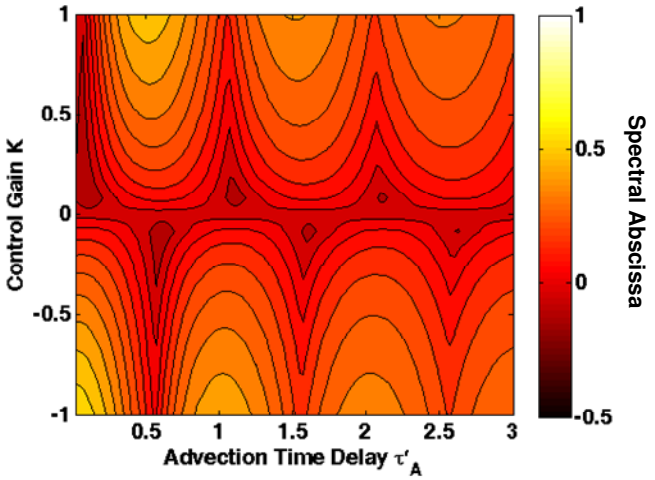

Figure 3-14: Spectral abscissa for a controlled self-excited, noise driven, combustor corresponding to case 1 in Appendix D as a function of k and τ'_A.

Understanding how the control operator excites the temporal mode shapes can go a long way in explaining the behavior in Figure 3-14 even if the vector of normalization constants is generally unknown. Selecting the gain and time delay of a proportional delay conmpensator (3.68) for a time delay system is very similar to selecting the gain and actuator position for proportional control of vibrating structures. For the structure vibration problem many different ways exists to optimize the actuator placement such as through Hankel singular vectors[182] or properly setting it up as a spatial $\mathcal{H}_2$ control problem.[183] These techniques do not translate well to time delay systems because high

frequency eigenvalues are hard to capture via discretization. As a result, large classes of optimization techniques will be very sensitive to how the state space is discretized.

One very simplistic way to place an actuator for controlling structural vibrations is to place it at the maxima of a mode that needs to be controlled. This method ignores the fact that feedback control will change the mode shapes. Time delay systems are very forgiving in this aspect because the temporal mode shapes are always exponentials. What does change is the location of the eigenvalues and hence the normalization constant but enough similarity exists to effectively explain certain trends in control effectiveness. To use this idea a figure of merit is needed. Drawing upon the structural vibrations example the desired result can come from taking the inner product of the spatial mode shape of interest with a control operator representing what fragment of the state space the actuator acts upon. For example, a point actuator would be represented by a gain and a Dirac delta function at the actuator position. A piezoelectric actuator would be a non-zero functional over the space that it covers with the gain determined by how the actuator distributes force. An appropriate analogue in time delay systems would correspond to a proportional delay controller and a distributed delay controller respectively. The corresponding operation for the time delayed Langevin's equation (3.8) with a proportional delay controller is shown in Eq. (3.69) below.

$$\left\langle \begin{matrix} c_i \\ c_i e^{\lambda_i(\bullet)} \end{matrix} , \begin{matrix} 0 \\ k\mathcal{S}\left(-\tau_c'\right)\delta(t) \end{matrix} \right\rangle = k c_i e^{-\lambda_i \tau_c} \tag{3.69}$$

Throughout the rest of this section the first argument in all inner products will be set up to only extract the pressure component of the temporal mode shapes because pressure based feedback (3.68) is being used for the thermo-acoustic control model.

$$\left\langle \begin{matrix} \begin{bmatrix} 0 & 1 & 0 & 0 & 0 \end{bmatrix}\vec{c}_i & 0 \\ \begin{bmatrix} 0 & 1 & 0 & 0 & 0 \end{bmatrix}\vec{c}_i e^{\lambda_i(\bullet)} & \begin{bmatrix} 0 & 0 & 0 & 0 & k \end{bmatrix}\left(\sum_{m=0}^{3} B_m \mathcal{S}\left(-\tau_m'\right)\right)\begin{pmatrix} \delta(t) \\ \mathcal{D}\delta(t) \\ \mathcal{D}^2\delta(t) \end{pmatrix} \end{matrix} \right\rangle$$

$$= c_i(2)k\Big[\left(B_1(3,1)-\lambda_i B_1(3,2)+\lambda_i^2 B_1(3,3)\right)+\left(B_2(3,1)-\lambda_i B_2(3,2)\right)e^{-\lambda_i\frac{\tau_V}{\beta^2}}\ldots \quad (3.70)$$

$$+\left(B_3(3,1)-\lambda_i B_3(3,2)\right)e^{-\lambda_i\tau_V}\Big]e^{-\lambda_i\tau_A}$$

Since the equivalence ratio modulations induced by the controller indirectly affects the acoustics through volumetric heat release perturbation the form of the control operator in Eq. (3.70) is much more complicated than Eq. (3.69). Derivatives of the control input (2.35) are represented by derivatives of the Dirac delta while the multiple time delays are represented using the corresponding shifts. The terms within the bracket make Eq. (3.70) looks hopelessly complicated but its functional dependence on the gain and advection delay are easily factored outside of the brackets.

For the purposes of this analysis the only features that matter in Eq. (3.70) is that the advection time delay only shows up in one term, $exp(-\lambda_i\tau_A)$, which is multiplied by an exponential polynomial of the eigenvalue of the temporal mode shape. This means that the time delays that yield the best control performance are the extrema of this expression. How the extrema of Eq. (3.70) are distributed is not immediately obvious in its current form but if the result is added to its complex conjugate, corresponding to the inner product of the temporal mode shape of the complex conjugate eigenvalue, then the resulting expression has a sinusoidally varying exponential. As a result, the stability islands in Figure 3-14 must appear with a period that is half of the fundamental mode (approximately 0.5) and alternate between minima and maxima; hence explaining the alternative gains and spacing of the stability islands. Additionally, the derivative of a sinusoidal exponential is a sinusoidal exponential with a phase offset. This explains why

the pattern of alternating stability islands does not start from zero advection delay but instead has an offset.

Currently, the normalization constant has been treated as a constant as its name would suggest; however, this constant is sensitive to the definition of the inner product of the extended state space and hence the advection delay. Although the exact value of these normalization constants cannot be generally solved for analytically their behavioral trends are the same as the one dimensional case (3.63) due to sharing the same form of the temporal mode shapes. When $Re(\lambda_i)\tau_A$ is small the normalization constant is relatively indifferent to the value of the advection delay; therefore, the previous discussion on stability islands trends hold. In the opposite limit the advection delay dependence in the normalization constant perfectly cancels out the explicit advection delay dependence of the inner product of the temporal mode shape with the control operator in Eq. (3.70). As a result, the performance of the control law (3.68) becomes indifferent to the value of the advection delay which means no more stability islands should exist at large enough delays. What is seen in Figure 3-14 is a transition between these two regimes which explains why each subsequent stability island does not push the spectral abscissa as deep in the LHCP as the previous stability island.

The final remaining mystery pertains to what determines the size of these islands. In particular, why are large gains destabilizing? This requires understanding how the other eigenvalues respond to the control input. Figure 3-15 shows how the eigenvalues change with gain at an advection delay corresponding to the midline of the third stability island in Figure 3-14. As the control gain is increased from the uncontrolled case ($k = 0$) the spectral abscissa is pushed deeper into the LHCP but the second rightmost eigenvalue is pulled towards the RHCP faster than the rightmost pair is pushed into the LHCP. When the gain is high enough ($k \approx 0.118$) the trajectories of these two eigenvalues cross such that the eigenvalue that was the 2nd rightmost eigenvalue becomes the new spectral abscissa. The reason this occurs is that the second rightmost eigenvalues in the

uncontrolled case has a larger value for $Re(-\lambda_i)\tau_A$ in the exponential in Eq. (3.70) and hence is more sensitive to control. This means that as the control gain is increased the placement of more eigenvalues have to be juggled; hence suggesting why large gains are destabilizing.

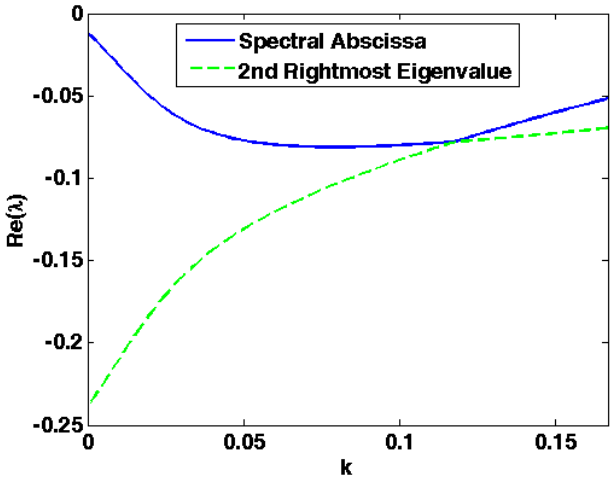

Figure 3-15: The two rightmost eigenvalues as a function of *k* corresponding to case 1 in Appendix D with $\tau'_A = 1.1$.

Two very interesting repercussions on control design result from the trajectories of these two eigenvalues crossing. As control becomes more effective the real part of the eigenvalues begins to cluster together such that the spectral abscissa becomes a less dominant component of the system response, weakening its ability to act as a predictor of system performance. The second interesting repercussion is that the trajectory of the spectral abscissa with respect to any parameter is not continuous in the first derivative. When a parameter is varied each eigenvalue follows its own trajectory in the complex plane. If an eigenvalue moving to the right overtakes the rightmost eigenvalue moving to the left an abrupt slope discontinuity appears in the spectral abscissa. Gradient search algorithms[184] can get confused while optimizing control gains which can lead to an incorrect minimum in the cost function being optimized. This will become increasing important as more complex controllers with more degrees of freedom are considered.

In the interest of fairness one discrepancy exists in Figure 3-15 that this simplistic temporal mode shape approach cannot explain. When tracking the eigenvalue corresponding to the spectral abscissa in the uncontrolled case the eigenvalue initially moves deeper into the LHCP as the gain is increased until $k \approx 0.08$ where the trajectory reaches a minimum. Afterwards, this trajectory begins to move this eigenvalue towards the RHCP. A hypothesis for why this could be occurring is that the normalization constant for pressure is being redistributed to the normalization constants of different derivatives of χ. Table 3-1 shows the numerically calculated eigenvector for this eigenvalue for three different values of k in Figure 3-15. Increasing the gain decreases the magnitude of $c_1(2)$, making the control effort less effective. While this creates some questionable trust in the results of this simple temporal mode shape approach it is hard to deny the advantage it has in explaining control effectiveness trends compared to the Rayleigh's criterion explanation.

To be rigorous, in the spirit of the modeling process illustrated in Figure 2-1, the control effectiveness trends just predicted and explained need to be corroborated with experimental evidence. At first glance a proportional delay compensator seems to offer marginal improvements in the spectral abscissa which seems to conflict with the summary of experimental results provided in §1.2. Most test results are for unstable combustors such that the large improvements in the pressure spectrum reported are for a system already in a limit cycle. The linear control then shrinks the orbit of this limit cycle.[26] On the other hand, this thesis and the thermo-acoustic model contained within it are concerned with self-excited noise driven combustors. This corresponds to a driven linearly stable system which may exhibit unwanted but acceptable performance characteristics which is a fairly common in industry. Currently, a dearth of experimental data exists for this case that will have to be addressed in the future. Figure 3-14 is clearly pessimistic in improving stability margins and performance in a driven linear combustor; however, this is a very simple controller and these results are not a proof of impossibility.

Table 3-1: How the eigenvector of the spectral abscissa in the uncontrolled case changes with feedback control corresponding to Figure 3-15.

K	0	1/12	1/6
$c_1(1)$	0.0001	0.0002	0.0002
$c_1(2)$	-0.0014	-0.0010	-0.0008
$c_1(3)$	-0.0021	-0.0055	-0.0074
$c_1(4)$	0.0546	0.0387	0.0284
$c_1(5)$	0.0779	0.1957	0.2621

3.7.2 Two Projected Spatial Mode Shapes

Harmonic coupling is one of the least understood aspects of feedback control of combustion instabilities. An analysis by Kopasakis[185] of the coherence of the fundamental mode of instability from an experimental aircraft engine simulator with the rest of the pressure spectrum found very strong coherence at higher harmonics of the instability frequency. Kopasakis then hypothesized that feedback control at higher harmonics could also be used to suppress combustion instabilities. Follow up experiments[61] at NASA Glenn greatly exceeded expectations where feedback control at the first harmonic proved to be twice as effective as feedback control based upon the fundamental frequency. Later work[186] at NASA Glenn proposes looking at wave asymmetry arguments based upon analogy with gravity waves in oceanography. The issue of why and when this occurs has never been satisfactorily explained and hence this is an excellent test of the viability of any thermo-acoustic model.

Instead of looking at the coherence this thesis will consider the correlation coefficient between the fundamental mode and the first harmonic. Systems with strong correlations should experience harmonic coupling. If the correlation is positive then

feedback control of one mode will also help suppress the other mode while if it is negative stabilizing one mode will destabilize the other. An analytical expression can be set up using the nomenclature introduced in §3.2 to describe pdf's.

$$\rho\left(Y_1,Y_2\right)=\frac{\sigma_{(y,1,2)}^{\ 2}}{\sigma_{(y,1,1)}\sigma_{(y,2,2)}} \tag{3.71}$$

As mentioned previously, writing out the power spectral density matrix (3.24) for more than one mode and including control gets prohibitively large. Luckily, all the information needed is contained in the quasi-polynomials structure of the individual terms in this matrix. The most important term in deciding the value of the correlation coefficient (3.71) is the covariance between these two modes. Inspection of the thermo-acoustic model (2.68) used in this thesis show that the terms responsible for modal coupling com from boundary condition and volumetric heat release perturbation interactions. Boundary condition terms are capable of being higher order in frequency and larger in magnitude compared to the volumetric heat release perturbation terms which suggests that boundary conditions are the dominant effect in this model. A simple inspection of the lack of influence the time delayed terms have on the pressure spectrum in Figure 3-3 compared to the boundary conditions reinforces this narrative.

In the first example to be explored is a case with no coupling at the boundary conditions. Figure 3-16 shows the best achievable spectral abscissa for all possible gains at a fixed advection delay for control based on the fundamental and the first harmonic. Feedback control based upon the fundamental mode performs as expected and shows the same type of trends discussed in the previous subsection. Higher harmonic control is more enigmatic revealing itself to be completely ineffective. This does not mean it is not doing anything. Changes in the spectral abscissa are more noticeable with the first harmonic based controller if the ordinate in Figure 3-16 is rescaled. What is causing these differences between these two controllers is the weakness of the modal coupling

from the volumetric heat release perturbation terms. Much larger gains are required by the first harmonic based controller to influence the spectral abscissa but before it can do this the controller destabilizes other eigenvalues which then become the new spectral abscissa, similar to what happens in Figure 3-15 as the control gain is increase for the one projected spatial mode case.

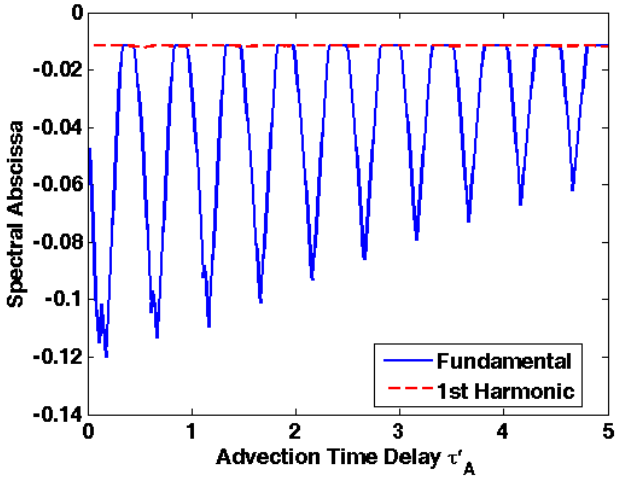

Figure 3-16: Best possible spectral abscissa for all gains at a give advection delay with feedback control at the fundamental frequency or first harmonic. Corresponds to case 2 in Appendix D.

When boundary condition coupling is added the first harmonic controller becomes much more responsive as shown in Figure 3-17. The feedback control based upon the fundamental mode is still performing much better for the vast majority of cases compared to a controller based upon the first harmonic. Another interesting behavior is that the performance trends are no longer matching the trends predicted for the single projected spatial mode shape example. Moving unanticipated eigenvalues becomes easier due to the stronger modal coupling such that the unfamiliar patterns in Figure 3-17 are due to different eigenvalues becoming the spectral abscissas parameters are changed. As a result, the controller based upon the fundamental mode does not perform as well in Figure 3-17 as in Figure 3-16. Meanwhile, the controller based upon the first harmonic

performs better in Figure 3-17 than Figure 3-16 because it can pull the eigenvalues associated with the fundamental mode easier with lower gains.

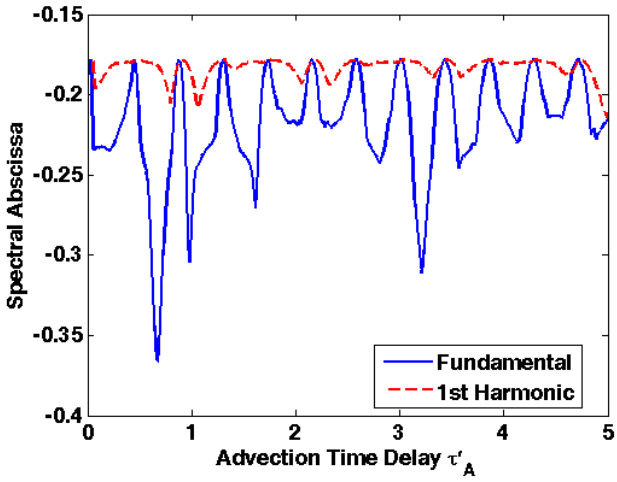

Figure 3-17: Best possible spectral abscissa for all gains at a give advection delay with feedback control at the fundamental or first harmonic. Corresponds to case 3 in Appendix D.

The results in Figure 3-17 are promising but does not explain how higher harmonic control did such a better job in the NASA Glenn results.[61] Associating this with a modeling mismatch of the volumetric heat release perturbation modeling under limit cycle behavior is much too simplistic because increasing the linear damping in one mode should decrease the limit cycle amplitude of that mode. In the experiments by NASA Glenn an adaptive phase controller was used that would dither the phase to see what direction to increment the phase. For NASA Glenn's higher harmonic experiments the phase compensated is such a way to add a frequency component at the fundamental frequency to the voltage commands going to the fuel actuator; therefore, what NASA Glenn labeled as higher harmonic control should have been labeled as mixed mode control. When control is applied based on the fundamental mode the combustion instability at the fundamental frequency is suppressed while aggravating the first harmonic, as seen in their SPL plots.[61] With mixed mode control the higher harmonic

controller can stabilize the aggravated modes so that the controller working on the fundamental frequency can continue to push the spectral abscissa deeper into the LHCP.

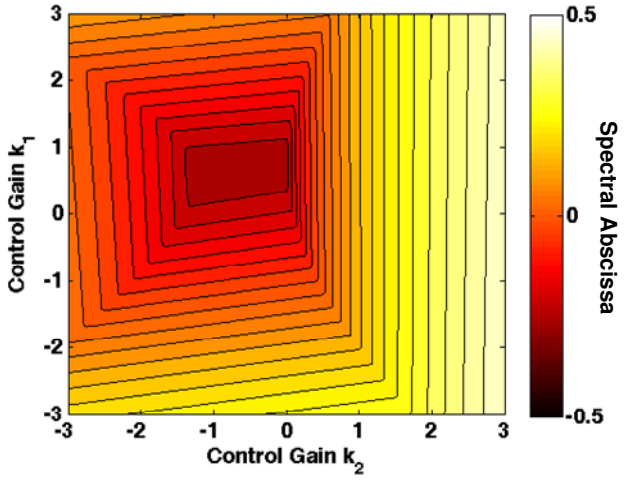

Figure 3-18: Performance map of the spectral abscissa placement achieved by a mixed mode controller corresponding to case 3 in Appendix D with τ'_A = 0.80.

Having two degree of freedom obviously allows a controller to perform better. Figure 3-18 shows a parameter map of how the spectral abscissa varies with gain in a mixed mode controller corresponding to the τ'_A = 0.80 data point in Figure 3-17. Improvements from using multimodal control are marginal over the feedback controller based upon the fundamental mode if the spectral abscissa is the only benchmark for performance. Benefits of mixed mode control come from increasing the robust performance of the control system. Both single mode controllers perform optimally near regions of sharp gradients in the spectral abscissa such that unmodeled behavior in the fuel actuator can greatly reduce control system performance. By moving the spectral abscissa to a less sensitive region in the parameter space allows a much more practical controller design. This is very similar to the more advanced stability radii concept introduced by Michiels and Roose.[187]

CHAPTER 4

FACTORS LIMITING CONTROL EFFECTIVENESS

Performance limitations in feedback control systems are strongly influenced by its state. The presence of time delays in the new thermo-acoustic model introduced in Chapter 2 requires using an extended state space which is why Chapter 3 spent so much effort on corroborating predicted results with prior experimental data. Time delay systems present new challenges for the control engineer. Infinite dimensional compensators can be difficult to design and implement. The first step to understanding what is mathematically achievable is investigating the concept of controllability in more detail. This will reveal how and where the eigenvalues of the infinitesimal generator can be relocated in the complex plane. Afterwards, what is physically achievable is investigated by introducing sensitivity functions to illustrate how feedback loops naturally create control constraints. These sensitivity functions show how disturbances at a given frequency are either attenuated or amplified. Merging both of these ideas together create a powerful lens into understanding the optimal control design problem and practical implementation issues. Despite having limited analysis tools, the design process illustrates that the factors that limit control effectiveness are closely related to the properties of the open loop system response. The implications this has on the combustor design process and the practicality of industrial adoption is then discussed.

4.1 Controllability

One of the most fundamental questions a control engineer can ask is what limits the ability of a control system to shape a system's performance. In finite-dimensional linear systems a controllable system is able to find a control input to steer every possible initial state to the origin in a finite time. A useful property that comes with controllability

is that it gives the control engineer the ability to place the closed loop eigenvalues anywhere in the complex plane independently of each other. Another closely related concept is a reachability which is the ability to find a control input to steer the state from the origin to every possible final state in a finite time. Reachability implies controllability and vice versa if the state transition matrix is invertible. These are basic facts that can be found in any introductory text in linear system theory.[188]

In infinite-dimensional linear system theory what is referred to as exact controllability is actually the extension of reachability in finite-dimensional linear system theory.[84] When the infinitesimal generator is unbounded but the control operator is bounded then a system can never be exactly controllable.[189] This is always true for linear functional differential equations even if delays exists or derivatives are acting on the system input because they appear in the infinitesimal generator using the extended state space introduced in §2.8 which ensures that the control operator is bounded. The definition of exact controllability is too strict because a state represents the system response for a span of time instead of a point in time in the finite-dimensional case. Arbitrarily assigning an infinite number of eigenvalues is impossible.

A weaker version of controllability is needed and no shortages of alternative definitions exists,[46] but not every definition has a clean interpretation in terms of the eigenvalues. Furthermore, many equivalent definitions were invented independently over the span of several decades making the literature murky. Some of the more useful alternative definitions are collected in the monograph by Curtain and Pritchard.[82] Of particular interest is the concept of exact-null controllability which is analogous to controllability in finite-dimensional linear system theory. In terms of the system eigenvalues, exact-null controllability is equivalent to arbitrarily assigning a finite number of eigenvalues. This is sufficient to drive the system to the origin because as discussed in §3.5 only a finite number of eigenvalues exists in the RHCP for retarded delay differential equations.

Pandolfi[190] was the first to develop a Popov-Belevitch-Hautus style test for linear functional differential equations to show under what conditions a finite number of eigenvalues can be assigned while holding all other eigenvalues in place. The matrix used in this test and subsequent work is nameless but for convenience this thesis will refer to it as the exact-null controllability matrix. If this matrix test fails to have full row rank at any point in the complex plane then there exists a vertical line in the complex plane passing through that point which the trajectories of the eigenvalues cannot move past as control is applied. A system that is not exact-null controllable is said to be β-exponentially stabilizable where β is the coordinate of this vertical line. The significance of β is that it represents the best possible spectral abscissa that feedback control can mathematically achieve. While this reveals nothing about the form of the optimal controller, nor its physically realizability, it does represent an upper limit to achievable stability margin. Any limit in achievable stability margin will also limit the control engineer's ability to shape the system response since the spectral abscissa determines the rate of decay of a bounding exponential for the system response to an impulse disturbance

An extension by Olbrot[191] allowed this test to include linear functional differential equations which have a functional of bounded variation acting upon the control input. This allows for time delays to be incorporated into the control input. These conditions almost cover the thermo-acoustic model (2.68) being investigated in this thesis except that derivatives acting on the control input exist which makes the control operator unbounded. Fortuitously, Olbrot's proof (Theorem 1) only requires minor modifications to include this case. The extended proof is given in Appendix E. When this modified theorem is applied to Eq. (2.68) the exact-null controllability matrix is given by Eq. (4.1).

$$\left[\begin{array}{c|c} \left[sI - A_0 - A_1 e^{-s\tau'}\right] & \left[B_1 e^{-s\tau'_A} + B_2 e^{-s\left(\tau'_A + \frac{\tau'_V}{\beta^2}\right)} + B_3 e^{-s(\tau'_A + \tau'_V)}\right]\begin{bmatrix} 1 \\ s \\ s^2 \end{bmatrix} \end{array}\right] \tag{4.1}$$

Matrix A_0 (2.72) has a large number of identity matrices hidden within it which ensures that the columns and rows that contain them cannot reduce the row rank of the exact-null controllability matrix (4.1). As a result, the only way for the exact-null controllability matrix to be row rank deficient is for the submatrix given by Eq. (4.2) to not have full rank; however, this is a necessary and not a sufficient condition to fail the exact-null controllability test.

$$\left[sI + \tilde{C}_0 + 2\frac{M}{\tau'_V}\tilde{S}_2 - 2\frac{M}{\tau'_V}\tilde{S}_2 e^{-s\tau'_V}\right] \tag{4.2}$$

The exact-null controllability matrix has more columns than rows. If the last column group in the exact-null controllability matrix has a component in the null-space of the characteristic matrix then the exact-null controllability matrix still has full row rank. Alternatively, the submatrix could have a rank deficiency greater than one if the zero has a multiplicity greater than one but this is uncommon for exponential polynomials. For all intensive purposes the thermo-acoustic model in this thesis is exact-null controllable.

This is a startling result considering how limited the improvements in the spectral abscissa were for the controllers investigated in §3.7. The exact-null controllability test allows for the controller to be a member of any possible subspace in the extended state space. Intuitively, a controller using the full extended state space instead of a finite dimensional subspace of an infinite dimensional space like a proportional delay compensator should exhibit superior performance. Although a superior controller may exist mathematically this does not mean it is physically realizable. Real control systems have constraints on their behavior which are not included in the exact-null controllability test. For example, a finite bandwidth fuel actuator with limited authority cannot faithfully reproduce any arbitrary control law in the extended state space. Constrained

controllability tests for infinite dimensional systems[192] work by forbidding the controller from being a member of certain subspaces in the extended state space. Unfortunately, a specific version corresponding to exact-null controllability does not exist. An alternative framework is needed to investigate these issues.

4.2 Sensitivity Functions

In physical systems conservation laws play an important role in creating fundamental limits because they create inviolable constraints in the behavior of the system. Control theory has many concepts similar to energy that can be cast as a conservation law.[193] A natural way of looking at energy concepts is in the frequency domain. The very presence of a feedback loop creates frequency response constraints in the closed loop system dynamics since the feedback loop must be physically realizable and analytic.[194] This creates the means to investigate the factors that limit control effectiveness and understand the system behavior as these limits are approached.

Typically, system behavior is benchmarked by the closed loop performance; however, the system behavior that is initially known is the open loop performance. Linking closed loop performance to open loop performance will require a common framework. A general feedback diagram applicable to both cases is shown in Figure 4-1 for a single-input single-output (SISO) system. Comments on the multiple-input multiple-output (MIMO) system will be made towards the end of this section. Inspection of Figure 4-1 shows that it is drawn using a feedback compensator. Precompensation is not included in Figure 4-1 because it corresponds to the controller altering the combustor geometry or boundary conditions. Here, a reference signal $R(s)$ is feed into the plant transfer function $P(s)$. An ideal sensor $Y(s)$ reads the output of $P(s)$ plus any system disturbances $D(s)$. $Y(s)$ plus any noise $N(s)$ that exists in the sensor is the input to the compensator $F(s)$. Afterwards, the compensator output is fed back into $P(s)$.

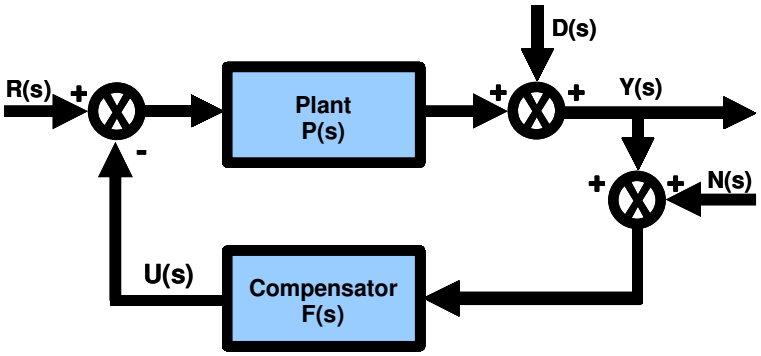

Figure 4-1: General SISO feedback diagram with feedback compensation.

Before proceeding, the feedback diagram that physically illustrates self-excited, noise driven, combustors, Figure 2-2, needs to be understood in the context of Figure 4-1. The plant $P(s)$ is the closed loop transfer function of the internal feedback loop which includes the transfer functions of the combustor $G(s)$, the self-excitation due to velocity perturbations $I(s)$, and the sensor $M(s)$ while the compensator $F(s)$ includes the effects of an estimator $E(s)$, if present, and the control response $K(s)$ due to equivalence ratio perturbations. All of the input terms in Figure 4-1 are not present in Figure 2-2 except for the reference signal $R(s)$ which can be interpreted as driving from combustion noise $C(s)$. When trying to write an expression for the closed loop response $Y_r(s)$ in the absence of disturbances and sensor noise the sensitivity function $S(s)$ naturally crops up.

$$Y_r(s) = S(s)P(s)R(s) \tag{4.3}$$

$$S(s) = \left[I_n + L(s)\right]^{-1} \tag{4.4}$$

$$L(s) = P(s)F(s) \tag{4.5}$$

The sensitivity function (4.4) is the transfer function between output disturbances $D(s)$ and the system output. It happens to be a function of the open loop transfer function $L(s)$ which is a mapping between the plant input and the controller output. This means that open loop performance (4.5) can be related to closed loop performance (4.3) via the sensitivity function (4.4).

Another important function is the complementary sensitivity function $T(s)$ (4.7) which is the transfer function between sensor noise $N(s)$ and the system output.

$$Y_n(s) = -T(s)N(s) \tag{4.6}$$

$$T(s) = L(s)\left[I_n + L(s)\right]^{-1} \tag{4.7}$$

The complementary sensitivity function can also be viewed as the transfer function between the reference signal R(s) and the control input $U(s)$ in the absence of output disturbances and sensor noise.

$$U(s) = T(s)R(s) \tag{4.8}$$

While the sensitivity function has a strong connection to system performance the complementary sensitivity function has a strong connection to the robustness of the system. On the $j\omega$-axis the magnitude of $T(s)$ at a given frequency decides the bounds on the system unstructured multiplicative uncertainty $M(\omega)$ at that frequency.[195]

$$\left|T(j\omega)\right| < \frac{1}{M(\omega)} \tag{4.9}$$

Inspection of the definition of the sensitivity function (4.4) and its complement (4.7) reveal that their sum must equal one which is called an algebraic constraint.

$$S(s) + T(s) = 1 \tag{4.10}$$

This shows that in any control design an inevitably tradeoff exists between system performance and robustness at the same frequency. At high frequencies where modeling is the least accurate and robustness is most needed requires that $|T(j\omega)|$ is very small, but in that limit $|S(j\omega)|$ is near one. Meanwhile, at low frequencies where $P(j\omega)$ is large requires $|S(j\omega)|$ to be very small to get good disturbance rejection of $R(j\omega)$, but in that limit $|T(j\omega)|$ is near one. Taken together, these two design goals do not interfere as long as the frequency range where good performance is needed does not overlap with the frequency range where robustness is needed. Sometimes the system performance and

robustness can both be poor at the same frequency when both $|S(j\omega)|$ and $|T(j\omega)|$ are greater than one.

Design constraints can also exist across different frequencies and are expressed as integral constraints. Bode[196] was the first person to formulate an integral constraint for stable rational SISO transfer functions with at least two more poles than zeros in $L(s)$. Freudenberg and Looze[197] extended Bode's sensitivity integral to work with unstable SISO systems for the case with at least two more poles than zeros in $L(s)$ or the case when $L(s)$ is factorable into the product of a strictly proper rational transfer function and a time delay.[198] All of these sensitivity integral constraints take the form of Eq. (4.11) and show dependence on how deep the poles are in the RHCP. Poles are zeros in the RHCP will be represented by p_i and z_i respectively throughout the rest of this thesis.

$$\int_0^\infty \log\left|S(j\omega)\right| d\omega = \pi \sum_{i=1}^{n_p} p_i \tag{4.11}$$

Intuitively, getting better performance out of a control system becomes more difficult as the open loop system becomes increasing unstable. Another extension valid for $L(s)$ as a proper rational transfer function comes from the monograph of Seron et al.[58] which add a second term to Eq. (4.11) related to the system response to the unit step function. Similar work by the same researchers has been done for Bode's complementary sensitivity integral with the additional constraint that $L(0)\neq 0$. A weighting function of ω^{-2} is used to help the integral to converge.

$$\int_0^\infty \log\left|T(j\omega)\right| \frac{d\omega}{\omega^2} = \pi \sum_{i=1}^{n_p} \frac{1}{z_i} + \frac{\pi}{2}\tau \tag{4.12}$$

When $L(s)$ is allowed to be a proper rational transfer function in Eq. (4.12) a third term is added related to the steady state error to a ramp input.

For the purposes of this thesis the assumptions constraining $L(s)$ to a rational transfer function with at most a single factorable time delay is too restrictive. Furthermore, the exact-null controllability test in the previous section suggests that high

performance controllers can take the form of a linear functional acting on the extended state space. As a result, an integral constraint that can handle distributed delays is required. The class of pseudo-rational transfer functions[199] is large enough to incorporate distributed delays. This class of transfer functions includes the ratio of entire functions of exponential type that are Laplace transforms of distributions with compact support. An example is given by the equation below.

$$L(\mathrm{s}) = \frac{\sum_{i=0}^{m}\sum_{l=0}^{n}\int_{-\tau_{a,l}}^{0} a_{il}(\kappa)\, s^i e^{s\kappa} d\kappa}{\sum_{i=0}^{m}\sum_{l=0}^{n}\int_{-\tau_{b,l}}^{0} b_{il}(\kappa)\, s^i e^{s\kappa} d\kappa} \tag{4.13}$$

In this thesis each of the kernels a_{il} and b_{il} are treated as a piecewise continuous function plus the sum of a finite number of Dirac delta functions. The time delays are sorted in such a way that their magnitude increases with j; therefore, the time delays at $j = 0$ are zero. If any coefficients of a_{ml} and b_{ml} are nonzero $\nexists\, l \geq 1$ then the closed loop system behaves as a neutral delay differential equation.

Sensitivity and complementary sensitivity integral constraints for pseudo-rational transfer functions that are similar to Eq. (4.12), due to ω^{-2} weighting function, are derived by evaluating the contour integral in Figure 4-2. Integral constraints without the weighting term similar to Eq. (4.11) will be revisited at the end of this section. The weighted integral constraints are expressed analytically in Eq. (4.14) and Eq. (4.15) respectively.

$$\oint_{C} \log\big(S(s)\big)\frac{ds}{s^2} = \oint_{C_0} \log\big(S(s)\big)\frac{ds}{s^2} + \sum_{i=1}^{n_p}\oint_{C_i} \log\big(S(s)\big)\frac{ds}{s^2} + \oint_{C_R} \log\big(S(s)\big)\frac{ds}{s^2} \tag{4.14}$$

$$\oint_{C} \log\big(T(s)\big)\frac{ds}{s^2} = \oint_{C_0} \log\big(T(s)\big)\frac{ds}{s^2} + \sum_{i=1}^{n_z}\oint_{C_i} \log\big(T(s)\big)\frac{ds}{s^2} + \oint_{C_R} \log\big(T(s)\big)\frac{ds}{s^2} \tag{4.15}$$

In the limit as $R \longrightarrow \infty$ the contour shown in Figure 4-2 is evaluated over the entire RHCP as an expanding semicircle, except for a number of branch cuts. These branch

cuts are needed because the complex logarithm is multivalued about any point where the argument of the complex logarithm is zero. For the weighted sensitivity function integral constraint (4.14) the number of branch cuts corresponds to the number of open loop poles, n_p, in the RHCP. Similarly, the number of branch cuts for the weighted complementary integral constraint (4.15) corresponds to the number of open loop zeros, n_z, in the RHCP. These RHCP zeros are called non-minimum phase zeros.

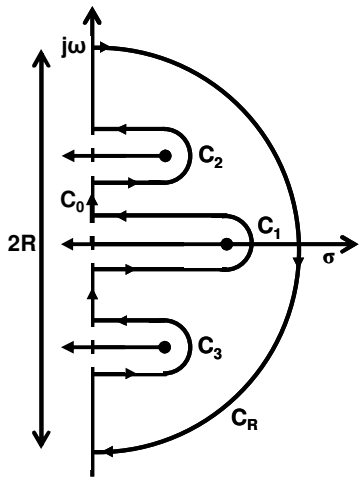

Figure 4-2: Contour integral needed to derive integral constraints for the sensitivity function and its complement.

Since the region on and within the closed contour C is analytic Cauchy's integral theorem can be used. This ensures that the left hand side of Eq. (4.14) and Eq. (4.15) are both zero. The contour on the $j\omega$-axis, C_0, can be simplified by taking advantage of conjugate symmetry. All of the contours around the branch cuts, C_i, have already been evaluated in simpler proofs[58] by invoking the inverted symmetry that exists due to the ω^{-2} weighting term.

$$\frac{f(j\omega)\,d\omega}{\omega^2} = f\left(\frac{1}{jv}\right)dv \tag{4.16}$$

Contour C_R is the most difficult to evaluate and it is where the previous proofs for rational $L(s)$ fails to extend to general time delay systems because it relies upon the

existence of a Laurent series expansion at infinity. Functional differential equations have unbounded roots which prevents this technique from being used. Instead, the integral has to be evaluated directly. Collectively, these evaluations result in Eq. (4.17) and Eq. (4.18).

$$-2j\int_0^{\infty}\log\left|S(j\omega)\right|\frac{d\omega}{\omega^2}+2j\pi\sum_{i=1}^{n_p}\frac{1}{p_i}-\lim_{R\to\infty}\frac{j}{R}\int_{-\frac{\pi}{2}}^{\frac{\pi}{2}}\log\left(S\left(R\mathrm{e}^{j\theta}\right)\right)e^{-j\theta}d\theta=0 \tag{4.17}$$

$$-2j\int_0^{\infty}\log\left|T(j\omega)\right|\frac{d\omega}{\omega^2}+2j\pi\sum_{i=1}^{n_z}\frac{1}{z_i}-\lim_{R\to\infty}\frac{j}{R}\int_{-\frac{\pi}{2}}^{\frac{\pi}{2}}\log\left(T\left(R\mathrm{e}^{j\theta}\right)\right)e^{-j\theta}d\theta=0 \tag{4.18}$$

Evaluating the third integral in Eq. (4.17) and Eq. (4.18) due to C_R by substituting Eq. (4.13) into one of the integral constraints looks daunting, but in the limit of large R many of the terms drop out. This assumes that the limit can be brought inside of the integral. A proper proof for showing that the limit and integral operation commute using the dominated convergence theorem[200] will not be attempted. Instead, this thesis will proceed as if interchanging these operators is valid and then compare the results to simpler problems with known solutions to offer a heuristic justification of this procedure. Several intermediate steps are required before this occurs; the first of which is expanding the sensitivity function and its complement.

$$S\left(R\mathrm{e}^{j\theta}\right)=\frac{\sum_{i=0}^{m}\sum_{l=0}^{n}\int_{-\tau_{b,l}}^{0}b_{il}(\kappa)\left(R\mathrm{e}^{j\theta}\right)^i e^{R\mathrm{e}^{j\theta}\kappa}d\kappa}{\sum_{i=0}^{m}\sum_{l=0}^{n}\left(\int_{-\tau_{a,l}}^{0}a_{il}(\kappa)\left(R\mathrm{e}^{j\theta}\right)^i e^{R\mathrm{e}^{j\theta}\kappa}d\kappa+\int_{-\tau_{b,l}}^{0}b_{il}(\kappa)\left(R\mathrm{e}^{j\theta}\right)^i e^{R\mathrm{e}^{j\theta}\kappa}d\kappa\right)} \tag{4.19}$$

$$T\left(R\mathrm{e}^{j\theta}\right)=\frac{\sum_{i=0}^{m}\sum_{l=0}^{n}\int_{-\tau_{b,l}}^{0}a_{il}(\kappa)\left(R\mathrm{e}^{j\theta}\right)^i e^{R\mathrm{e}^{j\theta}\kappa}d\kappa}{\sum_{i=0}^{m}\sum_{l=0}^{n}\left(\int_{-\tau_{a,l}}^{0}a_{il}(\kappa)\left(R\mathrm{e}^{j\theta}\right)^i e^{R\mathrm{e}^{j\theta}\kappa}d\kappa+\int_{-\tau_{b,l}}^{0}b_{il}(\kappa)\left(R\mathrm{e}^{j\theta}\right)^i e^{R\mathrm{e}^{j\theta}\kappa}d\kappa\right)} \tag{4.20}$$

Finding the dominant term inside the complex logarithm in the limit of large R will allow for the neglection of most of the terms. The R in the exponential terms is the most important because it drives each term to zero faster than any power of R going to infinity; therefore, the dominant term in the numerator or denominator of $L(s)$ is decided by the kernel a_{ij} or b_{ij} that is nonzero for the smallest value of the dummy variable κ. If multiple kernels satisfy this condition then the kernel that is multiplied by the largest power of R is dominant. Only one term in the numerator and denominator will survive inside the complex logarithm. Both of the remaining kernels can be bounded from above and below by a piecewise constant function. A substitution of this nature allows the functional inside the complex logarithm to be evaluated which results in a ratio of exponential polynomials.

$$\begin{aligned}&\lim_{R\to\infty} c_{S,L}\left(R\mathrm{e}^{j\theta}\right)^{\left(m_D^*-\max\left(m_N^*,m_D^*\right)\right)} e^{-R\mathrm{e}^{j\theta}\left(\tau_D^*-\min\left(\tau_N^*,\tau_D^*\right)\right)} \le \lim_{R\to\infty} S\left(R\mathrm{e}^{j\theta}\right) \le \\ &\lim_{R\to\infty} c_{S,U}\left(R\mathrm{e}^{j\theta}\right)^{\left(m_D^*-\max\left(m_N^*,m_D^*\right)\right)} e^{-R\mathrm{e}^{j\theta}\left(\tau_D^*-\min\left(\tau_N^*,\tau_D^*\right)\right)}\end{aligned} \tag{4.21}$$

$$\begin{aligned}&\lim_{R\to\infty} c_{T,L}\left(R\mathrm{e}^{j\theta}\right)^{\left(m_N^*-\max\left(m_N^*,m_D^*\right)\right)} e^{-R\mathrm{e}^{j\theta}\left(\tau_N^*-\min\left(\tau_N^*,\tau_D^*\right)\right)} \le \lim_{R\to\infty} T\left(R\mathrm{e}^{j\theta}\right) \le \\ &\lim_{R\to\infty} c_{T,L}\left(R\mathrm{e}^{j\theta}\right)^{\left(m_N^*-\max\left(m_N^*,m_D^*\right)\right)} e^{-R\mathrm{e}^{j\theta}\left(\tau_N^*-\min\left(\tau_N^*,\tau_D^*\right)\right)}\end{aligned} \tag{4.22}$$

In the nomenclature above in Eq. (4.21) and (4.22) c_L and c_U refer to lower and upper bounding constants for the sensitivity function or its complement. The time delays τ^*_N and τ^*_D refer to the smallest delay that exists for a nonzero value in any kernel in the numerator and denominator of the open loop transfer function respectively. Finally, m^*_N and m^*_D refer to the highest power of s corresponding to the time delays τ^*_N and τ^*_D.

When the bounds derived for the sensitivity function (4.21) or its complement (4.22) is substituted back into Eq. (4.17) and Eq. (4.18) the complex logarithm can be broken into the sum of three different complex logarithms: one for the constants, another for the powers in R, and the third for the exponential term.

$$\lim_{R\to\infty}\int_{-\frac{\pi}{2}}^{\frac{\pi}{2}}\left[\frac{\log\left(c_{S,L}\right)+\left(m_D^*-\max\left(m_N^*,m_D^*\right)\right)j\theta}{R}\right]e^{-j\theta}d\theta$$

$$+\lim_{R\to\infty}\int_{-\frac{\pi}{2}}^{\frac{\pi}{2}}\left[\frac{\log\left(R\right)}{R}\right]e^{-j\theta}d\theta+\lim_{R\to\infty}\int_{-\frac{\pi}{2}}^{\frac{\pi}{2}}\left[-\left(\tau_D^*-\min\left(\tau_N^*,\tau_D^*\right)\right)\right]d\theta$$

$$\le\lim_{R\to\infty}\int_{-\frac{\pi}{2}}^{\frac{\pi}{2}}\frac{\log\left(S\left(Re^{j\theta}\right)\right)}{R}e^{-j\theta}d\theta$$

$$\le\lim_{R\to\infty}\int_{-\frac{\pi}{2}}^{\frac{\pi}{2}}\left[\frac{\log\left(c_{S,U}\right)+\left(m_D^*-\max\left(m_N^*,m_D^*\right)\right)j\theta}{R}\right]e^{-j\theta}d\theta$$

$$+\lim_{R\to\infty}\int_{-\frac{\pi}{2}}^{\frac{\pi}{2}}\left[\frac{\log\left(R\right)}{R}\right]e^{-j\theta}d\theta+\lim_{R\to\infty}\int_{-\frac{\pi}{2}}^{\frac{\pi}{2}}\left[-\left(\tau_D^*-\min\left(\tau_N^*,\tau_D^*\right)\right)\right]d\theta \tag{4.23}$$

$$\lim_{R\to\infty}\int_{-\frac{\pi}{2}}^{\frac{\pi}{2}}\left[\frac{\log\left(c_{T,L}\right)+\left(m_N^*-\max\left(m_N^*,m_D^*\right)\right)j\theta}{R}\right]e^{-j\theta}d\theta$$

$$+\lim_{R\to\infty}\int_{-\frac{\pi}{2}}^{\frac{\pi}{2}}\left[\frac{\log\left(R\right)}{R}\right]e^{-j\theta}d\theta+\lim_{R\to\infty}\int_{-\frac{\pi}{2}}^{\frac{\pi}{2}}\left[-\left(\tau_N^*-\min\left(\tau_N^*,\tau_D^*\right)\right)\right]d\theta$$

$$\le\lim_{R\to\infty}\int_{-\frac{\pi}{2}}^{\frac{\pi}{2}}\frac{\log\left(T\left(Re^{j\theta}\right)\right)}{R}e^{-j\theta}d\theta$$

$$\le\lim_{R\to\infty}\int_{-\frac{\pi}{2}}^{\frac{\pi}{2}}\left[\frac{\log\left(c_{T,U}\right)+\left(m_N^*-\max\left(m_N^*,m_D^*\right)\right)j\theta}{R}\right]e^{-j\theta}d\theta$$

$$+\lim_{R\to\infty}\int_{-\frac{\pi}{2}}^{\frac{\pi}{2}}\left[\frac{\log\left(R\right)}{R}\right]e^{-j\theta}d\theta+\lim_{R\to\infty}\int_{-\frac{\pi}{2}}^{\frac{\pi}{2}}\left[-\left(\tau_N^*-\min\left(\tau_N^*,\tau_D^*\right)\right)\right]d\theta \tag{4.24}$$

Since the path integrals in Eq. (4.23) and Eq. (4.24) are divided by R, the first two natural logarithm terms go to zero in the limit as R goes to infinity. The first term goes to zero regardless if the kernels in the open loop transfer function (4.13) are replaced by

piecewise constant functions bounded from above or below; therefore, via the squeeze theorem[200] the approximated answer becomes the actually answer in the limit as R goes to infinity. For convenience the squeeze theorem is stated below for functions that are locally continuous at a limit point, a.

$$\begin{aligned} &\textit{if} \quad g(x) \le f(x) \le h(x) \quad \& \quad \lim_{x\to a} g(x) = \lim_{x\to a} h(x) = L \\ &\textit{then} \quad \lim_{x\to a} f(x) = L \end{aligned} \tag{4.25}$$

In the case of the second term the ratio of $\log(R)/R$ goes to zero because R grows faster than $\log(R)$. Only the third term is capable of being nonzero. When the complex logarithm cancels the exponential the R that was in that first exponential also cancels the R that was dividing the natural logarithm. Additionally, the exponential in the exponential in the complex logarithm also cancels the exponential multiplying the complex logarithm. This leaves behind the integral of a constant which is easily evaluated.

$$\lim_{R\to\infty} \int_{-\frac{\pi}{2}}^{\frac{\pi}{2}} \frac{\log\left(S\left(Re^{j\theta}\right)\right)}{R} e^{-j\theta} d\theta = -\pi\left[\tau_D^* - \min\left(\tau_N^*, \tau_D^*\right)\right] \tag{4.26}$$

$$\lim_{R\to\infty} \int_{-\frac{\pi}{2}}^{\frac{\pi}{2}} \frac{\log\left(T\left(Re^{j\theta}\right)\right)}{R} e^{-j\theta} d\theta = -\pi\left[\tau_N^* - \min\left(\tau_N^*, \tau_D^*\right)\right] \tag{4.27}$$

The term in brackets on the right hand side of Eq. (4.26) is always zero while the term in brackets on the right hand side of Eq. (4.27) is the net delay, τ_{net}.[201] For the thermo-acoustic model considered in this thesis τ^*_D is zero while τ^*_N is the advection delay τ'_A. As a result, time delays in the control system do not affect achievable performance but they do hurt the system's robustness with respect to bounded uncertainty. This explains why the stability islands found in Figure 3-14 decrease with increases in the advection delay and also suggests that adding artificial delay to improve control system performance may not be in the engineer's best interest. An

infinite-dimensional compensator is able to achieve the same performance without sacrificing robust performance.

Fully simplifying the integral constraints gives Eq. (4.28) and Eq. (4.29).

$$\int_0^\infty \log\left|S(j\omega)\right| \frac{d\omega}{\omega^2} = \pi \sum_{i=1}^{n_p} \frac{1}{p_i} \tag{4.28}$$

$$\int_0^\infty \log\left|T(j\omega)\right| \frac{d\omega}{\omega^2} = \pi \sum_{i=1}^{n_z} \frac{1}{z_i} + \frac{\pi}{2}\tau_{net} \tag{4.29}$$

The sensitivity integral constraint shows that the area under the complex logarithm of the magnitude of the sensitivity function is equal to a constant dependent upon how close the poles of the open loop transfer function L(s) are to the $j\omega$-axis in the open RHCP while the non-minimum phase zeros play a similar role for the complementary integral constraint. The dependence of these integral constraints on how close the poles or zeros are to the $j\omega$-axis makes sense because performance is dictated by the values on the $j\omega$-axis; therefore, poles and zeros closer to the $j\omega$-axis will exert a greater influence. No weighted sensitivity integral constraint analogous to Eq. (4.28) exists in the literature; however, the weighted complementary sensitivity integral constraint (4.29) is analogous to Eq. (4.12) for a strictly proper open loop transfer function, $L(s)$, with a single factorable delay. Inspection of these two equations shows that the difference between the finite and infinite dimensional systems comes from the evaluation of contour C_R in Figure 4-2. In this limit $\tau_{net} = \tau$ and which shows that Eq. (4.29) properly simplifies into Eq. (4.12). The same cannot be said when $L(s)$ is proper which suggest the interchanging of the limit and integral operator in Eq. (4.21) and Eq. (4.22) is invalid when the roll-off is less than -2.

Integral constraints act similar to conservation laws because their area cannot be arbitrarily reduced by good control design, although a bad design can increase this area. Feedback control can only shift how this area is distributed.[66] A good controller works by shifting this area onto frequencies where the gain of P(s) is low to minimize the

response of $Y_r(s)$ (4.3). Unfortunately, a price must be paid for shifting the area around due to the ω^{-2} weighting term in these integrals. Combustion dynamics, contained in $P(s)$, take place at lower frequencies while $P(s)$ is low at high frequencies. Disproportionately more area must be added at high frequencies to compensate for small area changes at low frequencies. In an ideal world this would not matter because the area can be shifted to infinitely higher frequencies and $P(s)$ has low pass characteristics; however, real fuel actuators have bandwidth constraints which prevent manipulating this area beyond some cutoff frequency. As a result, a tipping point exists where redistributing area can no longer improve performance.

Other integral constraints can reveal different design tradeoffs. One alternative set of integral constraint for strictly proper systems with a single factorable time delay are the Poisson's integral constraints.[197]

$$\int_{-\infty}^{\infty} \ln\left|S(j\omega)\right| \frac{\mathrm{Re}(z_i)}{(z_i - j\omega)(\overline{z}_i + j\omega)} d\omega = \pi \ln\left|B_p^{-1}(z_i)\right| \tag{4.30}$$

$$\int_{-\infty}^{\infty} \ln\left|T(j\omega)\right| \frac{\mathrm{Re}(p_i)}{(p_i - j\omega)(\overline{p}_i + j\omega)} d\omega = \pi \ln\left|B_z^{-1}(p_i)\right| + \pi \mathrm{Re}(p_i)\tau \tag{4.31}$$

The number of Poisson sensitivity integral constraints possible for a given open loop transfer function $L(s)$ is equal to n_z while n_p dictates the number of possible Poisson complementary sensitivity integral constraints. A Blaschke product,[202] B, appears on the right hand side of Eq. (4.30) and Eq. (4.31) which is used to factor out the RHCP poles or zeros in $L(s)$.

$$B_z(s) = \prod_{i=1}^{n_z} \frac{z_i - s}{\overline{z}_i + s} \tag{4.32}$$

$$B_p(s) = \prod_{i=1}^{n_p} \frac{p_i - s}{\overline{p}_i + s} \tag{4.33}$$

To keep the magnitude of these Blaschke products small the RHCP poles of $L(s)$ need to be far away from the RHCP zeros of $L(s)$. Additionally, the Poisson complementary

sensitivity integral constraint shows that RHCP poles should not be deep in the RHCP nor should time delays be large in order to get good robust performance out of a control system.

Extending these Poisson integral constraints to work for the case of pseudo-rational transfer functions is accomplished by taking Cauchy integral formula and subtracting Cauchy integral theorem.[202]

$$\frac{1}{\pi j}\oint_C f(s)\frac{\mathrm{Re}(s_0)}{(s-s_0)(s+\overline{s}_0)}ds = f(s_0) \tag{4.34}$$

The actual contour integral used in Eq. (4.34) is the same as the one used in Figure 4-2 except that it is in the counter-clockwise direction and that there are no branch cuts. If a zero of $f(s)$ appears on the $j\omega$-axis then the contour integration will also include an indentation into the RHCP to avoid this point. Poisson's integral constraint is formulated by considering a special form of the sensitivity function and its complement, marked by a tilde, such that their RHCP poles and zeros are reflected into the LHCP.

$$\tilde{S}(s) = S(s)B_p^{-1}(s) \tag{4.35}$$

$$\tilde{T}(s) = T(s)B_z^{-1}(s) \tag{4.36}$$

Substituting the natural logarithm of the magnitude of Eq. (4.35) for $f(s)$ in Eq. (4.34) and evaluating s_0 at one of the RHCP zeros of the open loop transfer function $L(s)$ formulates a Poisson integral constraint. Similarly, Eq. (4.36) can be used instead while evaluating s_0 at one of the RHCP poles of the open loop transfer function to formulate a complementary Poisson integral constraint.

$$\begin{aligned}&\int_{-\infty}^{\infty}\ln\left|S(j\omega)\right|\frac{\mathrm{Re}(z_0)}{(z_0-j\omega)(\overline{z}_0+j\omega)}d\omega = \pi\ln\left|B_p^{-1}(z_0)\right| \\ &-\mathrm{Re}(z_0)\lim_{R\to\infty}\int_{-\frac{\pi}{2}}^{\frac{\pi}{2}}\ln\left|S\left(Re^{j\theta}\right)\right|\frac{Re^{j\theta}}{\left(Re^{j\theta}-z_0\right)\left(Re^{j\theta}+\overline{z}_0\right)}d\theta\end{aligned} \tag{4.37}$$

$$\int_{-\infty}^{\infty} \ln\left|T(j\omega)\right| \frac{\mathrm{Re}(p_0)}{(p_0 - j\omega)(\overline{p}_0 + j\omega)} d\omega = \pi \ln\left|B_z^{-1}(p_0)\right| - \mathrm{Re}(p_0) \lim_{R\to\infty} \int_{-\frac{\pi}{2}}^{\frac{\pi}{2}} \ln\left|T\left(Re^{j\theta}\right)\right| \frac{Re^{j\theta}}{\left(Re^{j\theta} - p_0\right)\left(Re^{j\theta} + \overline{p}_0\right)} d\theta \tag{4.38}$$

In the limit of R going to infinity the integral on the right hand side of Eq. (4.37) and Eq. (4.38) are exactly the same the integrals in Eq. (4.26) and Eq. (4.27) with one distinction: an absolute value sign. The definition of the complex logarithm allows these two operations to be related to each other as long as the principal argument is known.

$$\log f(s) = \ln\left|f(s)\right| + j\mathrm{Arg}f(s) \tag{4.39}$$

No matter how complicated the expression for the principal argument is for a given function, it will always be bounded. This ensures that the integral that it appears in vanishes due to the R^{-2} term. As a result, the absolute value sign does not matter and both equations can be evaluated.

$$\int_{-\infty}^{\infty} \ln\left|S(j\omega)\right| \frac{\mathrm{Re}(z_0)}{(z_0 - j\omega)(\overline{z}_0 + j\omega)} d\omega = \pi \ln\left|B_p^{-1}(z_0)\right| \tag{4.40}$$

$$\int_{-\infty}^{\infty} \ln\left|T(j\omega)\right| \frac{\mathrm{Re}(p_0)}{(p_0 - j\omega)(\overline{p}_0 + j\omega)} d\omega = \pi \ln\left|B_z^{-1}(p_0)\right| + \pi \mathrm{Re}(p_0)\tau_{net} \tag{4.41}$$

In the limit of a strictly proper transfer function with a factorable delay Eq. (4.40) recovers Eq. (4.30) while Eq. (4.41) recovers Eq. (4.31). Poisson integral constraints also exist in the literature for systems with multiple discrete delays.[203] Those results also agree with Eq. (4.40) and Eq. (4.41).

So far in this section all of the integral constraints considered for pseudo-rational transfer functions have had a ω^{-2} weighting term. This weighting term skews the interpretation of these integral constraints such that they reveal more information about low frequencies than the frequencies where combustion dynamics are likely to occur. These weighting term guarantees the contour integral C_R converges in the general case

which is why this section started with the weighted integral constraints. When the weights are removed this contour integral diverges which ensures that the contour integral on the $j\omega$-axis also diverges. One workaround for this is to consider the contour C in Figure 4-2 without the weighting term for a finite size R.

$$\int_0^R \log\left|S(j\omega)\right| d\omega = \pi \sum_{i=1}^{n_p} \mathrm{Re}(p_i) - \frac{1}{2}\int_{-\frac{\pi}{2}}^{\frac{\pi}{2}} R\log\left(S\left(Re^{j\theta}\right)\right)e^{j\theta}d\theta \tag{4.42}$$

$$\int_0^R \log\left|T(j\omega)\right| d\omega = \pi \sum_{i=1}^{n_p} \mathrm{Re}(z_i) - \frac{1}{2}\int_{-\frac{\pi}{2}}^{\frac{\pi}{2}} R\log\left(T\left(Re^{j\theta}\right)\right)e^{j\theta}d\theta \tag{4.43}$$

Solving the contour integral for C_R in Eq. (4.42) and Eq. (4.43), the second term on the right hand side, via the same procedure as used for Eq. (4.14) and Eq. (4.15) cannot be accomplished because the squeeze theorem (4.25) fails. Additionally, the divergence of these integrals creates difficulties with moving the limit of large but finite R into the integrals. Despite the inability to evaluate these integrals Eq. (4.42) and Eq. (4.43) reestablish that having poles and zeros deep in the RHCP is bad for performance which was lost due to the frequency inversion (4.16) in the frequency weighted integral constraints.

All of the analysis in this section has been for SISO systems. Handling MIMO systems are much more difficult. Two different approaches are commonly used in the literature: analyzing the singular values and vectors of the open loop transfer function[204] or pre- and/or postmultiplying $L(s)$ and by an appropriate vector to force a SISO framework on the MIMO problem.[201] The singular value approach is difficult because it is based on the theory of sub-harmonic functions while the SISO case can be handled using the theory of harmonic functions.[194] A repercussion of this sub-harmonic behavior results in the MIMO singular integral constraints being inequalities which hurt their ability to be interpreted as a conservation law. Pursuing the second approach will result

in an equality but this requires solving for the transmission zeros by putting the system into Smith-McMillan form.[205] An additional complication comes from the zeros and poles having a vector associated with their input and output direction. MIMO integral constraints are a function of the angles between the input and output directions. Solving for and physically interpreting these vectors directions is not a simple task. For all of these reasons, extending the MIMO integral constraints to handle multiple distributed delays is not pursued in this thesis. This does not mean that they are unimportant. Additionally, this does not mean that the SISO integral constraints are useless in understanding the factors that limit control effectiveness in a MIMO system. Selecting an appropriate row and column vector to pre- and postmultiply $L(s)$ will recover the SISO integral constraints; therefore, the factors that limit control effectiveness in a SISO system are a subset of those in a MIMO and warrant investigation.

Cumulatively, the sensitivity function analysis in this section shows that the common rules of thumb used for finite dimensional compensator design also carry over to infinite dimensional compensator design. RHCP poles and zeros are undesirable near the $j\omega$-axis and deep in the complex plane. If they both exist then they need to be kept apart from each other. Additionally, the net delay needs to be minimized. Applying these design rules can be very complicated because an infinite number of degrees of freedom exist in shaping the kernel of a linear functional controller and nothing is known about how the form of this kernel affects the location of the RHCP poles and zeros. As a result, automated methods to optimize control design are very useful in the infinite dimensional setting and will be explored in the next section of this chapter. Even if the control law is not physically realizable the answer still suggests the form of the kernel which can be redesigned to be implementable.

4.3 Optimal and Suboptimal Control

Linear quadratic control problems are the most popular and simplest type of optimization problems that appear in control theory. The idea is to have a non-negative cost function *J* and to find a controller in the state space that yields a local minimum of that cost function. Since this thesis is concerned with steady state behavior the particular linear quadratic control problem that will be investigated is the infinite-time horizon linear quadratic regulator (LQR). An example of the type cost function used for the LQR problem in Hilbert spaces is given in Eq. (4.44).

$$J = \int_0^\infty \left\langle \vec{x}_e(t'), \mathcal{Q}\vec{x}_e(t') \right\rangle + \left\langle \vec{u}(t'), \mathcal{R}\vec{u}(t') \right\rangle dt' \tag{4.44}$$

The cost function has been set up using the extended state space introduced in §2.8. Two terms exist inside the integral: a state weighted cost due to the positive semi-definite operator $\mathcal{Q}$ and a control weighted cost due to the coercive (positive definite and self-adjoint) operator $\mathcal{R}$. State weights are selected to minimize the undesirable system behavior. For this thesis $\mathcal{Q}$ is the acoustic energy operator that recovers Eq. (3.36). Control weights are used as a soft constraint on the control response. Large control inputs can break the linearity of the model while very fast control response may require an actuator bandwidth that cannot be delivered in practice.

Krasovskii[206] was the first to address the LQR problem with time delays in the state space using the principles of dynamical programming.[207] The modern form using the extended state space came from Delfour et al.[208] which showed the optimal controller (4.46) comes from the solution of the operator algebraic Riccati equation (ARE) (4.45).

$$0 = \mathcal{A}^*\mathcal{P} + \mathcal{P}\mathcal{A}^* - \mathcal{P}\mathcal{B}\mathcal{R}^{-1}\mathcal{B}^*\mathcal{P} + \mathcal{Q} \tag{4.45}$$

$$\vec{u}(t) = -\mathcal{R}^{-1}\mathcal{B}^*\mathcal{P}\vec{x}_e(t) \tag{4.46}$$

Many other methodologies exist to arrive at the ARE or an equivalent form of it from Eq. (4.44). A good sampling of how diverse these methodologies can be is found in the

bibliographies in the monographs by Curtain and Zwart[84] and Bensoussan et al.[83] Solving the ARE analytically usually involves an eigen-decomposition but as explained in §3.7 the eigenvectors of the infinitesimal generator are non-orthogonal and need to be found numerically. As a result, the physical insight that would come from analytical work is not delivered and a purely numerical route is used instead in this thesis.

Ito[209] showed that the solution of the ARE of finite order orthogonal projections (4.47) will converge strongly to the solution of the ARE (4.45) in the limit of the projection order increasing to infinity. The pseudospectral differencing method used in this thesis, and detailed in Appendix A, is actually an oblique projection, but it converges to an orthogonal projection as the order of the projection increases towards infinity. This creates the means to solve to LQR problem by minimizing the finite order projection of the cost function (4.48) in the limit of the projection order going to infinity instead of minimizing the cost function (4.44) for the infinite dimensional system directly.

$$\begin{aligned} 0 = {} & P_N\left(\mathcal{A}\right)^* P_N\left(\mathcal{P}\right) + P_N\left(\mathcal{P}\right) P_N\left(\mathcal{A}\right)^* + P_N\left(\mathcal{Q}\right) \\ & - P_N\left(\mathcal{P}\right) P_N\left(\mathcal{B}\right) P_N\left(\mathcal{R}\right)^{-1} P_N\left(\mathcal{B}\right)^* P_N\left(\mathcal{P}\right) \end{aligned} \tag{4.47}$$

$$J = \int_0^\infty \left\langle P_N\left(\vec{x}_e\left(t'\right)\right), P_N\left(\mathcal{Q}\right) P_N\left(\vec{x}_e\left(t'\right)\right)\right\rangle + \left\langle P_N\left(\vec{u}\left(t'\right)\right), P_N\left(\mathcal{R}\right) P_N\left(\vec{u}\left(t'\right)\right)\right\rangle dt' \tag{4.48}$$

What is really powerful about this proof is the ARE being solved for is the ARE of the projections and not the projection of the ARE. This allows sidestepping very complicated analytical issues such as finding the adjoints and inverses of infinite dimensional operators before taking the projection. Instead, the projection is taken first and then the adjoints and inverse are found in a finite dimensional space. In the interest of fairness, Ito was not the first person to create a convergence proof for the ARE. Earlier work was done by Delfour[210] and Gibson;[211] however, the assumptions they use are more restricting and require extraneous knowledge about the system behavior to complete. Ito's proof works in the more general case.

Before the projections can be taken the LQR problem needs to be set up properly in the infinite dimensional setting. Unfortunately, the derivatives in the control input prevents the thermo-acoustic model (2.68) from fitting in the extended state space formulation introduced in §2.8. Cartesian products of Lebesgue spaces can be used to incorporate the past control derivative history into the extended state space but this excludes a two dimensional subspace consisting of $u'(t')$ and $u''(t')$ at the present time. An engineer may be tempted to just add these two points into the extended state space with more Cartesian product. This is incorrect. Physically, these two points are systems inputs and are automatically decided once the control law decides $u(t')$. As a result, if these two points are added to the extended state space they create uncontrollable false eigenvalues at the origin. The multiplicity of these false eigenvalues prevents the system from being stabilizable. If an engineer would naively proceed to try to solve this problem the algorithms used to solve finite dimensional AREs would fail because they require the pair $(P_N(\mathcal{A}), P_N(\mathcal{B}))$ to be stabilizable.[212] An alternative approach is to treat each derivative in the control input as a separate control input and then add a hard constraint to relate them together. When a hard constraint is incorporated the minimizing solution to the cost function (4.44) is no longer governed by the ARE. This solution may be governed by a general algebraic quadratic operator equation or even coupled algebraic operator equations. Convergence proofs do not exist yet for these types of equations.[84]

This thesis will deal with this problem in the rest of this section by ignoring the hard constraint and treating each derivative of the control input as independent control variables, creating a total of three control inputs. Although this is wrong, enough mathematical structure is preserved in this framework to capture useful information about the form of the control law. The controller derived from this process can be used as an initial guess for optimizing the correct problem and by using the adaptive gradient search algorithm[184] used in the previous chapter. As a result, the design process for an infinite dimensional compensator becomes a design problem with a finite number of parameters

instead of the infinite number that would result from skipping the unconstrained LQR problem. While this controller will be sub-optimal it will be an improvement over the proportional delay compensator used in the previous chapter.

Finite dimensional LQR's and its theoretical properties has been well-studied and algorithms for its numerical solution are widely available.[213] In finite dimensions $P_N(\mathcal{Q})$ and $P_N(\mathcal{R})$ are matrices. For the thermo-acoustic model (2.68) used in this thesis the state weighting matrix $P_N(\mathcal{Q})$ is sparsely populated and consists of mostly zeros. More freedom in allowed in defining the control weighting matrix $P_N(\mathcal{R})$. Since actuator constraints are mainly in the authority and bandwidth a diagonal weighting matrix makes the most sense. The simplest form possible (4.49) is to use equal weights on each term.

$$P_N\left(\mathcal{R}\right) = g_c I_3 \tag{4.49}$$

Two examples of the performance of a LQR is shown in Figure 4-3 and compared with the best possible proportional delay compensator for different advection delays in terms of the spectral abscissa. From inspection the performance of the LQR's are independent of the advection delay. This does not mean that the closed loop system at different advection delays have the same spectrum. The eigenvalues are different but these differences tend to be deep inside of the LHCP such that performance is not affected. Practically, this means a way to redesign the controller exists to compensate for the advection delay even when this delay is large. Proportional delay compensators have very little authority at large delays while the LQR's continue to make their presence felt.

Another observation that can be made from Figure 4-3 is that the performance of the LQR depends strongly upon the control weights. This makes sense. The exact-null controllability test in §4.1 shows that no limit to control performance exists if the actuator is unconstrained. As the soft constraint on the actuator become more severe the LQR algorithm tries to avoid certain regions in the extended state space which restricts the performance gains a controller can achieve. What limits control effectiveness is the lack

of authority and bandwidth in a fuel actuator. An unconstrained controller will deviate towards large gains, but eventually this breaks the assumptions in the linear equivalence ratio perturbation model (2.2).

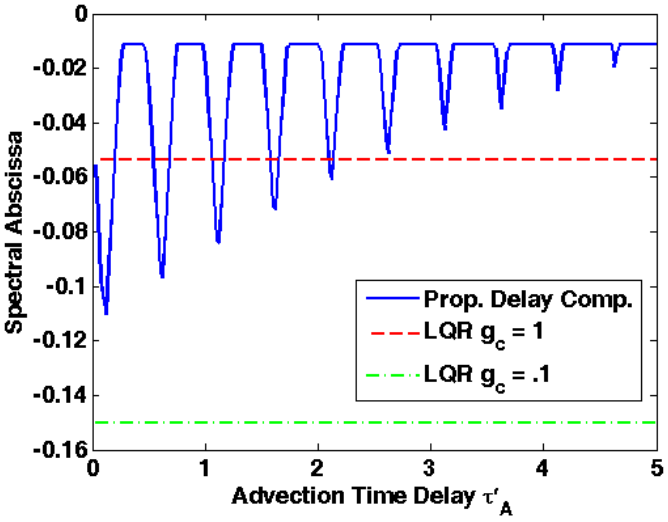

Figure 4-3: Best possible spectral abscissa for a few LQR's compared to a proportional delay compensator. Corresponds to case 1 in Appendix D.

The next step after understanding what the LQR is doing is to understand how it gets increased performance over the proportional delay compensator. When looking at the numerical solution to the LQR (4.46) what is striking about it is that no functional acting over the past history of the state variables present. Only proportional terms acting on the state variables exist. For the extended state variables a functional acting over the past control history is present. This gives the control law shown in Eq. (4.50).

$$\vec{u}(t') = k_0 \vec{x}(t') + \int_{-\tau'_A}^{0} K(\kappa)\vec{u}(t'+\kappa)\,d\kappa \tag{4.50}$$

Examples of these functionals are shown in Figure 4-4, but only two of the three are shown to keep the figure readable. Additionally, the pseudospectral differencing scheme[85] used to set up the extended state space views functionals as the coefficients of a Clenshaw-Curtis quadrature scheme[214] based upon the Chebyshev extremal points

detailed in Appendix A. To convert these coefficients into the actual value of the functional they need to be multiplied by the number of discretizations used for a given time interval. This has already been done in Figure 4-4.

Inspection of the control functional in Figure 4-4 shows that it looks like a beating sinusoid. The lower frequency is a function of the advection delay while the higher frequency is very close to the instability frequency ω'_1. A phase offset also exists between the different control functionals. Collectively, this suggests Eq. (4.51) is a good initial guest for the control functional over the interval $[-\tau'_A, 0]$.

$$K(\kappa) = a \sin\left(\frac{\pi}{\tau'_A}\kappa\right) \sin\left(\omega'_1 \kappa + \phi\right) \tag{4.51}$$

When expanding the thermo-acoustic model (2.68) to include higher harmonics the control functional is likely to become a linear combination of Eq. (4.51) based upon the higher harmonic frequencies. An explanation for why the control functional has this form was not found in the investigations under taken by this thesis. At this stage just synthesizing a better controller will have to suffice.

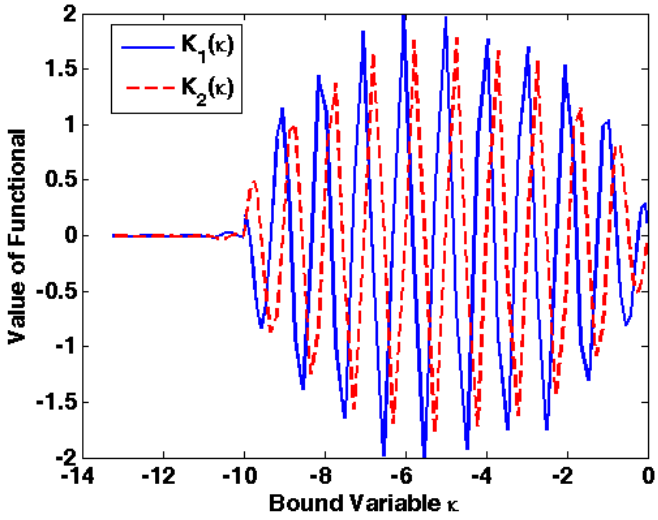

Figure 4-4: Gain functional acting over past control history for a LQR with g_c = 0.1. Corresponds to case 1 in Appendix D with τ'_A = 10.

A parameter mapping of the performance increases available with an infinite dimensional compensator is shown in Figure 4-5 as a function of the functional gain and phase. The proportional term with respect to the state variables in Eq. (4.50) was selected to correspond to the best possible proportional delay compensator found in Figure 3-14 at $\tau'_A = 1.1$. Using relatively low gains the addition of the infinite dimensional compensator is able to improve the spectral abscissa by 21% by pushing it from -0.0811 to -0.0984. All of this comes from an intelligent guess of the form of the control functional. Further improvements are possible with larger control gains but this shrinks the robustness with respect to the phase offset in the control functional.

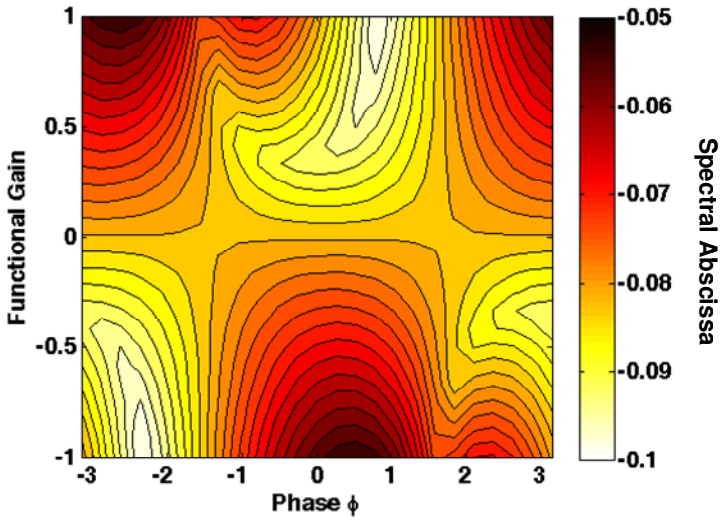

Figure 4-5: Spectral abscissa for an infinite dimensional compensator corresponding to case 1 with $\tau'_A = 1.1$ in Appendix D as a function of functional gain and phase.

Short of solving the constrained LQR problem, the form of the infinite dimensional compensator can be improved with some simple logic. The easiest correction to make is to have the proportional gain act on all derivatives of the state variable instead of just pressure, which would require a state estimator. Other clues can come from looking at how an infinite dimensional compensator affects the placement of the eigenvalues. Compared to the finite dimensional compensator shown in Figure 3-15 the spectral abscissa is pushed back a little more in the LHCP. All the other eigenvalues

are deep inside the LHCP beyond the line defined by $Re(\lambda) = -2$ just like the finite dimensional compensator. What is striking is that two complex conjugate pairs closely spaced in frequency near each other seems to always trade off on being the spectral abscissa for different control laws. Adding another linear functional to the control law (4.51) with the highest frequency determined by the frequencies of other eigenvalue near the spectral abscissa can be used to try to move both complex conjugate pair of eigenvalues simultaneously.

4.4 Implementation Issues

The ability to analyze and design infinite dimensional compensators through numerical means is a recent development enabled by intelligent methods to discretize time delay systems.[85] This thesis used an LQR solution to help guide the design of the control functional but this is not the only control methodology that leads to infinite dimensional compensators. Analytical techniques for constructing Lyapunov-Krasovskii functionals[81] have existed for more than half a century, yet a curious lack of infinite dimensional compensators exist in the literature which suggests that something exists that is holding back their adoption as the control law of choice. That barrier is how to implement an infinite dimensional controller. Real control system are digital. At best, an infinite dimensional compensator has to be approximated by a high order finite dimensional controller. Understanding how implementation hinders closed loop system performance is a recent research topic in the time delay systems community.

Early indications that something was amiss came from numerical experiments comparing different quadrature schemes for distributed delay controllers.[215] As the quadrature schemes became more accurate the stability and performance of the system decreased. Essentially, the performance of the approximated distributed delay controller was unable to converge to the performance of the predicted continuous time implementation regardless of how small the output response rate is made. This is quite

an alarming result considering Kamen et al.[216] showed that if a time delay system is stabilizable then it is also stabilizable via a finite dimensional compensator. A trivial extension of this result will show that if a time delay system is β-exponentially stabilizable then it is β-exponentially stabilizable via a finite dimensional compensator; therefore, a finite dimensional counterpart exist to the infinite dimensional compensator designed in the previous section. How useful the approximated distributed delay controller is depends upon how different it is from its unknown but equivalent finite dimensional counterpart.

Answers to how quadrature disrupts the performance of a distributed delay controller came from Mirkin[217] who showed that many quadrature schemes result in a non-strictly proper approximation of a strictly proper transfer function between the control input and the state variables. This means that the high frequency response of the approximated distributed delay control law is inaccurate and the $\mathcal{H}_\infty$ norm of the error at high frequencies is nonzero. The result is a high frequency robustness problem. How this occurs can be gleamed from the Laplace transform of Eq. (4.50).

$$u(s) = \frac{k_0 \vec{x}(s)}{1 - \int_{-\tau_A'}^{0} K(\kappa) e^{s\kappa} d\kappa} \tag{4.52}$$

When the integral in Eq. (4.52) is evaluated an s^{-1} factor naturally appears but for any quadrature scheme used in implementation this factor cannot be reproduced.[79]

$$u_N(s) = \frac{k_0 \vec{x}(s)}{1 - \sum_{i=1}^{N} k_i e^{s\tau_i'}} \tag{4.53}$$

This destroys the strictly properness of the transfer function. Additionally, the s^{-1} factor in the derived control law (4.52) provides low pass filter characteristics which is why the high frequency eigenvalues can lack robustness in the implementation of distributed delay control laws such as Eq. (4.53).

Losing the strict properness of a transfer function is not the only problem associated with distributed delay controllers. Engelborghs et al.[218] noticed that the denominator in Eq. (4.52) is of neutral type. When this control law is substituted into the Laplace transform of the closed loop system (2.68) both sides of the equation have to be multiplied by this denominator. This turns a retarded functional differential equation into a neutral functional differential equation. As a result, the distributed delay controller also needs to be strongly stable.[171] If a system is not strongly stable then the system is not exponentially stable with respect to infinitesimal perturbations to the time delays. The essential spectrum of the infinitesimal generator will not vary continuously with respect to infinitesimal changes to the time delays. Implementing a distributed delay controller can be viewed as a perturbation to the ideal infinite dimensional compensator. If a system behaves badly then the eigenvalues of the implemented system may jump beyond the spectral abscissa of the ideal controlled system. This explains why the performance of certain implementations cannot converge to the performance of the theoretical infinite dimensional controller as the output response rate of the control system increases.

The solution to both of these implementation problems are very similar: recover the low pass characteristics of the distributed delay controller or add a low pass filter to the control input.[219] More complicated quadrature implementation schemes are covered in the monograph by Zong.[79] Many of these schemes were designed for specific time delay systems using a unified Smith predictor and do not convert easily to different type of controllers. Other schemes create a pole near the $j\omega$-axis which effectively becomes the spectral abscissa of the closed loop system. A forward differencing quadrature scheme, as suggested by Zhong,[79] which does not enforce the strictly proper property will be to generate all the figures in this section of this thesis. Figure 4-6 shows how the best distributed delay controller found in Figure 4-5 behaves compared to its implementation with an output response rate of 0.01 which corresponds to one hundred voltage commands to the fuel actuator for every instability cycle.

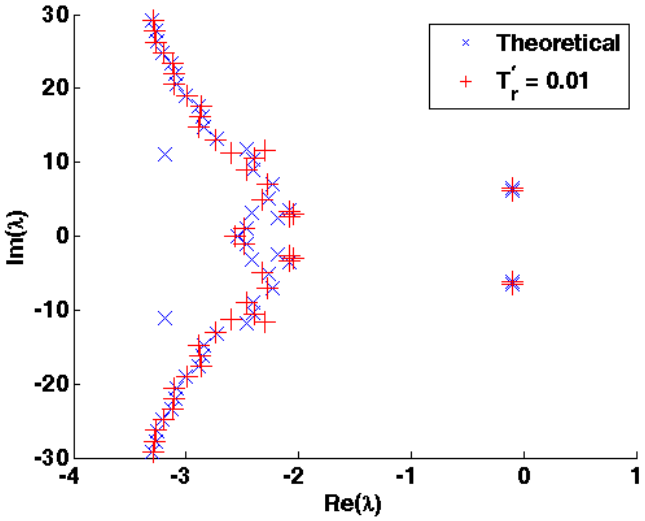

Figure 4-6: Comparison of the eigenvalues of the best distributed delay controller found in the previous figure and its implementation using a forward differencing quadrature rule.

For both cases the eigenvalues are very similar with most differences occurring deeper in the LHCP while the spectral abscissa is mainly unaffected. This narrative is in stark contrast to the warning in the preceding paragraphs and deserves an explanation. Many of the reported cases of implementation issues are due to Smith predictors and related controllers. These control laws have exponentials in their control functionals compared to the trigonometric functions (4.51) used in this thesis. Trigonometric functions are much better behaved such that their implementation converges to their infinite dimensional counterpart's performance at lower output response rates. While this suggests implementation issues are not as problematic, this lesson should not be applied too broadly. Adding higher harmonics will require faster output response rates and a proper solution to the optimal control problem may still yield some unpleasant surprises.

The other implementation problem of strong stability can be assessed numerically by looking at how the trajectory of the spectral abscissa changes as the output response rate is increased. If the spectral abscissa is stationary with respect to increasing the discretization order then the system is strongly stable; otherwise, different eigenvalues are discontinuous jumping beyond the spectral abscissa as the implementation scheme is

changed. Eigenvalue plots similar to Figure 4-6 at slight variations in the output response rates show that the location of the eigenvalues in the complex plane are indifferent to these rates which suggests strong stability. Just like the implementation issues associated with the loss of strict properness, the narrative of this strong stability experiment is in contrast to the warnings in the preceding paragraphs. What the thermo-acoustic modeler needs to keep in mind is if unmodeled behavior can cause a loss of strong stability. Additionally, more advanced controllers may not have a control functional that is as well behaved as Eq. (4.51). Good design practice seems to dictate redesigning the controller to revert the close loop system response back into a retarded functional differential equation.

Low pass filtering the control input will achieve this end. This lowers the effectiveness of the controller, but this may still be desirable in practice because it adds robustness. Furthermore, selecting the cutoff frequency based upon the actuator bandwidth will help ensure that the control response is still linear by avoiding unmodeled behavior such as hysteresis. Figure 4-5 is updated to include a low pass filter in Figure 4-7 with $\omega'_c = 2\omega'_1$ which corresponds to a representative worst case scenario in aircraft engines with current technology. The fundamental longitudinal frequency can be as high as 500 *Hz* while the best currently available fuel actuators discussed in §2.7 have a bandwidth up to 1 *kHz*. For ground power applications this worst case cutoff frequency will be about a factor of ten greater than the fundamental longitudinal frequency.

When comparing Figure 4-7 with Figure 4-5 three noticeable differences exist. Regions of superior and inferior performance have been shifted by approximately $\pi/2$ radians which makes sense considering that a low pass filter acts like an integrator. Another observation is that the region where the distributed delay controller improves performance is larger at higher functional gains showing successful containment of unwanted higher frequency dynamics. Finally, the contours level in the regions of superior performance are the same in both figures while reaching worst performing

contour levels is easier with the low pass filtered controller. This final observation is very interesting. Earlier work at UTRC[65] suggests that the actuator bandwidth should play a critical role in limiting controller effectiveness because it limits the ability to reshape the sensitivity function at high frequencies; however, these control designs show no such limit along with tremendous difficulty in relocating the spectral abscissa. The only way this can happen is if the assumed form of the controller (4.50) is incorrect. A similar narrative has been collaborated by the exact-null controllability test performed in §4.1. Understanding the factors that limit control effectiveness will require delving deeper into the flaws of this control design.

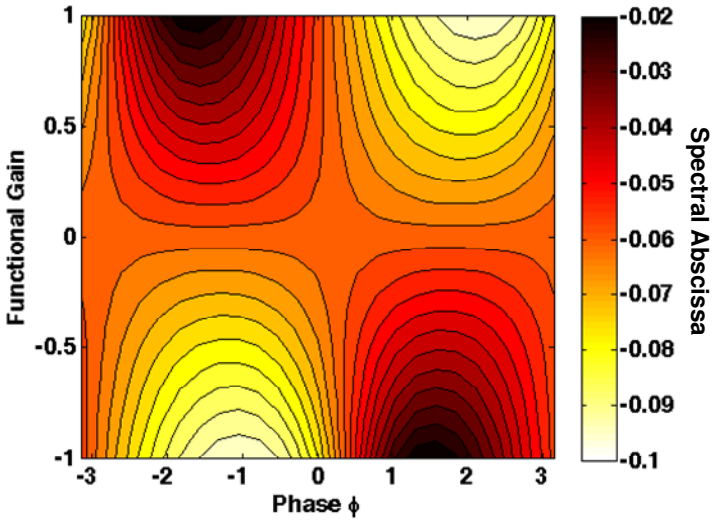

Figure 4-7: Spectral abscissa for an infinite dimensional compensator with a 1st order low pass filter at $\omega'_c = 2\omega'_1$ corresponding to case 1 with $\tau'_A = 1.1$ in Appendix D as a function of functional gain and phase.

4.5 Designing Combustors for Control Effectiveness

Blaming the controller deficiencies on the inability to incorporate the relationship between the control input and its derivatives in the LQR problem, while partially correct, is shortsighted because it does not lead to physical insight into the cause of the problem nor how to correct it. Sensitivity function analysis tools presented in §4.2 are a very

powerful way to investigate these currently unknown deficiencies. To get the thermo-acoustic model (2.68) into the proper framework a more detailed version of Figure 4-1 is required. In Figure 4-8 the transfer functions representing the plant $P(s)$ and the compensator $F(s)$ in Figure 4-1 have been fully expanded.

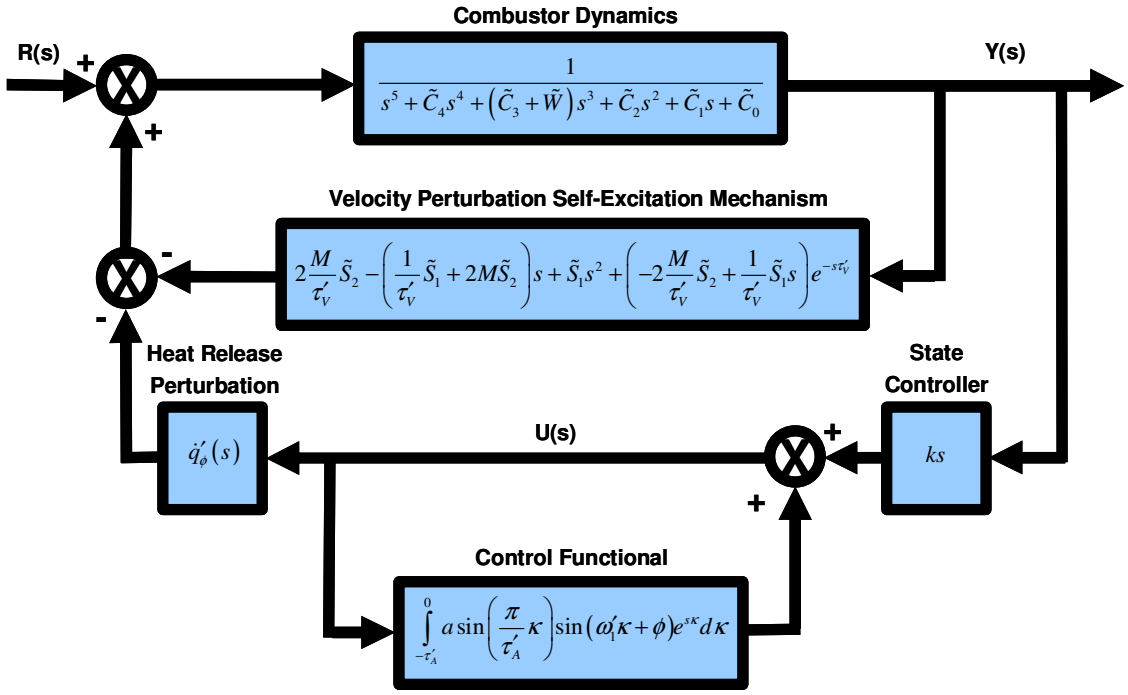

Figure 4-8: Detailed feedback diagram corresponding to case 1 in Appendix D with an LQR inspired controller.

The plant transfer function consists of a transfer function representing the combustor dynamics and the internal feedback loop in Figure 2-2 for velocity induced volumetric heat release rate perturbations. When the feedback loop representing the effect of control is expanded an additional feedback loop representing the effects of the control functional appears. Additional transfer functions exist in the forward path representing the effects of a state controller and how equivalence ratio perturbations cause volumetric heat release rate perturbations. This final transfer function is a bit too complicated to fit nicely in Figure 4-8 and is instead reproduced in Eq. (4.54).

$$\dot{q}'_{\phi}(s)=\left[\left(-2\beta^2 M\frac{\left(\beta^2-1\right)n_H+\beta^2 n_S}{\tau'_V\left(\beta^2-1\right)}\tilde{S}_4+\beta^2\frac{\left(\beta^2-1\right)n_H+\beta^2 n_S}{\tau'_V\left(\beta^2-1\right)}\tilde{S}_3 s\right)e^{-s\frac{\tau'_V}{\beta^2}}+\right.$$
$$\left(-\frac{\left(1+\beta^2\right)n_S+\beta^2 n_H}{\tau'_V}\left(\tilde{S}_3-2M\tilde{S}_4\right)-2\left(n_H+n_S\right)M\frac{n_C}{\tau'_V}\tilde{S}_4 s+\left(n_H+n_S\right)\tilde{S}_3 s^2\right) \qquad (4.54)$$
$$\left.+\left(2\frac{Mn_S}{\tau'_V\left(\beta^2-1\right)}\tilde{S}_4-\frac{n_S}{\tau'_V\left(\beta^2-1\right)}\tilde{S}_3 s\right)e^{-s\tau'_V}\right]e^{-s\tau'_A}$$

A major difference between Figure 4-1 and Figure 4-8 is the location of $U(s)$. In Figure 4-1, corresponding to the unconstrained LQR design problem, $U(s)$ feeds directly into the combustor dynamics because Eq. (4.54) is hiding inside the compensator $F(s)$ while in Figure 4-8, corresponding to the LQR inspired compensator, it is multiplied by Eq. (4.54) before feeding into the combustor dynamics. Equation (4.54) has the potential to contain non-minimum phase zeros. Back in §4.2 non-minimum phase zeros and right hand plane poles are shown to limit control effectiveness through the sensitivity integral constraint (4.28) and its complement (4.29). If these integral constraints can be related to the LQR design problem then a directly link can be made between the LQR performance and non-minimum phase zeros and right hand plane poles.

Applying the Cauchy-Schwarz inequality to the cost function (4.44) followed by Plancherel's theorem[134] can be used to get a workable inequality.

$$J=\int_0^{\infty}\left\langle\vec{x}(t'),\mathcal{Q}\vec{x}(t')\right\rangle+\left\langle\vec{u}(t'),\mathcal{R}\vec{u}(t')\right\rangle dt'\le\int_0^{\infty}\|\mathcal{Q}\|_2\left\|\vec{x}(t')\right\|_2^2+\|\mathcal{R}\|_2\left\|\vec{u}(t')\right\|_2^2 dt' \qquad (4.55)$$

$$\int_0^{\infty}\|\mathcal{Q}\|_2\left\|\vec{x}(t')\right\|_2^2+\|\mathcal{R}\|_2\left\|\vec{u}(t')\right\|_2^2 dt'=\int_0^{\infty}\|\mathcal{Q}\|_2\left\|Y(j\omega)\right\|_2^2+\|\mathcal{R}\|_2\left\|U(j\omega)\right\|_2^2 d\omega \qquad (4.56)$$

Since Eq. (4.56) is now in the frequency domain the transfer functions between the system's output $Y(s)$ (4.3) and control input $U(s)$ (4.8) to the reference signal $R(s)$ can be used to explicitly bound the cost function (4.55) by the sensitivity function and its complement.

$$J \le \int_0^\infty \left\| \mathcal{Q} \right\|_2 \left\| S(j\omega) P(j\omega) R(j\omega) \right\|_2^2 + \left\| \mathcal{R} \right\|_2 \left\| T(j\omega) R(j\omega) \right\|_2^2 d\omega \qquad (4.57)$$

The state cost is bounded by the sensitivity function. When open loop poles are deep in the RHCP the control system has to move the closed loop eigenvalues a larger distance to get them into the LHCP. As a result, the area under the sensitivity function is larger which limits the controlled system performance. Similarly, the control cost is bounded by the complementary sensitivity function. When the non-minimum phase zeros are deeper in the RHCP the more control effort that has to be used to move closed loop eigenvalues the same distance. This increases the area under the complementary sensitivity function which limits the controlled system performance.

If the demands placed on the control system are too great because of too many open loop poles or zeros deep in the RHCP then a point exists where the fuel actuator requires more bandwidth than it has available or it cannot exert enough authority to create large amplitude equivalence ratio oscillations. Additionally, large amplitude control response can break the linearity assumption of the thermo-acoustic model and can lead to unwanted increases in NO_x and the temperature profile approaching the high pressure turbine. Good design practice then dictates that a combustor should be designed in such a way to minimize these RHCP poles and zeros. The bound provided by Eq. (4.57) is true even if the LQR problem includes an actuator bandwidth constraint. Constraints typically prevent how the sensitivity function and its complement can be reshaped but not the fact that they are bounded from above by them. Only if a constraint makes structurally changes in the feedback diagram, like the relationship between control and its derivatives does in Figure 4-8, does the bound in Eq. (4.57) change. This constraint modifies the upper bound into Eq. (4.58) but the roles played by $S(j\omega)$ and $T(j\omega)$ are the same except that $T(j\omega)$ has a modified weighting term that is the reciprocal of Eq. (4.54) which behaves like a second order damped system with undulations in its transfer function due to the presence of time delays.

$$J \le \int_0^\infty \left\| \mathscr{Q} \right\|_2 \left\| S(j\omega) P(j\omega) R(j\omega) \right\|_2^2 + \left\| \mathscr{R} \right\|_2 \left\| T(j\omega) \dot{q}_\phi'^{-1}(j\omega) R(j\omega) \right\|_2^2 d\omega \qquad (4.58)$$

Understanding where the right hand plane poles and of the open loop transfer function $L(s)$ are coming from is the first step to developing some combustor design rules. In Figure 4-8 $P(s)$ and the control functional are creating right hand plane poles. Non-minimum phase zeros come from the control law and the equivalence ratio perturbation model (4.54) in this SISO model. If a MIMO model is considered then modal coupling due to boundary conditions or volumetric heat release perturbations can create additional non-minimum phase zeros. For the reasons discussed in §4.2 the role of non-minimum phase zeros from modal coupling will be neglected. Despite this necessary oversight, the design rules for the SISO model will be inherited by a MIMO model and are still worth investigating.

Reconsidering the constrained LQR problem in light of what was just learned reveals that the constraints affect how the LQR design process views Eq. (4.54). What the unconstrained LQR problem gets wrong is the control derivatives which appear as orders in s in Eq. (4.54). As a result, the location of the zeros from Eq. (4.54) behaves like an algebraic delay equation to the unconstrained LQR design problem while it actually behaves like a retarded delay differential equation. Considering that an algebraic delay equation has neutral delay characteristics, this is quite a difference. Although the unconstrained LQR design problem is based upon the incorrect location of zeros in $L(s)$ certain characteristic behavior is preserved. For example, the only term representing the advection delay factors out of Eq. (4.54) and does not contribute to the location of the zeros. This explains why the performance of an unconstrained LQR in Figure 4-3 is independent of the advection delay and suggests the constrained LQR will behave in a similar matter.

Equation (4.54) is also interesting from a combustion engineer's point of view. When combustion engineers design a combustor they are typically concerned about

resonance response frequencies which correspond to the poles of $L(s)$. The zeros affect feedback loops and closed loop performance. This explains the warning this thesis gives in §2.4.1 on how low *St* volumetric heat release perturbation models can be problematic. If high *St* errors in the open loop model causes the location of the zeros to be incorrect then low *St* errors are created in the closed loop model through the complementary sensitivity integral constraint (4.43). Combustion engineers need to pay attention to the placement of the zeros to make accurate performance predictions. Afterwards, these predictions can be used to design control effectiveness into the combustor. What is physically determining the locations of the zeros and hence limiting control effectiveness is how the flame is stabilized and its geometry! This is a very powerful and simple idea because it can be expressed as a simple design tool looking at the location of non-minimum phase zeros. Each exponential polynomial corresponds to an equivalent retarded delay differential equation; therefore, finding the zeros becomes an exercise in finding eigenvalues using the same techniques as in Chapter 3 and Appendix A.

From a design point of view the dependent variables in shaping the zeros of Eq. (4.54) are the flame geometry factor β and the internal time delay τ'_v which dictates the mean flame shape. Figure 4-9 shows how the logarithm of the sum of all of the non-minimum phase zeros depend on these factors. The logarithm does not naturally show up on the right hand side of the integral constraints in §4.2 but allows for easily interpretable contour plots. Inspection of Figure 4-9 immediately shows that non-minimum phase zeros always exists in an equivalence ratio modulation based controller; otherwise, the contour plot would have values going to negative infinity. This is a terrible property for a control system because at high gains the roots of the closed loop transfer function will migrate towards the zeros of the open loop transfer function.[220] As a result, high gain controllers are always destabilizing, illustrated for a simple controller in Figure 3-14, which create robustness problems for controllers that are prone to high gains, such as adaptive controllers.[221] Additionally, Figure 4-9 shows that a

control system seems to respond better at low flame geometry factors and high internal time delays. Physically, this corresponds to a long flame which pushes the position of mean heat release away from combustor inlet. This acts like a free gain multiplier in the control system without increasing the control cost.

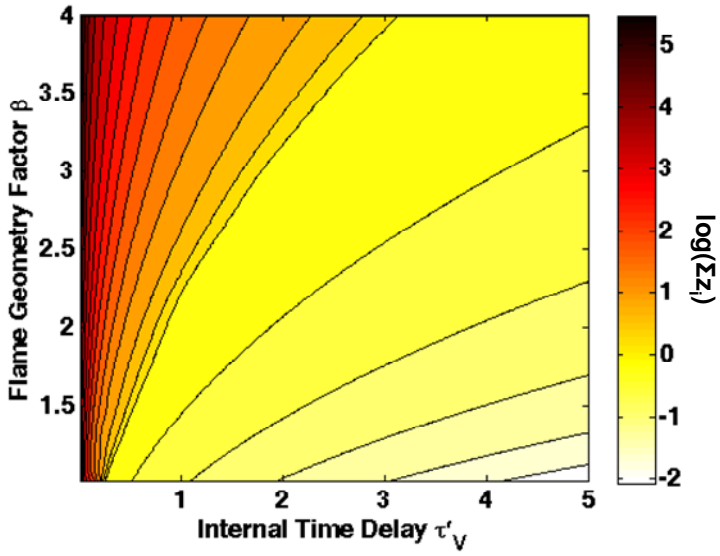

Figure 4-9: Logarithm of the sum of non-minimum phase zeros due to an equivalence ratio modulation controller corresponding to Case 1 in Appendix D.

A good question to ask is how the open loop poles are affected by changes that improve the location of the non-minimum phase zeros. The easiest way to do this would be to compare Figure 4-9 with Figure 3-8 but this is misleading. In Eq. (4.54) the zeros are indifferent to many of the parameters in the thermo-acoustic model (2.68) but the spectral abscissa plotted in Figure 3-8 is not. What really matters is how the velocity perturbation self-excitation mechanism (2.1) depends on the position of mean heat release. Just like the equivalence ratio modulation case, the volumetric heat release rate perturbations due to velocity disturbances also increases because the effective gain of the internal feedback loop is increasing as the position of mean heat release moves away

from the combustor inlet. This can be seen in Figure 4-10 where the sum of the RHCP poles is seen to be increasing as x'_f and n_C increases.

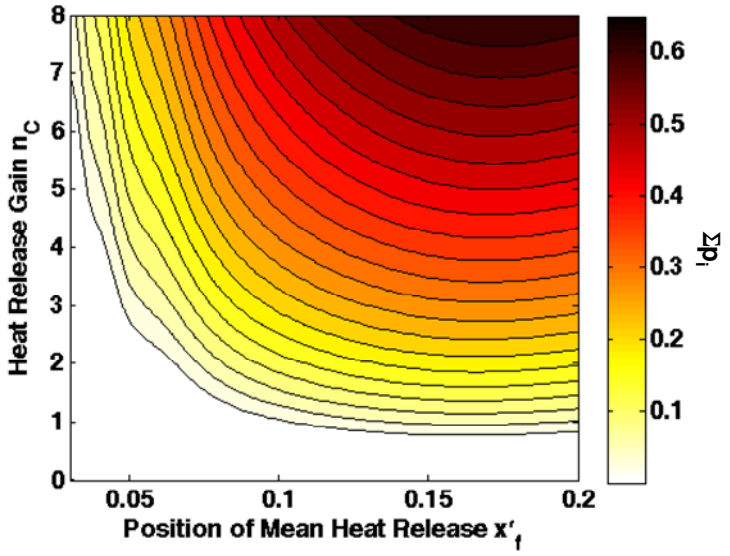

Figure 4-10: Sum of the RHCP poles for an uncontrolled self-excited, noise driven, combustor of case 1 in Appendix D but allowed to vary as a function of n_C and x'_f.

An interesting situation is created since the RHCP poles and zeros follow the same trends. The non-minimum phase zeros are much more sensitive to the position of mean heat release which is shown by the necessitation of the logarithm to plot meaningful contours in Figure 4-9 but not in Figure 4-10. As a result, by increasing the position of mean heat release the upper bound on the control cost in Eq. (4.58) due to the non-minimum phase zeros decreases faster than the upper bound on the state cost due to the RHCP poles. For the constrained control problem the area under the frequency weighting term also needs to be considered. In Figure 4-11 this area is shown to be increasing as the position of mean heat release increases. While the weighting function weakens the trend of decreasing the upper bound on the cost function by pushing the non-minimum phase zeros back into the LHCP, the weighting function influence is not enough to reverse this trend. $T(j\omega)$ is small at low frequencies and large at high

frequencies while the increase in the weighting term is mostly at low frequencies which is why the weighting function is not as detrimental as Figure 4-11 suggests. All the trends in the behavior of the upper bound on the cost function (4.58) suggest that the combustors most responsive to control are the ones most likely to be intrinsically unstable. This means that if the control engineer designed a control system for two different combustors, one stable and the other unstable, then the controlled unstable combustor will have better disturbance rejection than the controlled stable combustor.

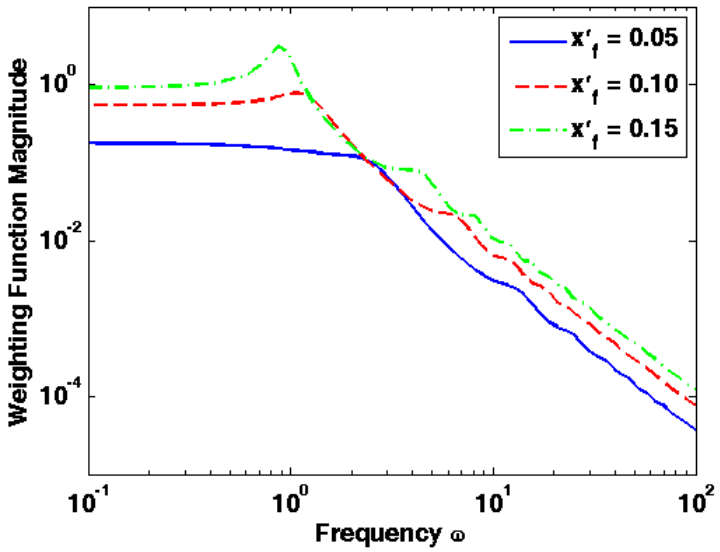

Figure 4-11: Frequency dependent magnitude of the weighting function multiplying $T(j\omega)$ corresponding to case 1 in Appendix D with $\tau'_A = 1.1$ as a function of x'_f.

Current combustors are not designed to be unstable nor will they be in the near future as long as the thermo-acoustic models are unreliable. Great pains have been taken in Chapter 2 to improve the physically realizable and mathematically tractable of current thermo-acoustic models, but there is always room for improvement. Certain physical processes are not well understood or properly experimentally validated and certain tools for time delay system are not fully developed. Why design a combustor to be unstable

but responsive to control if the control performance cannot be predicted ahead of time? Without this capability performance and stability cannot be guaranteed.

The poor robustness qualities of time delay systems, demonstrated in §3.7, place stronger demands on the thermo-acoustic modeler. As a result, reduced order models for controlling combustion instabilities need to be quite detailed. Getting the phase information at high frequencies correct is very important to accurately model stability because of uncertain time delays. Most robustness tools for time delay systems are related to the small gain theorem[222] used for magnitude uncertainty although some work exists on extending passivity concepts for phase uncertainty to alleviate these difficulties.[98] At the very least, enough information about modeling deficiencies need to known to set up a structured uncertainty problem because delay independent stability is too strong of a property to achieve. The stability islands in Figure 3-14 will attest to this fact. This pushes the complexity of the required physics and the mathematical tools needed to make useful predictions. While other important factors exists that are responsible for limiting control effectiveness, particularly behavioral constraints on the fuel actuator, these factors will remain secondary as long as the effects of their idealized counter parts cannot be predicted and consistently reproduced.

Prediction of feedback control performance on the behavior of combustion instabilities has been historically unsuccessful, which §1.3 can attest. This has confounded the combustion instability community. Now the culprits are found: the non-minimum phase zeros. In a SISO system they come from the volumetric heat release rate mechanism while in a MIMO system modal coupling also becomes important. The non-minimum phase zeros exclusive to MIMO systems may even follow different behavioral trends then their SISO system counterparts which would modify the design implications for designing combustor that are responsive to feedback control. These ideas create a path forward because it reveal where future research needs to be directed.

CHAPTER 5

CONCLUSION

Feedback control of combustion instabilities is a discipline ripe with profound subtleties. The existence of these subtleties is well known because physics based thermo-acoustic models have not successfully predicted the results of feedback control experiments. How these subtleties manifest themselves and their implications is a major constraint in understanding the factors that limit control effectiveness. This thesis focuses on the subtleties introduced by time delays in self-excited, noise driven, combustors. Results from this investigation are summarized in this chapter. A suggested research roadmap to tackle the issues hindering industrial adoption follows with some parting comments and encouragement for future researchers.

5.1 Thesis Accomplishments

In aggregate, the contributions of this thesis to the study of feedback control to suppress combustion instabilities fall into three broad categories: improved thermo-acoustic modeling, the introduction of new analysis tools, and an increased understanding of what limits control effectiveness. To help deconstruct communication barriers between combustion and control engineers this thesis pursued a deliberate policy of developing and interpreting results in two different ways to individually cater to the technical backgrounds of combustion and control engineers. The lack of collaboration between both types of engineers in studying the effects of feedback control on combustion instabilities has been a major impediment to progress since the birth of this area of research.[8] By developing the means to exchange information a research plan can be developed so that individual research by a combustion or control engineer can help

support the other discipline, and hence, accelerate the rate progress in this field. Such a plan will be purposed in the next section.

This thesis considers a thermo-acoustic model for self-excited, noise driven, combustor that has multiple independent time delays. Previous studies have not included multiple time delays. Most modeling work on the feedback control of combustion instabilities either had a noise driven stable linear system with no self-excitation mechanism or the control input and self-excitation mechanism overlapped. For industrial purposes the overlapping scenario is the most likely but this does not mean they are governed by the same physics, and hence, the same time delay. Practical thermo-acoustic models need to be able to handle multiple time delays in multiple feedback loops.

Developing better thermo-acoustic models consist of more than just adding new physical processes. How a physical process is implemented can be just as important as what physical processes are included. This is why this thesis makes such a strong emphasis starting in §2.1 on preserving physical realizability and mathematical tractability. Modeling assumptions for each component of a feedback diagram, such as Figure 2-2, need to be compatible with each other but often this attention to detail is lacking. Historically, thermo-acoustic modelers have placed too much weight on mathematical tractability and used many assumptions to get the individual transfer functions in Figure 2-2 as simple as possible while correctly reproducing the behavior of interest in a given frequency range. Such an approach is valid for an open loop transfer function like a forced combustor, but a self-excited and/or controlled combustor depends upon the closed loop transfer function. In §4.2 the sensitivity function analysis shows how the response of a closed loop transfer function depends upon the open loop transfer function over the entire frequency spectrum. This creates the means for modeling errors in the open loop transfer function in a frequency regime of seemingly no interest to the modeler to propagate to a frequency regime of interest in the closed loop transfer function.

To prevent these errors in the closed loop transfer function, any simplifying assumptions need to preserve the location of the RHCP poles, the location of the non-minimum phase zeros, and the magnitude of the net time delay on the open loop transfer function. Of these items the non-minimum phase zeros are the most sensitive to modeling as seen in §4.5 which come the volumetric heat release perturbation modeling. As a result, this thesis relaxes three commonly used assumptions in thermo-acoustic modeling to ensure that the closed loop transfer function response is correct. The first assumption not used is the low *St* assumption ($St << 1$) which can lead to getting the location of the non-minimum phase zeros incorrect. This thesis the first to include a full *St* model in its feedback loops for volumetric heat release perturbations. Additionally, this assumption distorts the order of the derivative in which time delays appear in which causes certain control schemes to behave like neutral functional differential equations when they should behave like retarded functional differential equations. Another relaxed assumption that distorts the order of the derivative of time delayed terms is the use of the linearized Galerkin expansion discussed in §2.6. Physically, the linearized Galerkin expansion assumes that the classical acoustic relations between pressure and velocity are valid. For this to be true the equi-partition of acoustic energy must hold; however, §3.6 shows how the presence of time delays in a linear system breaks the equi-partition of acoustic energy. As a result, this thesis uses the standard Galerkin expansion. The final relaxed assumption is that the order of magnitude of the volumetric heat release perturbations are $O(M\varepsilon)$[136] which is a historic holdover from when the combustion instability lacked first principle's model. Analysis in §2.5 shows that the order of magnitude of these terms are actually $O(\varepsilon)$ which means that a term in the wave equation (2.33) involving the spatial gradient of the volumetric heat release perturbations that is commonly neglected needs to be retained. Collectively, relaxing these three assumptions lead to a radically different heat release source terms in the thermo-acoustic model used in this thesis compared to previously used models.

Inclusion of multiple time delays in the thermo-acoustic model creates enough mathematical complexity to necessitate new analysis techniques. The combustion instability community has been lethargic incorporating advancements from external communities, particularly in applied mathematics and control theory. One of the accomplishments of this thesis is refreshing the dated tool set of the combustion instability community from the 1960's with modern analysis techniques for time delay systems. Emphasis is placed on tailoring to the individual backgrounds of the combustion or the control engineer work. For the combustion engineer a pdf approach is developed to describe steady state behavior starting in §3.2. In the process, expressions for the exact pdf and statistics of a general system of linear stochastic functional differential equations are derived. This is a new result. Prior work was based on Monte Carlo methods[117] and its application was limited to estimating statistical properties.[59] Equipped with exact solutions, this thesis began to explore the physical origins of the statistical behavior of combustion instabilities which lead to the identification of two key parameters in §3.4: a shape parameter related to deviations in the equi-partition of acoustic energy and a spread parameter related to the total acoustic energy in each temporal mode shape. An alternative approach based upon the spectrum of the infinitesimal generator is introduced for the control engineer. The spectral abscissa can be used to describe stability margins in a linear system which is very easy to find numerically, making it a powerful analysis tool. Parameter studies performed in this thesis show that the behavioral trends in the spectral abscissa tend the mirror to behavioral trends in the steady state statistics. As a result, design studies can be done using the spectral abscissa to quickly find interesting design points before switching to the slower evaluation of statistical properties to quantify performance. Pseudospectra was also introduced in §3.6 to show the poor robustness characteristics of self-excited combustors which will has repercussion on the factors that limit control effectiveness.

This thesis begins its study of the factors that limit control effectiveness by looking at the concept of controllability in §4.1. By extending a proof by Olbrot[191] in Appendix E the thermo-acoustic model is shown to be exact-null controllable which reveals the mathematical possibility that a finite number of eigenvalues can be arbitrarily placed. The physical constraints on control are explored by using sensitivity functions[194] but this thesis had to first extend this concept to work for linear functional differential equations. Previous sensitivity integral constraints only worked with a single factorable delay,[58] except for the Poisson integral constraints which can work with multiple discrete delays.[201] Such an analysis reveals the role of open loop RHCP poles and zeros along with the magnitude of the net delay play in limiting control effectiveness. A key implication found for combustor design in §4.5 is that they need to be nominally unstable to be the most responsive to feedback control, but due to the current state of thermo-acoustic modeling this design suggestion will see significant resistance from industry. Future control systems will require significantly increased robustness or more precise modeling to build a level trust that a control system will work as intended.

5.2 Research Roadmap

The number of possible variations of research directions in studying the factors that limit control effectiveness is boundless. More complicated geometries, combustion regimes, boundary conditions, and acoustic modes can always be considered. A prerequisite to studying these problems is to correct the most glaring flaw damaging the credibility of using feedback control to suppress combustion instabilities: the inability to predict the performance of a feedback control experiment. Completing this task will provide a sturdy foundation to expand upon in any direction. Research focus can then shift to explaining predicted results and evaluating the conclusions of this thesis and other prior work on the factors that limit control effectiveness.

Subdividing this research is best done by discipline. A certain amount of enabling work needs to be done separately by the combustion and control engineer to allow for fruitful collaborations. This body of work can be further subdivided into theory and experimental work. Historically, these two types of investigations have been done separately and not cross verified which is the exact same problem experienced between combustion and control engineering. Until this problem is rectified looking at more realistic operating conditions involving unstable combustion in a limit cycle due to combustion nonlinearities or multiplicative noise may result in wasted effort. Instead, emphasis needs to be placed on generating the simplest possible experiment that can be described theoretically. Unfortunately, limits exist to how far an experimental setup can meet the theory halfway.

5.2.1 Combustion Engineering

Many of the obstacles facing the combustion engineer can be expressed by looking at the feedback diagram from Figure 2-2. To verify closed loop system performance each of the individual transfer functions needs independent verification. This task has not been completed yet for the volumetric heat release rate perturbation model due to equivalence ratio perturbations and the combustion noise model. Both of these are central to the conclusions of this thesis. The non-minimum phase zeros are coming from the volumetric heat release rate perturbations while certain physical interpretations of controlled combustion instability behavior rely on the combustion noise being additive and Gaussian.

Some of the details relating to the volumetric heat release perturbations have already been discussed in §2.4.1. Experimentally determined FTFs exists for more complex flame configurations than available in theoretical models which do not overlap. Even the simple laminar conical flame used in this thesis and reproduced in Figure 2-4 is very difficult to experimentally evaluate the effects of equivalence ratio perturbations.[223]

A fuel actuator does not supply a spatially uniform equivalence ratio oscillation. Additionally, premixing the fuel and oxidizer smoothes the waveform emitted from the fuel actuator. As a result, the theory assumes the flame sees an equivalence ratio perturbation that is not matched in practiced. Other potentially problematic assumptions include the prescription of a mean flame shape and fixing certain parameters. Feedback control could change the mean flame shape and the jump conditions across the flame which includes the velocity ratio affecting the combustor Mach number. These changes affect the position of mean heat release, the internal time delay, and the flame geometry factor. Uncertainty in the time delay is particularly worrisome when it comes to robust control system performance.

The other weak link in the thermo-acoustic model is the combustion noise modeling introduced in §2.4.2. No theoretical model exists which forces this thesis to make a heuristic argument that the noise is additive and Gaussian. Of these two properties the Gaussianity rests on the strongest foundation based on the nature of turbulence and the central limit theorem.[119] Experimental evidence[120] seems to indicate that linearly stable combustors are driven by additive noise but the really question is what happens when feedback control is added. If the governing equations are semi-linear with respect to the control input then the system's stability becomes a function of the variance of the noise[126] and that variance will scale with the control gain. The good news is that this can be tested at the same time as the equivalence ratio modulation mechanism. In §3.4 the family of allowed pdf responses for the amplitude and phase response is derived for a general infinite dimensional linear system. Any deviations imply the existence of nonlinearities or the presence of more complicated noise interactions.

So far the suggested research has covered necessary steps to understanding the factors that limit control effectiveness. Other research is needed to address the accessibility of thermo-acoustic modeling and the efficiency of related analysis tools. This relates back to the modeling process illustrated in Figure 2-1. These problems are

more mathematical and subtle in nature. For example, how the individual transfer functions are linked together can be called into question. Each of the mathematical frameworks discussed in §2.3 have deficiencies. How modified Galerkin methods,[8] used in this thesis, applies boundary conditions has never been given a rigorous mathematical derivation. The awkwardness of incorporating acoustic impedance is very evident in §2.6.

Other possible improvements in the analysis tools will most likely come from the control engineer because of the emphasis of using the spectral abscissa instead of amplitude statistics in this thesis due to numerical efficiency considerations; however, this does not mean that the pdf based methods cannot be improved. Numerically evaluating the inverse Fourier transform may not be the best approach, although it is orders of magnitude faster than a Monte Carlo simulation. An alternative may be to write a driven functional differential equation to solve for the steady state variance. Appendix B forms a similar equation using abstract operators. If large enough step sizes can be used to rapidly approach a steady state solution while controlling the numerical error then statistical methods may become competitive against the spectral methods used in this thesis. Building these two methods to work together could lead to increased physical insight because of the similarity of the Fourier and Laplace transforms. Exploring how the sensitivity function constraints in §4.2 influences the allowed pdf behavior such as the coefficient of variation in Figure 3-5 is one such example of the benefits of such an approach.

5.2.2 Control Engineering

While the combustion engineer needs to be focused upon improving the reliability of the thermo-acoustic model the control engineer needs to focus on improving what can be done with that model. How to reach the limits of control effectiveness is one vein of research while another is why a limit to control effectiveness exists. This can be restated

as two design problems: how to design a robustified optimal controller and how to design the combustor to take advantage of future control systems. Both of these ideas are partially addressed in Chapter 4 but this discussion is limited by mathematical barriers in extending preexisting finite dimensional analysis tools to work with time delays.

Putting robustness concerns aside for a moment, what makes the task of synthesizing an optimal controller so difficult is incorporating the design constraints on the fuel actuator and the derivatives acting on the control input. When working with the unconstrained LQR problem the ARE (4.45) needs to be solved to synthesis the optimal controller. As constraints are added the equation that needs to be solved deviates from the ARE. In finite dimensional systems these deviations tend to take the form of coupled generalized Riccati equations.[224] The infinite dimensional counter part still needs to be determined. Once this is accomplished the next step would be to try to recycle existing finite dimensional tools to solve these equations. This requires a convergence proof to show that the solution to finite dimensional projections of these equations converges to the solution of the infinite dimensional problem. Only a small subset of these equations has been looked at in the infinite dimensional setting.[84]

Once the optimal controller is synthesizable concerns about robustness can be addressed. Some of these will be very specific to the gain functional derived such as implementation issues and assurances of strong stability. What can be looked at are the effects of uncertainty. This thesis has focused on robustness analysis tools for unstructured uncertainty based upon the small gain theorem[222] which is useful when the uncertainty is in the magnitude of the open loop transfer function. Uncertainty in the time delay will manifest as an uncertainty in the phase of the open loop transfer function. Some work exists on generalizing Popov's theorem and the concept of passivity to time delay system which may create a path forward.[98] The actually problem considered in this thesis is a bit more complicated because the time delays in the volumetric heat release perturbations show up in the argument and the gain of these FTFs. Multiple robustness

concepts will have to be weaved together to create effective analysis tools. Ultimately, the goal should be the ability to set up and solve the mixed $\mathcal{H}_2$-$\mathcal{H}_\infty$ problem.[224]

Most control problems include the need to synthesize a state estimator. Throughout this thesis a major implicit assumption used is the availability of full information. This is intentional. The famous separation principle which allows optimal control and optimal estimator design to proceed independently of each other will hold for a large class of linear infinite dimensional systems, including time delay systems.[225] As a result, the conclusions in this thesis about the factors that limit control effectiveness are unaffected. A similar thesis can be written on the factors that limit effective estimation. This is not the end of the story because the separation principle does break down when additionally constraints are added such as robustness[224] or reduced order control.[226] When the separation principal fails the design for the best controller and estimator becomes coupled. Despite this, understanding the LQG problem and what limits effective estimation is a useful stepping stone to progressing to the mixed $\mathcal{H}_2$-$\mathcal{H}_\infty$ problem.

When trying to develop a state estimator for a time delay system most of the analysis tools in this thesis can be recycled. The main difficulty is the inadequacy of relying upon spectra alone. If there was no sensor noise a Luenberger type observer[227] could be designed using pole placement techniques. In an estimator problem, called the Kalman filter problem, the signal to noise ratio becomes an important parameter.[228] Synthesizing the Kalman filter is part of the LQG problem which requires solving an associated ARE. How to discretize the abstract operators for the covariance of the state and sensor noise that appear in this ARE runs into a tradeoff between numerical accuracy and precision. Since the ARE is a quadratic operator equation and this particular ARE depends on the noise the rules of stochastic calculus need to be followed. The discretization method used in Appendix A does not correspond to an appropriate stochastic integral interpretation rule. An incorrect discretization scheme will distort the

answer to this ARE. Ito integration would correspond to a 1st order Euler discretization scheme which has a significantly slower spectral convergence rate compared to the pseudospectral method.[96] Either a new discretization scheme is needed or a way to correct the solution to the ARE when an improper stochastic integration interpretation rule is used. The only reason the LQR problem escapes this difficulty is that the optimal controller is independent of the presence of additive Gaussian noise, although its performance is not.

So far this subsection has only addressed how to build a better control and estimation system but not how to design a better combustor to extend the limits of attainable performance. In this thesis these design implications stem from the sensitivity function analysis introduced in §4.2 and focused on the role on non-minimum phase zeros in SISO systems. Addressing MIMO integral constraints are important because non-minimum phase zeros can be caused by modal coupling due to the volumetric heat release mechanism or the boundary conditions. The first step requires solving for transmission zeros by putting the open loop transfer function into Smith-McMillan form[205] which is a prerequisite for their numerical computation. Afterwards, the input and output direction of the poles and zeros can be solved to fully specify the MIMO integral constraints.[201] Interpreting the results will require an analytical understanding of what determines the input and output directions, an area that needs additional study. Another shortcoming is that that a complete set of MIMO integral constraints exists for a open loop transfer function with a single factorable delay while the thermo-acoustic instability problem requires being able to handle multiple distributed delays. Scattered results do exists for multiple discrete delays in the MIMO setting.[201] Sensitivity functions analysis can also be used to explore constraints in filtering[58] which can tied back to the Kalman filter problem. Eventually the sensitivity function analysis for control and estimation can be merged to look at coupling effects such as the collocation of actuation and sensing. Such a problem has only been looked at in non-reacting duct

flows.[229] Other conservations laws also exist in control theory that have not been investigated in this thesis.[230] One of the most promising is based upon marrying concepts in communication and control theory using the mutual information rate because it is written as a function of the pdf of the system response.[231] This framework is general enough to handle nonlinear time delay systems with multiplicative noise as long as the combustion engineer can feed response pdfs to the control engineer.

5.3 Final Comments

Significant work remains to be done to understand the factors that limit control effectiveness. Since the late 1990's progress has slowed considerably. Fortuitously, current events are in favor of a resurgence of interest in feedback control of combustion instabilities which are driven entirely by environmental concerns. NO_x regulations will continue to increase which will drive combustors to designs with less acoustic damping. Integration of renewable energy sources with the electricity grid and their non-constant supply of energy are forcing gas turbine power plants to run at off-design conditions to smooth the variations in the electrical supply. As a result, gas turbine power plants need to have a larger operability envelope which increases the odds of encountering combustion instabilities. Similarly, fuel flexible combustors using biofuels or other low carbon fuels will also place new demands on the operability envelope.

Despite the seemingly endless supply of complications present in the feedback control of combustion instabilities the work is very rewarding for people that enjoy the challenge of thinking differently. Ultimately, enabling feedback control will lead to disruptive change in combustor design. Future combustors could be designed to be unstable but controllable for large operability envelopes compared to present combustors that are designed to be stable for carefully defined operability envelopes. This change would be akin to that experienced by military aircraft several decades ago as control

systems became reliable enough to enable unstable designs. The task at hand is hard but not impossible. Feedback control of combustion instabilities is worth pursuing.

APPENDIX A

PSEUDOSPECTRAL DIFFERENCING METHODS

Digital computers operate in finite dimensions so any numerical calculation with an infinite dimensional system will have to discretize the state space. A time delay system will appear as a high order ordinary differential equation after discretizing the differentiation operator $\mathscr{D}$ in Eq. (3.60). Early attempts at this were based on Runge-Kutta or linear multistep methods.[96] This thesis uses a piecewise pseudospectra method[85] which works on a large class of time delay problems including neutral functional differential equations.[232] To use this method the time delays need to be enumerated by a sequence of time delays intervals $[-\tau_{i+1}, -\tau_i]$ of increasing magnitude. Each time delay interval is discretized using Chebyshev extremal points.[214]

The *i-th* Chebyshev extremal point of the $(N+1)$ order discretization of $[-\tau_{i+1}, -\tau_i]$ is given by Eq. (A.1).

$$t_i = \frac{(\tau_i - \tau_{i+1})}{2}\left(\cos\left(i\frac{\pi}{N}\right) - 1\right) - \tau_i \tag{A.1}$$

This collection of Chebyshev extremal points can be used to create a set of Lagrange basis polynomials which are used to discretize the differentiation operator $\mathscr{D}$.[214]

$$l_j(t) = \prod_{\substack{m=0 \\ m \neq j}}^{N} \frac{t - t_m}{t_j - t_m} \tag{A.2}$$

$$D_{ij} = l_j'(t_i) \tag{A.3}$$

For most calculation in this thesis these discretization algorithms are sufficient; however, some times a linear functional will need to be evaluated. A quadrature scheme will be need for this. Since Chebyshev extremal points are already used a Clenshaw-Curtis[233] quadrature makes the most sense to implement.

APPENDIX B

STABILITY OF THE SECOND MOMENT

Notions of stability in stochastic systems are numerous and a nuanced understanding would require a prolonged detour into probability theory that is inappropriate for this thesis.[116] The minimum amount of knowledge required is an ability to relate the exponential stability of the moments of some stochastic process to the stability of its deterministic counterpart. Since this thesis only considers additive Gaussian processes in linear systems only the first two moments need to be considered. For generality the abstract operator approach is used so that this appendix is applicable to linear stochastic systems of infinite dimension.

$$dx = \mathcal{A}\,x dt + \mathcal{W}\,dw \tag{B.1}$$

If the expectation of Eq. (B.1) is taken an abstract operator equation for the mean is recovered. From inspection of Eq. (B.2) the stability of the mean is determined from the eigenvalues of the infinitesimal generator $\mathcal{A}$ because it satisfies the spectrum determining growth condition.[83] For the purposes of this thesis $\mathcal{A}$ is an infinitesimal generator for a strongly continuous semigroup.

$$d\langle x\rangle = \mathcal{A}\langle x\rangle dt \tag{B.2}$$

Similar work can be done to write an operator equation for the second moment but this will require the application of the Itô product rule.[126]

$$dxx^T = \mathcal{A}xx^T dt + \mathcal{W}x^T dw + xx^T\mathcal{A}^T dt + x\mathcal{W}^T dw + \mathcal{W}\mathcal{W}^T dw^2 \tag{B.3}$$

$$d\langle xx^T\rangle = \mathcal{A}\langle xx^T\rangle dt + \langle xx^T\rangle\mathcal{A}^T dt + \mathcal{W}\mathcal{W}^T dt \tag{B.4}$$

Equation (B.4) is a bit unusual because the state is a matrix instead of a vector; however, it can be placed in a more familiar form using the vectorization operator.[234]

$$dVec\left(\langle xx^T\rangle\right) = \left(\mathcal{I}\otimes\mathcal{A} + \mathcal{A}\otimes\mathcal{I}\right)Vec\left(\langle xx^T\rangle\right)dt + Vec\left(\mathcal{W}\mathcal{W}^T\right)dt \tag{B.5}$$

The tensor product of two infinitesimal generators for a strongly continuous semigroup will also generate a strongly continuous semigroup. This ensures that Eq. (B.5) satisfies the spectrum determining growth condition.[83] Eigenvalues from $\mathcal{I}\otimes\mathcal{A}$ and $\mathcal{A}\otimes\mathcal{I}$ are just the eigenvalues of $\mathcal{A}$ except they now have infinite algebraic multiplicity; therefore, if $\mathcal{A}$ is stable, and hence a negative definite operator, then $\mathcal{I}\otimes\mathcal{A}$ and $\mathcal{A}\otimes\mathcal{I}$ are also negative definite. This proves that the stability of the mean (B.2) automatically ensures that the second moment (B.5) is also stable because the sum of two linear negative definite operators is also negative definite.

APPENDIX C

GASEQ CALCULATIONS

Solving for the sensitivity of the heat of reaction with equivalence ratio (2.4) can be solved using a midpoint difference rule between three equilibrium states calculated using Gaseq. Data from three calculations are shown in Table C-1. Gaseq does not calculate the heat of reaction but it gives enough information to calculate it using the enthalpy of formation which can be looked up in the JANNAF tables.[235]

$$\Delta H_R = \sum_{i=1}^{N\ species} \left(n_i'' - n_i'\right) h_f^\circ \tag{C.1}$$

Equation (C.1) shows that the heat of reaction is just the sum of the moles produced of each species times its heat formation.

Table C-1: Equilibrium composition of a methane-air flame at T = 575 K and P = 18 atm.

ϕ	0.649	0.650	0.651
$T_{ad}(K)$	1960	1962	1963
$N_2(mol)$	0.79000 / 0.7879	0.79000 / 0.7879	0.79000 / 0.7879
$O_2(mol)$	0.2100 / 0.07143	0.2100 / 0.07121	0.2100 / 0.07099
$CH_4(mol)$	0.06815 / --	0.06825 / --	0.06836 / --
$H_2O(mol)$	-- / 0.1359	-- / 0.1361	-- / 0.1363
$CO_2(mol)$	-- / 0.06809	-- / 0.06819	-- / 0.06830
$CO(mol)$	-- / 5.753e-5	-- / 5.856e-5	-- / 5.960e-5
$OH(mol)$	-- / 7.508e-4	-- / 7.572e-4	-- / 7.637e-4
$H(mol)$	-- / 1.525e-6	-- / 1.555e-6	-- / 1.587e-6
$O(mol)$	-- / 3.156e-5	-- / 3.193e-5	-- / 3.232e-5
$H_2(mol)$	-- / 2.609e-5	-- / 2.652e-5	-- / 2.695e-5
$NO(mol)$	-- / 0.00425	-- / 0.00426	-- / 0.00427
$\overline{MW}(g/mol)$	28.04 / 28.03	28.03 / 28.03	28.03 / 28.03

APPENDIX D

TEST CASES

Graphically illustrating how system performance changes with respect to system parameters limits the number of parameters that can be varied at one time. This thesis emphasized the role of time delays and what parameters are important to them in expressing their influence on system behavior. As a result, a large number of parameters need to be held constant. For simplicity a few representative test cases in Table D-1 have been judiciously selected to illustrate key performance trends unique to time delay systems.

Table D-1: Parameters for different combustor operating conditions.

Case #	1	2	3
M	0.15	0.15	0.15
β	2	2	2
n_C	1.25	1.25	1.25
τ'_V	3.25	3.25	3.25
C_0	$32\pi^5$	$\begin{bmatrix} 32\pi^5 & 0 \\ 0 & 1024\pi^5 \end{bmatrix}$	$\begin{bmatrix} 32\pi^5 & 105.6\pi^5 \\ 105.6\pi^5 & 1024\pi^5 \end{bmatrix}$
C_1	$16.64\pi^4$	$\begin{bmatrix} 16.64\pi^4 & 0 \\ 0 & 276.48\pi^4 \end{bmatrix}$	$\begin{bmatrix} 16.64\pi^4 & 29.512\pi^4 \\ 29.512\pi^4 & 276.48\pi^4 \end{bmatrix}$
C_2	$8.6464\pi^3$	$\begin{bmatrix} 8.6464\pi^3 & 0 \\ 0 & 74.4448\pi^3 \end{bmatrix}$	$\begin{bmatrix} 8.6464\pi^3 & 8.3091\pi^3 \\ 8.3091\pi^3 & 74.4448\pi^3 \end{bmatrix}$
C_3	$8.1664\pi^2$	$\begin{bmatrix} 8.1664\pi^2 & 0 \\ 0 & 17.3824\pi^2 \end{bmatrix}$	$\begin{bmatrix} 8.1664\pi^2 & 2.5548\pi^2 \\ 2.5548\pi^2 & 17.3824\pi^2 \end{bmatrix}$
C_4	1.16π	$\begin{bmatrix} 1.16\pi & 0 \\ 0 & 2.64\pi \end{bmatrix}$	$\begin{bmatrix} 1.16\pi & 0.38\pi \\ 0.38\pi & 2.64\pi \end{bmatrix}$

APPENDIX E

EXTENSION OF OLBROT'S PROOF

Tests for exact-null controllability or β-exponentially stabilizable for linear functional differential equations all assume that the controller directly influences the systems response. Unfortunately, heat release perturbations have to be controlled indirectly in combustors. This leads to the existence of derivatives of control input acting on the system such as the general system of linear functional differential equations shown below.

$$\dot{\vec{x}}(t) = \int_{-\tau}^{0} A(t+\theta)\vec{x}(\theta)d\theta + \sum_{i=0}^{n}\int_{-\tau}^{0} B_i(t+\theta)\frac{d^i}{dt^i}\vec{u}(\theta)d\theta \tag{E.1}$$

The goal of this appendix is to extend Olbrot's proof[191] for testing exact-null controllability or β-exponentially stabilizable to incorporate these extra derivatives subject to the same assumptions. These assumptions are that the elements of A are of bounded variation, the elements of B_i are piecewise constant functions with finitely many jumps plus an absolutely continuous function with its derivative a member of a Lebesgue space $\mathbb{L}^q$, the initial state trajectory is a bounded continuous function with at most one jump at the initial time, and that the control input belongs to the Lebesgue space $\mathbb{L}^p$ such that $p^{-1}+q^{-1}=1$.

Theorem: System (E.1) is β-exponentially stabilizable if and only if the exact-null controllability matrix (E.2) has full row rank $\forall\ s \in \mathbb{C}$ with $Re(s) \geq \beta$ where the characteristic matrix of Eq. (E.1) is represented by $\Delta(s)$.

$$\left[\Delta(s) \quad ; \quad \sum_{i=0}^{n} s^i B_i(s)\right] \tag{E.2}$$

Proof of Necessity: Assume that Eq. (E.1) is β-exponentially stabilizable but the full row rank condition on the exact-null controllability matrix is not satisfied. Then $\exists\ s_0 \in \mathbb{C}$ with $Re(s) \geq \beta$ and $q \in \mathbb{C}^n : q\Delta(s_0) = 0$ and $q\sum s^i{}_0 B_i(s_0) = 0$. The Laplace transform of Eq. (E.1) is given by Eq. (E.3) where ξ represents an arbitrary initial condition.

$$sI - A(s) - \sum_{i=0}^{n} s^i B_i(s) = \xi \tag{E.3}$$

If Eq. (E.3) is multiplied by q and evaluated at s_0 then the left hand side is zero but the right hand side cannot be equal to zero for any arbitrary initial condition. This leads to a contradiction; therefore, if Eq. (E.1) is β-exponentially stabilizable then the full row rank condition on the exact-null controllability matrix (E.2) is satisfied.

Proof of Sufficiency: Equation (E.1) can be rewritten in the extended state space introduced in §2.8.

$$\begin{bmatrix} \dot{\vec{x}}(t) \\ \dot{\vec{u}}(t) \\ \vdots \\ \vec{u}^{(n+1)}(t) \end{bmatrix} = \int_{-\tau}^{0} \begin{bmatrix} A(t+\theta) & \cdots & B_{n-1}(t+\theta) & B_n(t+\theta) \\ \vdots & \ddots & \vdots & \vdots \\ 0 & \cdots & 0 & \delta(\theta - t) \\ 0 & \cdots & 0 & 0 \end{bmatrix} \begin{bmatrix} \vec{x}(\theta) \\ \vec{u}(\theta) \\ \vdots \\ \vec{u}^{(n)}(\theta) \end{bmatrix} d\theta + \begin{bmatrix} 0 \\ 0 \\ \vdots \\ I \end{bmatrix} \vec{u}_{vir}(t) \tag{E.4}$$

Pandolfi's β-exponential stabilizability test[190] for retarded functional differential equations can now be used on Eq. (E.4). If the exact-null controllability matrix (E.5) from Pandolfi's test has full row rank then the system is β-exponentially stabilizable.

$$\begin{bmatrix} \Delta(s) & -B_0(s) & -B_1(s) & \cdots & -B_n(s) & 0 \\ 0 & sI & I & \ldots & 0 & 0 \\ \vdots & \vdots & \vdots & \ddots & \vdots & \vdots \\ 0 & 0 & 0 & \cdots & I & 0 \\ 0 & 0 & 0 & \cdots & sI & I \end{bmatrix} \tag{E.5}$$

A linear combination of column groups two through n+1 can recover the second column group in Eq. (E.2). This new column group can replace the second column group in Eq. (E.5) without changing the row rank. Finally, the large number of identity matrices

ensures that certain row and column group cannot reduce the row rank of the exact-null controllability matrix (E.5); therefore, they can be deleted. The reduced form of the exact-null controllability matrix is the same as given by Eq. (E.2). As a result, if the full row rank condition on the exact-null controllability matrix is satisfied then Eq. (E.1) is β-exponentially stabilizable.

REFERENCES

[1] Sewell, J. B. and Sobieski, P. A., "Monitoring of Combustion Instabilities: Calpine's Experience," in *Combustion Instabilities in Gas Turbine Engines: Operational Experience, Fundamental Mechanisms, and Modeling*. vol. 210, T. C. Lieuwen and V. Yang, Eds. Reston: AIAA, 2005, pp. 147-162.

[2] Goy, C. J., James, S. R., and Rea, S., "Monitoring Combustion Instabilities: E.ON UK's Experience," in *Combustion Instabilities in Gas Turbine Engines: Operational Experience, Fundamental Mechanisms, and Modeling*. vol. 210, T. C. Lieuwen and V. Yang, Eds. Reston: AIAA, 2005, pp. 163-175.

[3] Boluriaan, S. and Morris, P. J., "Acoustic Streaming: From Rayleigh to Today," *International Journal of Aeroacoustics,* vol. 2, pp. 255-292, 2003.

[4] Pierce, A. D., *Acoustics: An Introduction to Its Physical Principles and Applications*, Melville: Acoustical Society of America, 1989.

[5] Bellows, B. D., Neumeier, Y., and Lieuwen, T. C., "Forced Response of a Swirling Premixed Flame to Flow Disturbances," *Journal of Propulsion and Power,* vol. 22, pp. 1075-1084, 2006.

[6] Keller, J. O., Vaneveld, L., Korschelt, D., Hubbard, G. L., Ghoneim, A. F., Daily, J. W., and Oppenheim, A. K., "Mechanism of Instabilities in Turbulent Combustion Leading to Flashback," *AIAA Journal,* vol. 20, pp. 254-262, 1981.

[7] Lefebvre, A. H., *Gas Turbine Combustion*, 2nd ed., New York: Taylor and Francis Group, 1999.

[8] Culick, F. E. C., "Unsteady Motions in Combustion Chambers for Propulsion Systems," DTIC Document AG-AVT-039, 2006.

[9] Lewis_Laboratory_Staff, "A Summary of Preliminary Investigations into the Characteristics of Combustion Screech in Ducted Burners," Cleveland NACA-TR-1384 1958.

[10] Oefelein, J. C. and Yang, V., "Comprehensive Review of Liquid-Propellant Combustion Instabilities in F-1 Engines," *Journal of Propulsion and Power,* vol. 9, pp. 657-677, 1993.

[11] Rubin, S., "Longitudinal Instability of Liquid Rockets Due to Propulsion Feedback (POGO)," *Journal of Spacecraft and Rockets,* vol. 3, pp. 1188-1195, August 1966.

[12] Zinn, B. T., "A Theoretical Study of Nonlinear Combustion Instability in Liquid Propellant Rocket Engines," *AIAA journal,* vol. 6, pp. 1966-1972, 1968.

[13] Culick, F. E. C., "Nonlinear Behavior of Acoustic Waves in Combustion Chambers - I," *Acta Astronautica,* vol. 3, pp. 715-734, 1976.

[14] Awad, E. and Culick, F. E. C., "On the Existence and Stability of Limit Cycles for Longitudinal Acoustic Modes in a Combustion Chamber," *Combustion Science and Technology,* vol. 46, pp. 195-222, 1986.

[15] Kim, S., "Nonlinear Combustion Instabilities in Combustion Chambers," in *Mechanical Engineering* Ph.D University Park: Pennsylvania State, 1989, p. 192.

[16] Marble, F. E. and Candel, S. M., "Acoustic Disturbance from Gas Non-Uniformities Convected through a Nozzle," *Journal of Sound and Vibration,* vol. 55, pp. 225-243, 1977.

[17] Eckstein, J., Freitag, E., Hirsch, C., and Sattelmayer, T., "Experimental Study on the Role of Entropy Waves in Low-Frequency Oscillations in a RQL Combustor," *Journal of Engineering for Gas Turbines and Power,* vol. 128, pp. 264-270, April 2006.

[18] Konrad, W., Brehm, N., Kameier, F., Freeman, C., and Day, I. J., "Combustion Instability Investigations on the BR710 Jet Engine," *Journal of Engineering for Gas Turbines and Power,* vol. 120, pp. 34-40, January 1998.

[19] Sattelmayer, T., "Influence of the Combustor Aerodynamics on Combustion Instabilities from Equivalence Ratio Fluctuations," *Journal of Engineering for Gas Turbines and Power,* vol. 125, pp. 11-19, January 2003.

[20] Bake, F., Kings, N., and Roehle, I., "Fundamental Mechanism of Entropy Noise in Aero-Engines: Experimental Investigations," *Journal of Engineering for Gas Turbines and Power,* vol. 130, January 2008.

[21] Schadow, K. C. and Gutmark, E. J., "Combustion Instability Related to Vortex Shedding in Dump Combustors and Their Passive Control," *Progress in Energy and Combustion Science,* vol. 18, pp. 117-132, 1992.

[22] Vuillot, F. and Casalis, G., "Motor Flow Instabilities - Part 1," NATO RTO-EN-023, 2002.

[23] Brown, R. S., Dunlap, R., Young, S. W., and Waugh, R. C., "Vortex Shedding as a Source of Acoustic Energy in Segmented Solid Rockets," *Journal of Spacecraft and Rockets,* vol. 18, pp. 312-319, July-August 1981.

[24] Stow, S. R., Dowling, A. P., and Hynes, T. P., "Reflection of Circumferential Modes in a Choked Nozzle," *Journal of Fluid Mechanics,* vol. 467, pp. 215-239, 2002.

[25] Putnam, A. A., *Combustion Driven Oscillations in Industry*, Fuel and Energy Science Series, New York: Elsevier, 1971.

[26] Dowling, A. P., "Nonlinear Self-Excited Oscillations of a Ducted Flame," *Journal of Fluid Mechanics,* vol. 346, pp. 271-290, 1997.

[27] Lieuwen, T. C., "Modeling Premixed Combustion - Acoustic Wave Interactions: A Review," *Journal of Propulsion and Power,* vol. 19, pp. 765-781, September-October 2003.

[28] Annaswamy, A. M., "Nonlinear Modeling and Control of Combustion Dynamics," in *Control of Fluid Flow`*. vol. 330, M. Thoma and M. Morari, Eds. The Netherlands: Springer-Verlag, 2006, pp. 95-121.

[29] Rayleigh, J. W. S., *The Theory of Sound*, 2nd ed., vol. 2: Dover Publishing, 1945.

[30] Chu, B. T., "On the Energy Transfer to Small Disturbances in Fluid Flow (Part I)," *Acta Mechanica,* vol. 3, pp. 215-234, September 1965.

[31] Tsien, H. S., "Servo-Stabilization of Combustion in Rocket Motors," *Journal of the American Rocket Society,* vol. 22, pp. 256-263, 1952.

[32] Marble, F. E. and Cox Jr., D. W., "Servo-Stabilization of Low-Frequency Oscillations in a Liquid Bipropellant Rocket Motor," *Journal of the American Rocket Society,* vol. 23, pp. 63-81, March-April 1953.

[33] Dines, P. J., "Active Control of Flame Noise," Ph.D. Cambridge: Cambridge University, 1983, p. 172.

[34] Heckl, M., "Heat Sources in Acoustic Resonators," Ph.D. Cambridge: Cambridge University, 1985, p. 181.

[35] Langhorne, P. J., Dowling, A. P., and Hooper, N., "Practical Active Control System for Combustion Oscillations," *Journal of Propulsion and Power,* vol. 6, pp. 324-333, 1989.

[36] Huang, Y. and Yang, V., "Dynamics and Stability of Lean Premixed Swirl Stabilized Combustion," *Progress in Energy and Combustion Science,* vol. 35, pp. 293-364, 2009.

[37] Annaswamy, A. M. and Ghoniem, A. F., "Active Control of Combustion Instability: Theory and Practice," in *IEEE Control Systems Magazine* 22 Ann Arbor: IEEE Control Systems Society, 2002, pp. 37-54.

[38] Dowling, A. P. and Morgans, A. S., "Feedback Control of Combustion Oscillations," *Annual Review of Fluid Mechanics,* vol. 37, pp. 151-182, January 2005.

[39] Bloxsidge, G. J., Dowling, A. P., Hooper, N., and Langhorne, P. J., "Active Control of Reheat Buzz," *AIAA Journal,* vol. 26, pp. 783-790, July 1988.

[40] Hoffmann, S., Weber, G., Judith, H., Hermann, J., and Orthmann, A., "Application of Active Control to Siemens Heavy Duty Gas Turbine," in *Symposium of the AVT Panel on*

"Gas Turbine Engine Combustion, Emissions, and Alternative Fuels," Lisbon, Portugal, 1998, pp. 40-1 to 40-13.

[41] Moran, A. J., Steele, D., and Dowling, A. P., "Active Control of Combustion and its Applications," in *RTO AVT Symposium on "Active Control Technology for Enhanced Performance Operational Capabilities of Military Aircraft, Land Vehicles and Sea Vehicles."* Braunschweig, Germany, 2000, pp. 2-1 to 2-8.

[42] Johnson, C. E., Neumeier, Y., Neumaier, M., Zinn, B. T., Darling, D. D., and Sattinger, S. S., "Demonstration of Active Control of Combustion Instabilities on a Full Scale Gas Turbine Combustor," in *Turbo Expo* New Orleans: ASME, 2001, p. 7.

[43] Cohen, J. M. and Banaszuk, A., "Factors Affecting the Control of Unstable Combustors," in *Combustion Instabilities in Gas Turbine Engines: Operational Experience, Fundamental Mechanisms and Modeling*. vol. 210, T. Lieuwen and V. Yang, Eds. Reston: AIAA, 2005, pp. 581-610.

[44] Summerfield, M., "A Theory of Unstable Combustion in Liquid Propellant Rocket Systems," *Journal of the American Rocket Society,* vol. 21, pp. 108-114, September 1951.

[45] Crocco, L. and Cheng, S.-I., "Theory of Combustion Instability in Liquid Propellant Rocket Motors," AD0688924, 1956.

[46] Richard, J., "Time-Delay Systems: An Overview of Some Recent Advances and Open Problems," *Automatica,* vol. 39, pp. 1667-1694, October 2003.

[47] Murugappan, S., Park, S., Annaswamy, A. M., Ghoniem, A. F., Acharya, S., and Allgood, D. C., "Optimal Control of a Swirl Stabilized Spray Combustor Using System Identification Approach," *Combustion Science and Technology,* vol. 175, pp. 55-88, 2003.

[48] Chu, Y. C., Glover, K., and Dowling, A. P., "Control of Combustion Oscillations via H_∞ Loop-Shaping, μ-Analysis and Integral Quadratic Constraints," *Automatica,* vol. 39, pp. 219-231, 2003.

[49] Evesque, S., Dowling, A. P., and Annaswamy, A. M., "Self-Tuning Regulators for Combustion Oscillations," *Proceedings: Mathematical, Physical and Engineering Sciences,* vol. 459, pp. 1709-1749, July 8th 2003.

[50] Silva, G. J., Datta, A., and Bhattacharyya, S. P., "Controller Design via Pade Approximation Can Lead to Instability," in *40th IEEE Conference on Decision and Control* Orlando, Florida, 2001, pp. 4733-4737.

[51] Hong, B. S., Yang, V., and Ray, A., "Robust Feedback Control of Combustion Instability with Modeling Uncertainty," *Combustion and Flame,* vol. 120, pp. 91-106, 2000.

[52] Evesque, S. and Dowling, A. P., "LMS Algorithm for Adaptive Control of Combustion Oscillations," *Combustion Science and Technology,* vol. 164, pp. 65-93, 2001.

[53] Hathout, J. P., Fleifil, M., Annaswamy, A. M., and Ghoniem, A. F., "Heat Release Actuation for Control of Mixture-Inhomogeneity-Driven Combustion Instability," *Proceedings of the Combustion Institute,* vol. 28, pp. 721-730, 2000.

[54] Palmor, Z. J., "Time-Delay Compensation: Smith Predictor and its Modifications," in *The Control Handbook*, W. S. Levine, Ed. Boca Raton: CRC-Press, 1996, pp. 224-237.

[55] Morgans, A. S. and Annaswamy, A. M., "Adaptive Control of Combustion Instabilities for Combustion Systems with Right-Half Plane Zeros," *Combustion Science and Technology,* vol. 180, pp. 1549-1571, 2008.

[56] Kopasakis, G. and DeLaat, J. C., "Adaptive Instability Suppression Controls in a Liquid Fueled Combustor," in *38th Joint Propulsion Conference* Indianapolis, Indiana: AIAA, 2002.

[57] Johnson, C. E., Neumier, Y., Cohen, J. M., Lee, J. Y., Lubarsky, E., and Zinn, B. T., "Effects of Time Delay and System Noise Upon Active Control of Unstable Combustors," in *39th Aerospace Science Meeting and Exhibit* Reno, Nevada: AIAA, 2001.

[58] Seron, M., Braslavsky, J., and Goodwin, G., *Fundamental Limitations in Filtering and Control*, New York: Springer-Verlag, 1997.

[59] Cohen, J. M., Banaszuk, A., Hibshman, J. R., Anderson, T. J., and Alholm, H. A., "Active Control of Pressure Oscillations in a Liquid-Fueled Sector Combustor," *Journal of Engineering for Gas Turbines and Power,* vol. 130, September 2008.

[60] Coker, A., Neumier, Y., Zinn, B. T., Menon, S., and Lieuwen, T. C., "Active Instability Control Effectiveness in a Liquid Fueled Combustor," *Combustion Science and Technology,* vol. 178, pp. 1251-1261, 2006.

[61] Kopasakis, G., DeLaat, J. C., and Chang, C. T., "Validation of an Adaptive Combustion Instability Control Method for Gas-Turbine Engines," in *40th Joint Propulsion Conference and Exhibit* Fort Lauderdale, Florida: AIAA, 2004.

[62] Fleifil, M., Hathout, J. P., Annaswamy, A. M., and Ghoniem, A. F., "The Origin of Secondary Peaks with Active Control of Thermoacoustic Instability," *Combustion Science and Technology,* vol. 133, pp. 227-265, 1998.

[63] Annaswamy, A. M., Fleifil, M., Hathout, J. P., and Ghoniem, A. F., "Impact of Linear Coupling on the Design of Active Controllers for the Thermoacoustic Instability," *Combustion Science and Technology,* vol. 128, pp. 131-180, 1997.

[64] Fleifil, M., Annaswamy, A. M., Ghoneim, A., and Ghoniem, A. F., "Response of a Laminar Premixed Flame to Flow Oscillations: A Kinematic Model and Thermoacoustic Instability Results," *Combustion and Flame,* vol. 106, pp. 487-510, 1996.

[65] Banaszuk, A., Mehta, P. G., Jacobson, C. A., and Khibnik, A. I., "Limits of Achievable Performance of Controlled Combustion Process," *IEEE Transactions on Control Systems Technology,* vol. 14, pp. 881-895, September 2006.

[66] Stein, G., "Respect the Unstable," in *IEEE Control Systems* 23: IEEE, 2003, pp. 12-25.

[67] Kopasakis, G., "High Frequency Adaptive Instability Suppression Controls in a Liquid-Fueled Combustor," in *39th Joint Propulsion Conference and Exhibit* Huntsville, Alabama: AIAA, 2003.

[68] Lieuwen, T. C., "Phase Drift Characteristics of Self-Excited Combustion Driven Oscillations," *Journal of Sound and Vibration,* vol. 242, pp. 893-905, 2001.

[69] Lieuwen, T. C. and Banaszuk, A., "Background Noise Effect on Combustor Stability," *Journal of Propulsion and Power,* vol. 21, pp. 25-31, January-February 2005.

[70] Haldane, J. B. S., "A Contribution to the Theory of Price Fluctuations," *The Review of Economic Studies,* vol. 1, pp. 186-195, 1934.

[71] Statz, H., DeMars, G. A., Wilson, D. T., and Tang, C. L., "Problem of Spike Elimination in Lasers," *Journal of Applied Physics,* vol. 36, pp. 1510-1514, 1964.

[72] Coleman, B. D., Gurtin, M. E., and Herrera, R. I., "Waves in Materials with Memory: I. The Velocity of One-Dimensional Shock and Acceleration Waves," *Archive for Rational Mechanics and Analysis,* vol. 19, pp. 1-19, 1965.

[73] Ergen, W. K., "Kinetics of Circulating- Fuel Nuclear Reactor," *Journal of Applied Physics,* vol. 25, pp. 702-711, 1953.

[74] Doi, S. and Kate, S., "Chatter Vibrations of Lathe Tools," *Transactions of the ASME,* vol. 78, pp. 1126-1137, 1955.

[75] Ziegler, J. G. and Nichols, N. B., "Optimum Settings for Automatic Controllers," *Transactions of the ASME,* vol. 64, pp. 759-768, November 1942.

[76] Smith, O. J. M., "Closer Control of Loops with Dead Time," *Chemical Engineering Progress,* vol. 53, pp. 217-220, 1957.

[77] Manitius, A. Z. and Olbrot, A. W., "Finite Spectrum Assignment Problem for Systems with Delays," *IEEE Transactions on Automatic Control,* vol. 24, pp. 541-553, August 1979.

[78] Watanabe, K. and Ito, M., "A Process-Model Control for Linear Systems with Delay," *IEEE Transactions on Automatic Control,* vol. 26, pp. 1261-1269, December 1981.

[79] Zhong, Q., *Robust Control of Time-Delay Systems*, 1st ed., Berlin: Springer, 2006.

[80] Bellman, R. and Cooke, K. L., *Differential-Difference Equations*, Mathematics in Science and Engineering, vol. 6, New York: Academic Press, 1963.

[81] Hale, J. K. and Lunel, S. M. V., *Introduction to Functional Differential Equations*, 1st ed., Applied Mathematical Sciences, vol. 99, New York: Springer-Verlag, 1993.

[82] Cutain, R. F. and Pritchard, A. J., *Infinite Dimensional Linear Systems Theory*, Lecture Notes in Control and Information Sciences, vol. 8, Berlin: Springer-Verlag, 1978.

[83] Bensoussan, A., Da Prato, G., Delfour, M. C., and Mitter, S. K., *Representation and Control of Infinite Dimensional Systems*, 2nd ed., Systems & Control: Foundations & Applications, Boston: Birkhäuser, 2007.

[84] Curtain, R. F. and Zwart, H., *An Introduction to Infinite-Dimensional Linear System Theory*, Texts in Applied Mathematics, vol. 21, New York: Springer-Verlag, 1995.

[85] Breda, D., Maset, S., and Vermiglio, R., "Pseudospectral Differencing Method for Characteristic Roots of Delay Differential Equations," *SIAM Journal of Scientific Computing,* vol. 27, pp. 482-495, 2005.

[86] Curtain, R. F. and Glover, K., "Robust Stabilization of Infinite Dimensional Systems by Finite Dimensional Controllers," *Systems & Control Letters,* vol. 7, pp. 41-47, February 1986.

[87] Lyapunov, A. M., *General Problem of the Stability of Motion*, 1st ed.: Taylor & Francis, 1992.

[88] Niculescu, S., Verriest, E. I., Dugard, L., and Dion, J., "Stability and Robust Stability of Time-Delay Systems: A Guided Tour," in *Stability and Control of Time-Delay Systems*. vol. 228, L. Dugard and E. I. Verriest, Eds. London: Springer, 1998, pp. 1-71.

[89] Kolmanovskiĭ, V. and Myshkis, A., *Introduction to the Theory and Applications of Functional Differential Equations*, Mathematics and Its Applications, vol. 463, Dordrecht: Kluwer Academic Publishers, 1999.

[90] Michiels, W., Engelborghs, K., Vansevenant, P., and Roose, D., "Continuous Pole Placement for Delay Equations," *Automatica,* vol. 38, pp. 747-761, May 2002.

[91] Michiels, W., Fridman, E., and Niculescu, S., "Robustness Assessment Via Stability Radii in Delay Parameters," *International Journal of Robust control,* vol. 19, pp. 1405-1426, September 2009.

[92] Bailly, C., Bogey, C., and Candel, S., "Modelling of Sound Generation by Turbulent Reacting Flows," *International Journal of Aeroacoustics,* vol. 9, pp. 461-491, 2010.

[93] Dowling, A. P. and Stow, S. R., "Acoustic Analysis of Gas Turbine Combustors," *Journal of Propulsion and Power,* vol. 19, pp. 751-764, September-October 2003.

[94] Stépán, G., *Retarded Dynamical Systems: Stability and Characteristic Functions*, Pitman Research Notes in Mathematics Series, vol. 210, London: Longman Scientific & Technical, 1989.

[95] Dowling, A. P., "The Calculation of Thermoacoustic Oscillations," *Journal of Sound and Vibration,* vol. 180, pp. 557-581, 1993.

[96] Breda, D., Maset, S., and Vermiglio, R., "Computing the Characteristic Roots for Delay Differential Equations," *IMA Journal of Numerical Analysis,* vol. 24, pp. 1-19, 2004.

[97] Foias, C., Manley, O. P., and Temam, R., "Approximate Inertial Manifolds and Effective Viscosity in Turbulent Flows," *Physics of Fluids A,* vol. 3, pp. 898-911, 1991.

[98] Niculescu, S., *Delay Effects on Stability: A Robust Control Approach*, Lecture Notes in Control and Information Sciences, vol. 269, Germany: Springer, 2001.

[99] Kim, W., Menon, S., and Mongia, H. C., "Large-Eddy Simulation of a Gas Turbine Combustor Flow," *Combustion Science and Technology,* vol. 143, pp. 25-62, 1999.

[100] Tacina, K. M., Lee, C., and Wey, C., "NASA Glenn High Pressure Low NOx Emissions Research," Cleveland NASA/TM-2008-214974, 2008.

[101] Ballal, D. R. and Zelina, J., "Progress in Aeroengine Technology (1939-2003)," *Journal of Aircraft,* vol. 41, pp. 43-50, 2004.

[102] Abdel-Gayed, R. G., Bradley, D., and Lung, F. K. K., "Combustion Regimes and the Straining of Turbulent Premixed Flames," *Combustion and Flame,* vol. 76, pp. 213-218, 1989.

[103] Poinsot, T. and Veynante, D., *Theoretical and Numerical Combustion*, 2nd ed., Philadelphia: R. T. Edwards, 2005.

[104] Dowling, A. P., "A Kinematic Model of a Ducted Flame," *Journal of Fluid Mechanics,* vol. 394, pp. 51-72, 1999.

[105] Cho, J. H. and Lieuwen, T. C., "Laminar Premixed Flame Response to Equivalence Ratio Oscillations," *Combustion and Flame,* vol. 140, pp. 116-129, 2005.

[106] Kerstein, A. R., Ashurst, W. T., and Williams, F. A., "Field Equation for Interface Propagation in an Unsteady Homogeneous Flow Field," *Physical Review A,* vol. 37, pp. 2728-2731, April 1988.

[107] Ducruix, S., Durox, D., and Candel, S. M., "Theoretical and Experimental Determinations of the Transfer Function of a Laminar Premixed Flame," *Proceedings of the Combustion Institute,* vol. 28, pp. 765-773, 2000.

[108] Karimi, N., Brear, M. J., Jin, S., and Monty, J. P., "Linear and Non-Linear Forced Response of a Conical, Ducted, Laminar Premixed Flame," *Combustion and Flame,* vol. 156, pp. 2201-2212, 2009.

[109] Schuller, T., Durox, D., and Candel, S., "A Unified Model for the Prediction of Laminar Flame Transfer Functions: Comparisons Between Conical and V-Flame Dynamics," *Combustion and Flame,* vol. 134, pp. 21-34, 2003.

[110] Palies, R., Schuller, T., Durox, D., and Candel, S., "Modeling of Premixed Swirling Flames Transfer Functions," *Proceedings of the Combustion Institute,* vol. 33, pp. 2967-2974, 2011.

[111] Preetham, Lieuwen, T. C., and Santosh, H., "Dynamics of Laminar Premixed Flames Forced by Harmonic Velocity Disturbances," *Journal of Propulsion and Power,* vol. 24, pp. 1390-1402, November-December 2008.

[112] Yi, T. and Santavicca, D. A., "Flame Transfer Functions for Liquid Fueled Swirl Stabilized Turbulent Lean Direct Fuel Injection Combustion," *Journal of Engineering for Gas Turbines and Power,* vol. 132, pp. 021506-1 to 021506-6, February 2010.

[113] Shreekrishna, Hemchandra, S., and Lieuwen, T. C., "Premixed Flame Response to Equivalence Ratio Perturbations," *Combustion Theory and Modelling,* vol. 14, pp. 681-714, 2010.

[114] Abu-Orf, G. M. and Cant, R. S., "Reaction Rate Modelling for Premixed Turbulent Methane-Air Flames," in *Proceedings of the Joint Meeting of Spanish, Portuguese, Swedish, and British Sections of the Combustion Institute* Madeira, 1996, p. 4.

[115] Candel, S., Durox, D., Ducruix, S., Birbaud, A. L., Noiray, N., and Schuller, T., "Flame Dynamics and Combustion Noise: Progress and Challenges," *International Journal of Aeroacoustics,* vol. 8, pp. 1-56, 2009.

[116] Liu, K., *Stability of Infinite Dimensional Stochastic Differential Equations with Applications*, 1st ed., Monographs and Surveys in Pure and Applied Mathematics, vol. 135, New York: Chapman and Hall, 2005.

[117] Burnley, V. S., "Nonlinear Combustion Instabilities and Stochastic Sources," in *Mechanical Engineering* Ph.D Pasadena: California Institute of Technology, 1996, p. 171.

[118] Chu, B. T. and Kovásznay, L. S. G., "Nonlinear Interactions in a Viscous Heat Conducting Compressible Gas," *Journal of Fluid Mechanics,* vol. 3, pp. 494-514, 1957.

[119] Clavin, P., Kim, J. S., and Williams, F. A., "Turbulence-Induced Noise Effects on High-Frequency Combustion Instabilities," *Combustion Science and Technology,* vol. 96, pp. 61-84, 1994.

[120] Lieuwen, T. C., "Experimental Investigation of Limit Cycle Oscillations in an Unstable Gas Turbine Combustor," *Journal of Propulsion and Power,* vol. 18, pp. 61-67, January-February 2002.

[121] Janson, S., *Gaussian Hilbert Spaces*, 1st ed., Cambridge Tracts in Mathematics, vol. 129, Cambridge: Cambridge University Press, 1997.

[122] Rajaram, R., Gray, J., and Lieuwen, T. C., "Premixed Combustion Noise Scaling: Total Power and Spectra," in *12th AIAA/CEAS Aeroacoustics Conference* Cambridge, MA, 2006, p. 9.

[123] Clavin, P. and Siggia, E. D., "Turbulent Premixed Flames and Sound Generation," *Combustion Science and Technology,* vol. 78, pp. 147-155, 1991.

[124] Bibbona, E., Panfilo, G., and Tavella, P., "The Ornstein-Uhlenbeck Process as a Model of a Low Pass Filtered White Noise," *Metrologia,* vol. 45, pp. S117-S126, December 2008.

[125] Gardiner, C., *Stochastic Methods: A Handbook for the Natural and Social Sciences*, 4th ed., Springer Series in Synergetics, vol. 13, Berlin: Springer, 2009.

[126] Mao, X., *Stochastic Differential Equations and Applications*, 1st ed., Horwood Series in Mathematics and Applications, Chuchester: Horwood Publishing, 1997.

[127] van Kämpen, N. G., "Itô Versus Stratonovich," *Journal of Statistical Physics,* vol. 24, pp. 175-187, January 1981.

[128] Kloeden, P. E. and Platen, E., *Numerical Solution of Stochastic Differential Equations*, 2nd ed., Applications of Mathematics: Stochastic Modeling and Applied Probability, vol. 23, Germany: Springer, 2000.

[129] Blackstock, D. T., *Fundamentals of Physical Acoustics*, 1st ed., New York: Wiley-Interscience, 2000.

[130] Marble, F. E., "Dynamics of Dusty Gases," *Annual Review of Fluid Mechanics,* vol. 2, pp. 397-446, January 1970.

[131] Holmes, M. H., *Introduction to Perturbation Methods*, 1st ed., Texts in Applied Mathematics, vol. 20, New York: Springer-Verlag, 1995.

[132] Patel, N. and Menon, S., "Simulation of Spray-Turbulence-Flame Interactions in a Lean Direct Injection Combustor," *Combustion and Flame,* vol. 153, pp. 228-257, April 2008.

[133] Huang, Y., Sung, H., Hsieh, S., and Yang, V., "Large Eddy Simulation of Combustion Dynamics of Lean Premixed Swirl Stabilized Combustor," *Journal of Propulsion and Power,* vol. 19, pp. 782-794, 2003.

[134] Bracewell, R., *The Fourier Transform and Its Applications*, 3rd ed., New York: McGraw-Hill Science/Engineering/Math, 1999.

[135] Culick, F. E. C., "Combustion Instabilities in Liquid-Fuelled Propulsion Systems - An Overview," NATO Document AGARD-CP-450, 1988.

[136] Culick, F. E. C., "A Note on Ordering Perturbations and the Insignificance of Linear Coupling in Combustion Instabilities," *Combustion Science and Technology,* vol. 126, pp. 359-379, 1997.

[137] Farassat, F., "Discontinuities in Aerodynamics and Aeroacoustics: The Concept and Applications of Generalized Derivatives," *Journal of Sound and Vibration,* vol. 55, pp. 165-193, February 1977.

[138] Docquier, N. and Candel, S., "Combustion Control and Sensors: A Review," *Progress in Energy and Combustion Science,* vol. 28, pp. 107-150, 2002.

[139] Culley, D., Garg, S., Hiller, S. J., Horn, W., Kumar, A., Mathews, H. K., Moustapha, H., Pfoertner, H., Rosenfeld, T., Rybarik, P., Schadow, K., Stiharu, I., Viassolo, D. E., and Webster, J., "More Intelligent Gas Turbine Engines," TR-AVT-128, 2009.

[140] Li, G. and Gutmark, E. J., "Effects of Installation on Dynamic Pressure Measurements," in *44th AIAA Aerospace Sciences Meeting and Exhibit* Reno, Nevada: AIAA, 2006, p. 5.

[141] Neumeier, Y., Lubarsky, E., Heising, R., Israeli, O., Neumaier, M., and Zinn, B. T., "Liquid Injector Actuator for Control of Combustion Processes," in *34th AIAA/ASME/SAE/ASEE Joint Propulsion Conference & Exhibit* Cleveland, Ohio, 1998, p. 20.

[142] Goeke, J. L. and Overman, N. R., "Active Combustion Control System Rig Testing," in *46th AIAA/ASME/SAE/ASEE Joint Propulsion Conference & Exhibit*, Nashville, Tennessee, 2010, p. 11.

[143] Yu, K. H., Wilson, K. J., and Schadow, K. C., "Liquid-Fueled Active Instability Suppression," *27th Symposium International on Combustion,* vol. 27, pp. 2039-2046, 1998.

[144] Barooah, P., Anderson, T. J., and Cohen, J. M., "Active Combustion Instability Control with Spinning Valve Actuator," *Journal of Engineering for Gas Turbines and Power,* vol. 125, pp. 925-932, 2003.

[145] Coleman, B. D. and Mizel, V. J., "Norms and Semi-Groups in the Theory of Fading Memory," *Archive for Rational Mechanics and Analysis,* vol. 23, pp. 87-123, 1966.

[146] Delfour, M. C. and Mitter, S. K., "Hereditary Differential Systems with Constant Delays. I: General Case," *Journal of Differential Equations,* vol. 12, pp. 213-235, 1972.

[147] Lions, J. L., *Optimal Control of Systems Governed by Partial Differential Equations*, Fundamentals of Mathematical Sciences, vol. 170, New York: Springer-Verlag, 1971.

[148] Ichikawa, A., "Quadratic Optimal Control of Evolution Equations with Delays in Control," *SIAM Journal of Control and Optimization,* vol. 20, pp. 645-668, 1982.

[149] Gillespie, D. T., "The Mathematics of Brownian Motion and Johnson Noise," *American Journal of Physics,* vol. 64, pp. 225-240, March 1996.

[150] Stratonovich, R., *Topics in the Theory of Random Noise*, Mathematics and its Applications, vol. 2, New York: Gordon and Breach Science Publishers, 1967.

[151] Risken, H., *The Fokker-Planck Equation: Methods of Solution and Applications*, 2nd ed., Springer Series in Synergetics, vol. 18, Berlin: Springer, 1989.

[152] Kryloff, N. and Bogoliuboff, N., *Introduction to Non-Linear Mechanics*, Annals of Mathematics Studies, vol. 11, Princeton: Princeton University Press, 1949.

[153] Roberts, J. B. and Spanos, P. D., "Stochastic Averaging: An Approximate Method of Solving Random Vibration Problems," *International Journal of Non-Linear Mechanics,* vol. 21, pp. 111-134, 1986.

[154] Solomos, G. P. and Spanos, P. D., "Oscillator Response to Nonstationary Excitation," *Journal of Applied Mechanics,* vol. 51, pp. 907-912, December 1984.

[155] Küchler, U. and Mensch, B., "Langevin's Stochastic Differential Equation Extended by a Time-Delayed Term," *Stochastics and Stochastics Reports,* vol. 40, pp. 23-42, 1992.

[156] Diekmann, O., van Gils, S. A., Verduyn Lunel, S. M., and Walther, H.-O., *Delay Equations: Functional-, Complex-, and Nonlinear Analysis*, 1st ed., Applied Mathematical Sciences, vol. 110, New York: Springer-Verlag, 1995.

[157] Sipahi, R., "Cluster Treatment of Characteristic Roots, CTCR, a Unique Methodology for the Complete Stability Robustness Analysis of Linear Time Invariant Multiple Time Delay Systems Against Delay Uncertainties," in *Mechanical Engineering* Ph.D Storrs: University of Connecticut, 2005, p. 97.

[158] Hsu, C. S. and Bhatt, S. J., "Stability Charts for Second-Order Dynamical Systems with Time Lag," *Journal of Applied Mechanics,* vol. 33, pp. 119-124, 1966.

[159] Papoulis, A. and Pillai, S. U., *Probability, Random Variables, and Stochastic Processes*, 4th ed., McGraw-Hill Series in Electrical and Computer Engineering, New York: McGraw-Hill, 2002.

[160] Crawford, J. H. and Lieuwen, T. C., "Time Delay and Noise Coupling in Limiting Control Effectiveness in Unstable Combustors," in *48th AIAA Aerospace Sciences Meeting*, Orlando, Florida, 2010, p. 16.

[161] Shampine, L. F., "Vectorized Adaptive Quadrature in MATLAB," *Journal of Computational and Applied Mathematics,* vol. 211, pp. 131-140, February 2008.

[162] Myers, M. K., "An Exact Energy Corollary for Homentropic Flow," *Journal of Sound and Vibration,* vol. 109, pp. 277-284, 1986.

[163] Zolotarev, V. M., *One-Dimensional Stable Distributions*, Translations of Mathematical Monographs, vol. 65, Providence: American Mathematical Society, 1986.

[164] Nadarajah, S., "A Review of Results on Sums of Random Variables," *Acta Applicandae Mathematicae,* vol. 103, pp. 131-140, 2008.

[165] Alouini, M., Abdi, A., and Kaveh, M., "Sum of Gamma Variates and Performance of Wireless Communication Systems Over Nakagami-Fading Channels," *IEEE Transactions on Vehicular Technology,* vol. 50, pp. 1471-1480, November 2001.

[166] Moschopoulos, P. G., "The Distribution of the Sum of Independent Gamma Random Variables," *Annals of the Institute of Statistical Mathematics,* vol. 37, pp. 541-544, 1985.

[167] Isserlis, L., "On a Formula for the Product-Moment Coefficient of any Order of a Normal Frequency Distribution in any Number of Variables," *Biometrika,* vol. 12, pp. 134-139, November 1918.

[168] Hoyt, R. S., "Probability Functions for the Modulus and Angle of the Normal Complex Variate," *Bell System Technical Report,* vol. 26, pp. 318-359, April 1947.

[169] Nakagami, M., "The m-Distribution - A General Formula of Intensity Distribution of Rapid Fading " in *Statistical Methods in Radio Wave Propagation*, W. Hoffman, Ed. Oxford: Pergamon Press, 1960, pp. 3-36.

[170] Michiels, W. and Niculescu, S., *Stability and Stabilization of Time-Delay Systems*, 1st ed., Advances in Design and Control, Philadelphia: SIAM, 2007.

[171] Hale, J. K. and Lunel, S. M. V., "Strong Stabilization of Neutral Functional Differential Equations," *IMA Journal of Mathematical Control and Information,* vol. 19, pp. 5-23, 2002.

[172] McManus, K. R., Poinsot, T., and Candel, S. M., "A Review of Active Control of Combustion Instabilities," *Progress in Energy and Combustion Science,* vol. 19, pp. 1-29, January 1993.

[173] Neumeier, Y., Markopoulos, N., and Zinn, B. T., "A Procedure for Real-Time Mode Decomposition Observation and Prediction for Active Control of Combustion

Instabilities," in *IEEE International Conference on Control Applications*, Hartford, CT, 1997, p. 6.

[174] Balas, M. J., "Modal Control of Certain Flexible Dynamic Systems," *SIAM Journal of Control and Optimization,* vol. 16, pp. 450-462, 1978.

[175] Wie, B. and Bryson Jr., A. E., "Modeling and Control of Flexible Space Structures," in *3rd VPI&SU Symposium on Dynamics and Control of Large Flexible Spacecraft* Blacksburg, VA, 1981, p. 22.

[176] Berberian, S. K., *Introduction to Hilbert Space*, 2nd ed., New York: American Mathematical Society, 1976.

[177] Trefethen, L. N., "Pseudospectra of Linear Operators," *SIAM Review,* vol. 39, pp. 383-406, September 1997.

[178] Harrje, D. T. and Reardon, F. H., "Liquid Propellant Rocket Combustion Instability," NASA, D.C. SP-194, 1972.

[179] Subramanian, P. and Sujith, R. I., "Non-Normality and Internal Flame Dynamics in Premixed Flame-Acoustic Interaction," *Journal of Fluid Mechanics,* vol. 679, pp. 315-342, July 2011.

[180] Trefethen, L. N. and Embree, M., *Spectra and Pseudospectra: The Behavior of Nonnormal Matrices and Operators*, 1st ed., Princeton: Princeton University Press, 2005.

[181] MacDonald, N., "Harmonic Balance in Delay-Differential Equations," *Journal of Sound and Vibration,* vol. 186, pp. 649-656, 1995.

[182] Gawronski, W., "Actuator and Sensor Placement for Structural Testing and Control," *Journal of Sound and Vibration,* vol. 208, pp. 101-109, 1997.

[183] Moheimani, S. O. R., Halim, D., and Fleming, A. J., *Spatial Control of Vibration: Theory and Experiment*, Stability, Vibration, and Control of Systems, vol. 10, London: World Scientific, 2003.

[184] Burke, J. V., Lewis, A. S., and Overton, M. L., "A Robust Gradient Sampling Algorithm for Nonsmooth Nonconvex Optimization," *SIAM Journal of Optimization,* vol. 15, pp. 751-779, 2005.

[185] Kopasakis, G., "System Characterization of Combustor Instabilities with Controls Design Emphasis," in *42nd AIAA Aerospace Sciences Meeting and Exhibit* Reno, NV: AIAA, 2004, p. 12.

[186] Kopasakis, G., DeLaat, J. C., and Chang, C. T., "Adaptive Instability Suppression Controls Method for Aircraft Gas Turbine Engine Combustors," *Journal of Propulsion and Power,* vol. 25, pp. 618-627, May-June 2009.

[187] Michiels, W. and Roose, D., "An Eigenvalue Based Approach for the Robust Stabilization of Linear Time-Delay Systems," *International Journal of Control,* vol. 76, pp. 678-686, 2003.

[188] Brogan, W. L., *Modern Control Theory*, 3rd ed., Upper Saddle River: Prentice Hall, 1990.

[189] Triggiani, R., "On the Lack of Exact Controllability for Mild Solutions in Banach Spaces," *Journal of Mathematical Analysis and Applications,* vol. 50, pp. 438-446, 1975.

[190] Pandolfi, L., "On Feedback Stabilization of Functional Differential Equations," *Bolletino della Unione Matematica Italiana,* vol. 4, pp. 626-635, 1975.

[191] Olbrot, A. W., "Stabilizability, Detectability, and Spectrum Assignment for Linear Autonomous Systems with General Time Delays," *IEEE Transactions on Automatic Control,* vol. 23, pp. 887-890, October 1978.

[192] Klamka, J., *Controllability of Dynamical Systems*, Mathematics and Its Applications (East European Series), vol. 48, Boston: Kluwer Academic Publishers, 1991.

[193] Ortega, R., van der Schaft, A. J., Mareels, I., and Maschke, B., "Putting Energy Back in Control," in *IEEE Control Systems Magazine* 21 Ann Arbor: IEEE Control Systems Society, 2001, pp. 18-33.

[194] Freudenberg, J. S. and Looze, D. P., *Frequency Domain Properties of Scalar and Multivariable Feedback Systems*, Lecture Notes in Control and Information Sciences, vol. 104, New York: Springer-Verlag, 1988.

[195] Doyle, J. C. and Stein, G., "Multivariable Feedback Design: Concepts for a Classical/Modern Synthesis," *IEEE Transactions on Automatic Control,* vol. 26, pp. 4-16, 1981.

[196] Bode, H. W., *Network Analysis and Feedback Amplifier Design*, 1st ed., Bell Telephone Labs Series, New York: Van Nostrand, 1945.

[197] Freudenberg, J. S. and Looze, D. P., "Right Half Plane Poles and Zeros and Design Tradeoffs in Feedback Systems," *IEEE Transactions on Automatic Control,* vol. 30, pp. 555-565, 1985.

[198] Freudenberg, J. S. and Looze, D. P., "A Sensitivity Tradeoff for Plants with Time Delay," *IEEE Transactions on Automatic Control,* vol. 32, pp. 99-104, 1987.

[199] Yamamoto, Y., "Pseudorational Transfer Functions - A Survey of a Class of Infinite Dimensional Systems," in *46th IEEE Conference on Decision and Control* New Orleans, LA, 2007, pp. 848-853.

[200] Bartle, R. G., *The Elements of Real Analysis*, 2nd ed., New York: Wiley, 1976.

[201] Gomez, G. and Goodwin, G. C., "Integral Constraints on Sensitivity Vectors for Multivariable Linear Systems," *Automatica,* vol. 32, pp. 499-518, 1996.

[202] Levinson, N. and Redheffer, R. M., *Complex Variables*, 1st ed., Holden-Day Series in Mathematics, San Francisco: Holden-Day, 1970.

[203] Gomez, G. I. and Goodwin, G. C., "Generalization of Integral Constraints on Sensitivity to Time-Delay Systems," *IEEE Transactions on Automatic Control,* vol. 43, pp. 1008-1012, July 1998.

[204] Chen, J., "Logarithmic Integrals, Interpolation Bounds, and Performance Limitations in MIMO Feedback Systems," *IEEE Transactions on Automatic Control,* vol. 45, pp. 1098-1115, June 2000.

[205] Antsaklis, P. J. and Michel, A. N., *Linear Systems*, Boston: Birkhauser, 2005.

[206] Krasovskii, N. N., "On the Analytic Construction of an Optimal Control in a System with Time Lags," *Journal of Appiled Mathematics and Mechanics,* vol. 26, pp. 39-51, 1962.

[207] Bellman, R., *Dynamic Programming*, Princeton: Princeton University Press, 1957.

[208] Delfour, M. C., McCalla, C., and Mitter, S. K., "Stability and the Infinite-Time Quadratic Cost Problem for Linear Hereditary Differential Systems," *SIAM Journal of Control,* vol. 13, pp. 48-88, 1975.

[209] Ito, K., "Strong Convergence and Convergence Rates of Approximating Solutions for Algebraic Riccati Equations in Hilbert Spaces," in *Distributed Parameter Systems*. vol. 102, F. Kappel, K. Kunisch, and W. Schappacher, Eds. Berlin: Springer, 1987, pp. 153-166.

[210] Delfour, M. C., "The Linear Quadratic Optimal Control Problem for Hereditary Differential Systems: Theory and Numerical Solution," *Applied Mathematics and Optimization,* vol. 3, pp. 101-162, 1977.

[211] Gibson, J. S., "Linear Quadratic Control of Hereditary Differential Systems: Infinite Dimensional Riccati Equations and Numerical Approximations," *SIAM Journal of Control and Optimization,* vol. 21, pp. 95-139, 1983.

[212] Sima, V., *Algorithms for Linear-Quadratic Optimization*, Monographs and Textbooks in Pure and Applied Mathematics, vol. 200, New York: Marcel Dekker, 1996.

[213] Mehrmann, V. L., *The Autonomous Linear Quadratic Control Problem: Theory and Numerical Solution*, Lecture Notes in Control and Information Sciences, vol. 163, New York: Springer-Verlag, 1991.

[214] Trefethen, L. N., *Spectral Methods in MATLAB*, Software, Environments, and Tools, Philadelphia: SIAM, 2000.

[215] Van Assche, V., Dambrine, M., and Lafay, J. F. R., J P, "Some Problems Arising in the Implementation of Distributed-Delay Control Laws," in *38th Conference on Decision and Control* Phoenix, AZ: IEEE, 1999, p. 5.

[216] Kamen, E. W., Khargonekar, P. P., and Tannenbaum, A., "Stabilization of Time-Delay Systems Using Finite-Dimensional Compensators," *IEEE Transactions on Automatic Control,* vol. 30, pp. 75-78, January 1985.

[217] Mirkin, L., "On the Approximation of Distributed-Delay Control Laws," *Systems & Control Letters,* vol. 51, pp. 331-342, April 2004.

[218] Engelborghs, K., Dambrine, M., and Roose, D., "Limitations of a Class of Stabilization Methods for Delay Systems," *IEEE Transactions on Automatic Control,* vol. 46, pp. 336-339, 2001.

[219] Michiels, W., Mondie, S., Roose, D., and Dambrine, M., "The Effects of Approximating Distributed Delay Control Law on Stability," in *Advances in Time-Delay Systems*. vol. 38, S. Niculescu and K. Gu, Eds. New York: Springer, 2004, pp. 207-222.

[220] Ogata, K., *Modern Control Engineering*, 5th ed., Upper Saddle River: Prentice Hall, 2009.

[221] Ortega, R. and Tang, Y., "Robustness of Adaptive Controllers - A Survey," *Automatica,* vol. 25, pp. 651-677, 1989.

[222] Zames, G., "On the Input-Output Stability of Time-Varying Nonlinear Feedback Systems Part I: Conditions Derived Using Concepts of Loop Gain, Conicity, and Positivity," *IEEE Transactions on Automatic Control,* vol. 11, pp. 228-238, 1966.

[223] Schwarz, H., Zimmer, L., Durox, D., and Candel, S., "Detailed Measurements of Equivalence Ratio Modulations in Premixed Flames Using Rayleigh Scattering and Absorption Spectroscopy," *Experiments in Fluids,* vol. 49, pp. 809-821, 2010.

[224] Bernstein, D. S. and Haddad, W. M., "LQG Control with an H_s Performance Bound: A Riccati Equation Approach," *IEEE Transactions on Automatic Control,* vol. 34, pp. 293-305, March 1989.

[225] Curtain, R. F. and Ichikawa, A., "The Separation Principle for Stochastic Evolution Equations," *SIAM Journal of Control and Optimization,* vol. 15, pp. 367-383, May 1977.

[226] Bernstein, D. S. and Hyland, D. C., "The Optimal Projection Equations for Finite-Dimensional Fixed-Order Dynamic Compensation of Infinite-Dimensional Systems," *SIAM Journal of Control and Optimization,* vol. 24, pp. 122-151, January 1986.

[227] Bhat, K. P. M. and Koivo, H. N., "An Observer Theory for Time Delay Systems," *IEEE Transactions on Automatic Control,* vol. 21, pp. 266-269, April 1976.

[228] Simon, D., *Optimal State Estimation: Kalman, H Infinity, and Nonlinear Approaches*, Hobeken: Wiley-Interscience, 2006.

[229] Hong, J. and Bernstein, D. S., "Bode Integral Constraints, Collocation, and Spillover in Active Noise and Vibration Control," *IEEE Transactions on Control Systems Technology,* vol. 6, pp. 111-120, January 1998.

[230] Haddad, W. M. and Chellaboina, V. S., *Nonlinear Dynamical Systems and Control: A Lyapunov-Based Approach*, Princeton: Princeton University Press, 2008.

[231] Li, D., "Closed-Loop Analysis and Feedback Design in the Presence of Limited Information," in *Mechanical Engineering* Ph.D Urbana: University of Illinois at Urbana-Champaign, 2011, p. 113.

[232] Breda, D., Maset, S., and Vermiglio, R., "Pseudospectral Approximation of Eigenvalues of Derivative Operators with Non-Local Boundary Conditions," *Applied Numerical Mathematics,* vol. 56, pp. 318-331, 2006.

[233] Gentleman, W. M., "Implementing Clenshaw-Curtis Quadrature I: Methodology and Experience," *Numerical Mathematics,* vol. 15, pp. 337-342, 1972.

[234] Bernstein, D. S., *Matrix Mathematics: Theory, Facts, and Formulas*, 2nd ed., Princeton: Princeton University Press, 2009.

[235] Chase Jr, M. W., *NIST-JANAF Thermochemical Tables*, 4th ed., Journal of Physical Chemical Reference Data, vol. 9: American Institute of Physics, 1998.